PURDUE UNIVERSITY | Purdue Institute of Inflammation, Immunology and Infectious Disease

2024 PI4D Symposium

Poster Abstracts
E-Booklet

Table of Contents

Poster Number: #1

Activation of the Innate Immune System to Prevent Flavivirus Induced Viremia Using a Bispecific Small Molecule Targeting Ligand

Magdalena Alvis

Biological Sciences

Dengue is a mosquito-borne disease that infects around 400 million people every year, with 10-25% of these cases becoming severe and requiring hospitalization. Currently, 3.6 billion people are at risk for Dengue infections, but this number is predicted to rise to 6.1 billion in 2080 as climate change expands mosquito habitat. No effective treatments or vaccines exist for Dengue due to its unique pathophysiology involving antibody-dependent enhancement. Therefore, there is a substantial need to develop an antiviral that can treat Dengue. Previously, we have produced a novel, bifunctional small molecule capable of targeting and eliminating severe influenza infection via activation of the host‚Äôs innate immune system with a single dose. We have adapted this platform technology to successfully target the Dengue Envelope (E) protein, a protein expressed on the exterior of the virus and highly conserved across all serotypes and several other flaviviruses, including Zika, Yellow Fever, West Nile, and Japanese Encephalitis. The E protein targeting ligand is linked to two distinct hapten molecules, each capable of binding to two different, naturally occurring human antibodies. These antibodies recruited to the virus engage the innate immune effector cells to kill the virus particles. Preclinical in vitro and in vivo experiments have been performed and show that binding of our compound is effective in stopping infection and reduces viremia in animals more effectively than any previous compounds when administered orally or subcutaneously. This dual targeting tactic is a novel approach for the rapid and effective treatment of severe Dengue and other flaviviruses.

Activation of the Innate Immune System to Prevent Flavivirus Induced Viremia Using a Bispecific Small Molecule Targeting Ligand

PURDUE UNIVERSITY

Purdue Institute of Inflammation, Immunology and Infectious Disease

Conrrad Nicholls, PhD, Jeffery Nielsen, PhD, Magdalena Alvis, Charity Campbell, Joshua Ramsey, McLayne Houin, Jeramiah Budd, Ian Alford, Imrul Shariar, PhD, Philip Low, PhD

Eradivir Inc., West Lafayette, IN 47907

PURDUE CHEMISTRY

ERADIVIR

Abstract

Dengue is a mosquito-borne disease that infects around 400 million people every year, with 10-25% of these cases becoming severe and requiring hospitalization. Currently, 3.6 billion people are at risk for Dengue infections, but this number is predicted to rise to 6.1 billion in 2080 as climate change expands mosquito habitat. No effective treatments or vaccines exist for Dengue due to its unique pathophysiology involving antibody-dependent enhancement. Therefore, there is a substantial need to develop an antiviral that can treat Dengue. Previously, we have produced a novel, bifunctional small molecule capable of targeting and eliminating severe influenza infection via activation of the host's innate immune system with a single dose. We have adapted this platform technology to successfully target the Dengue Envelope (E) protein, a protein expressed on the exterior of the virus and highly conserved across all serotypes and several other flaviviruses, including Zika, Yellow Fever, West Nile, and Japanese Encephalitis. The E protein targeting ligand is linked to two distinct hapten molecules, each capable of binding to two different, naturally occurring human antibodies. These antibodies recruited to the virus engage the innate immune effector cells to kill the virus particles. Preclinical in vitro and in vivo experiments have been performed and show that binding of our compound is effective in stopping infection and reduces viremia in animals more effectively than any previous compounds when administered orally or subcutaneously. This dual targeting tactic is a novel approach for the rapid and effective treatment of severe Dengue and other flaviviruses.

Background

Platform Technology:

BAiT™

Bispecific Antigenic immuno-Therapy

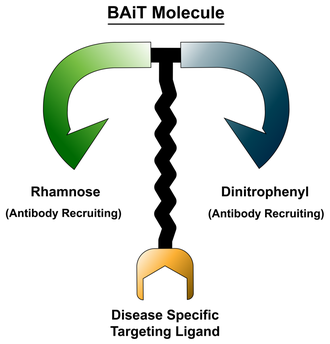

Figure 1 - Bispecific Antigenic Immuno-Therapy (BAiT) molecule general structure: The BAiT molecule is a highly modular tool capable of being altered to meet the demand of a wide variety of diseases.

Mechanism:

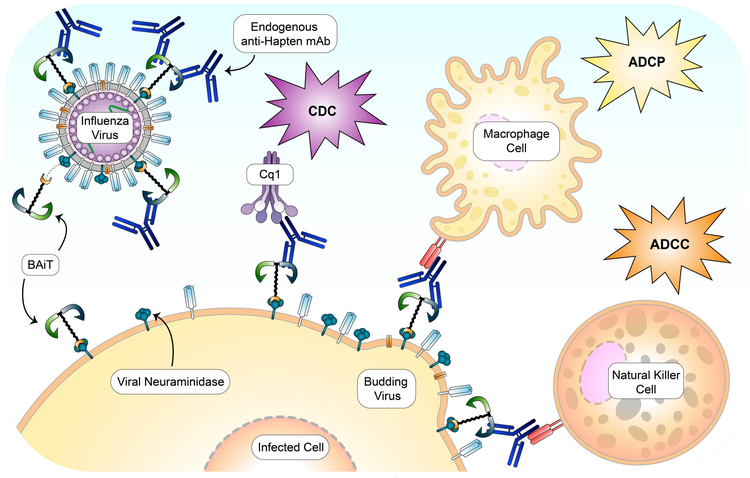

Figure 2 - Mechanism of Action of the BAiT Platform: Relying on the high binding affinity of disease specific targeting ligands, BAiT molecules link proteins of interest to endogenously produced anti-Hapten antibodies abundant in all humans. The tethering of these antibodies to disease specific proteins via BAiT molecules recruits complement proteins, macrophages, and even natural killer cells to sites of infection, effectively eliminating infected cells and removing virus particles.

Foundation in Influenza:

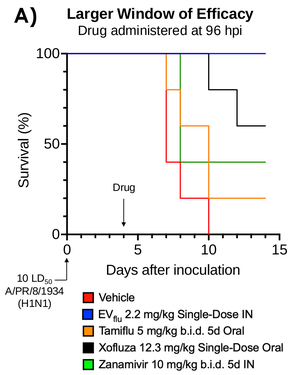

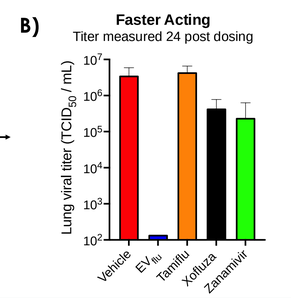

Figure 3 – Proof of concept in influenza: **A)** EVflu, our lead molecule for the treatment of influenza infection, has demonstrated robust antiviral efficacy when administered out to 96 hours post infection, protecting all mice treated. **B)** EVflu was shown to reduce viral titer to limit of quantification after only 24 hours post treatment.

Experimental Design

Target of Interest: Flavivirus E protein

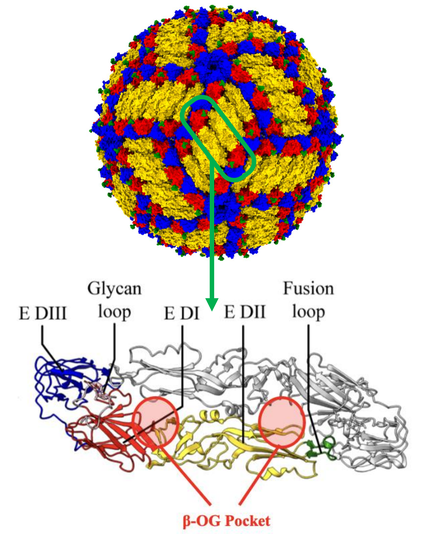

Figure 4 – Flavivirus Protein Region of Interest: One location of the flavivirus E protein – the beta-OG-pocket, was evaluated with 10 different ligands to determine the most reliable ligand capable of bridging the E protein to effector cells.

Results

Lead Molecule EV58 Retains Pan Flavivirus Direct Antiviral Activity

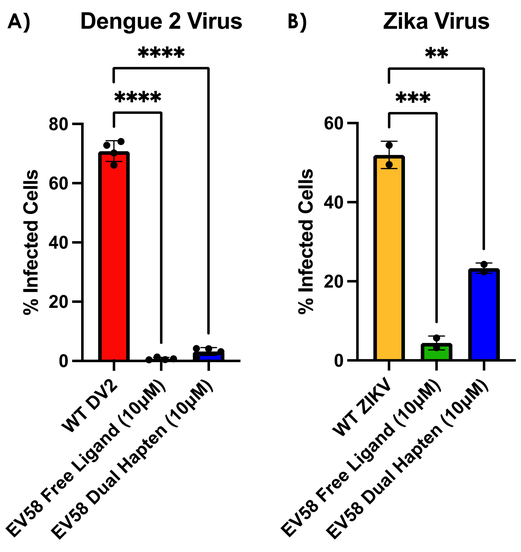

Figure 5 – Cell Based Flavivirus Infection Assay: **A)** BHK cells were infected with DV2, or **B)** Vero cells were infected with ZIKV, both at an MOI of 5 for 36 hours in the presence of EV58 Free Ligand (FL) or EV58 Dual Hapten (DH), each at a final concentration of 10 μM. An immunofluorescence assay was then used to determine the ratio between infected cells to non-infected cells via an Opera Phenix high resolution cell imager. One-Way ANOVA was used to determine statistical significance between WT infection and treatment with EV58 FL or DH. These results demonstrate that EV58 DH retains the pan flavivirus direct antiviral activity of the free ligand, suggesting that the addition of the dual haptens onto the free ligand does not drastically impair antiviral activity.

EV58 is Immunologically Active and Specific to RSF F

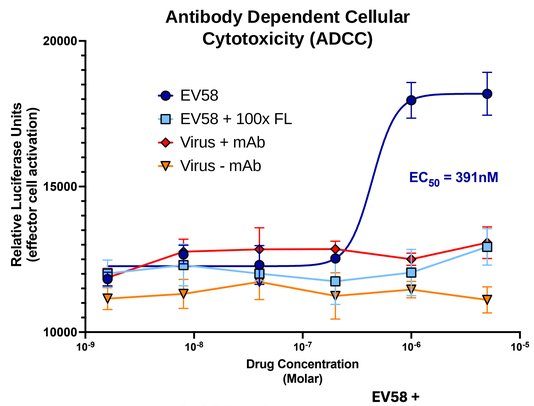

Figure 6 – Immunological Activity of EV58: The ability for EV58 to present its dual haptens to the surrounding environment when bound to DV2 was determined via ADCC assay with clarified virus particles ($1x10^6$ PFU / well). Results show that EV58 elicits a robust and site-specific activation of effector (i.e., NK) cells with an EC_{50} value of 391 nM. These results suggest that the dual haptens attached to EV58 are not obstructed from interacting with immune cells, confirming our mechanism of action.

Figure 7 – Competitive Specificity of EV58: Immunofluorescence assay of DV2 infected cells demonstrates the specificity of EV58 to the flavivirus E protein, as EV58 was shown to be out competed by the addition of 100x FL. These results suggest that EV58 co-localizes with DV2 E protein while retaining hapten presentation to the external environment.

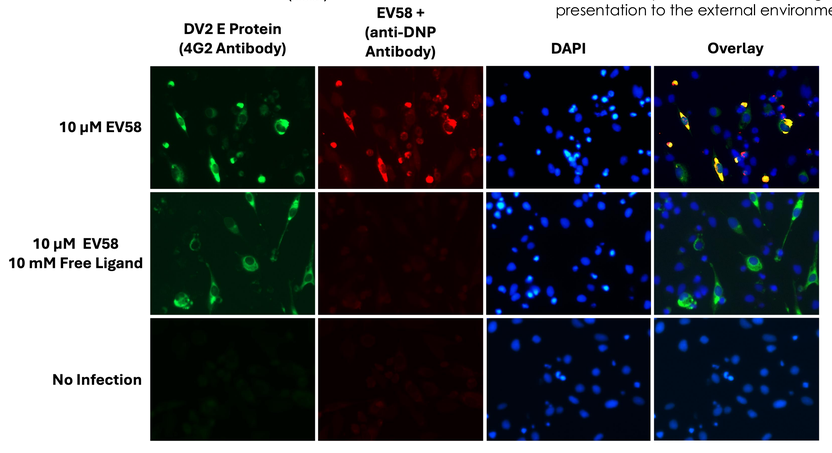

EV58 Demonstrates In Vivo Therapeutic Efficacy

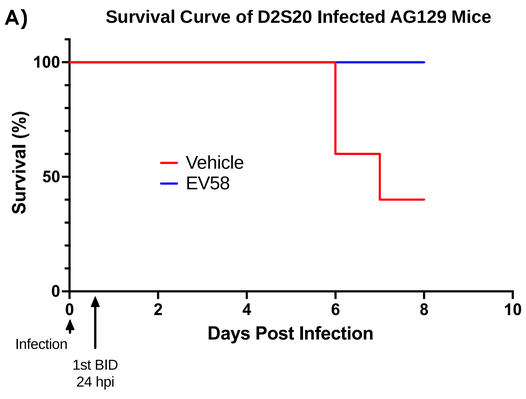

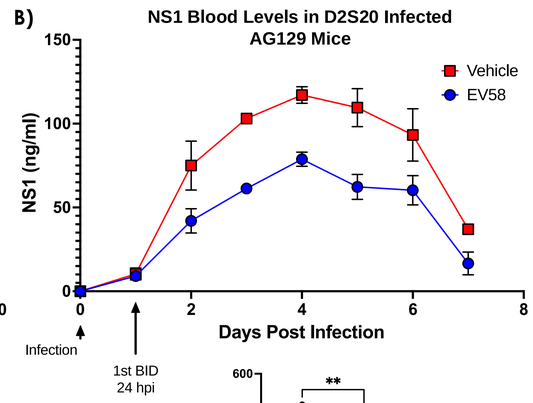

Figure 8 – In Vivo Efficacy of EV58 in AG129 mice: AG129 mice lacking interferon alpha/beta and gamma were infected with $1x10^6$ mouse adapted dengue virus serotype 2 strain D2S20. The first dose of EV58 was given 24 hours post infection. Blood samples (serum) and body weights were obtained daily. **A)** EV58 treatment resulted in 100% of mice surviving throughout the duration of the study, while only 40% of vehicle treated mice survived. **B)** NS1 levels in the blood serum of infected mice was shown to be noticeably higher in the vehicle treated mice over the EV58 treated mice, suggesting that the infection was still present, but was significantly blunted by EV58 treatment. **C)** AUC analysis of the EV58 and vehicle curves show that EV58 treatment significantly reduced blood NS1 levels (Student's t test ** = P value of 0.004).

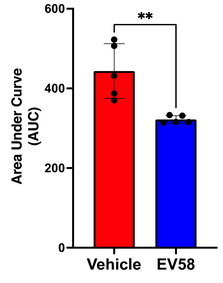

Conclusions

Initial results indicate that our bispecific molecules protect against DV2 and ZIKV infection in vitro. This suggests that our targeting ligands are still able to bind to flavivirus particles, disrupting some early stage of virus entry or fusion. In addition, effector cell activation suggests that the binding is specific, and the haptens linked to our targeting ligands are still accessible to antibodies. Lastly, positive in-vivo data suggest that our mechanism of action is effective at protecting AG129 mice from lethal infection.

Acknowledgements

I would like to thank Eradivir Inc for allowing me to present this work and a special thank you to Dr. Jeffery Nielsen for his continued guidance as VP of Discovery Research. Lastly, I would like to thank Dr. Phil Low for his continued support of our company as our academic partner at Purdue University.

Poster Number: #2

New tools to study fungal pathogens and find antifungal drug targets.

Emily Danzeisen

Biochemistry

Systemic fungal infections are on the rise, accounting for a staggering 6.5 million invasive infections and an estimated 3.6 million deaths each year. This global health concern was highlighted in 2022 by the World Health Organization‚Äôs fungal priority pathogens list which listed Candida albicans and emerging pathogen Candida auris as critical priority pathogens. Several Candida species including C. auris show emerging resistance to the few antifungals available, reducing the efficacy of prescribed therapeutics. With the increase in invasive fungal infections, limited treatment options available, and rise in antifungal resistance, there is an urgent need for novel antifungal therapies and drug targets. To address this need, we are developing the auxin inducible degradation (AID) system in Candida species that can be used in animal infection models to provide a platform for identifying novel antifungal drug targets. The AID system enables rapid degradation of a target protein upon addition of the plant hormone auxin and has been used in various eukaryotic organisms for protein characterization. We hypothesize that use of the system can extended into the realm of drug discovery by serving as a platform to screen for potential antifungal drug targets. We predict that the addition of auxin will induce degradation of the target protein during infection and will simulate the effects of a small molecule inhibitor or degrader drug, with auxin acting as a surrogate drug. To validate this approach, we are targeting the known C. albicans virulence factor Cdc14 for degradation in genetically modified C. albicans strains. These strains are being used to test if auxin-induced degradation of Cdc14 decreases virulence in two well-established models of invasive fungal infection: Galleria mellonella larvae and mice. If Cdc14 degradation reduces the virulence of C. albicans, the AID system could be used to broadly test if degradation of other proteins is sufficient to impair pathogenesis and thereby identify potential novel antifungal targets.

New tools to study fungal pathogens and find antifungal drug targets

Emily L. Danzeisen[1] and Mark C. Hall[1,2]
[1]Department of Biochemistry, Purdue University, West Lafayette IN
[2]Institute for Cancer Research, Purdue University, West Lafayette, IN

The rising problem of fungal diseases

Invasive fungal diseases are a global health concern and a serious problem for immune-comprised people.

- Around 3.6 million people succumb to these infections annually.[1]
- *Candida* species (42%), *Aspergillus* (29%), and *Cryptococcus* (4%) are among the primary contributors.[2]

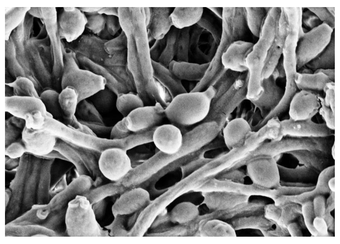
Candida albicans

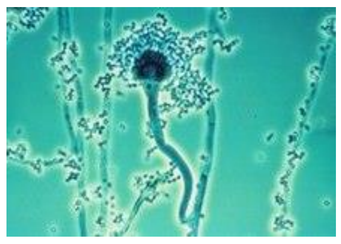
Aspergillus fumigatus

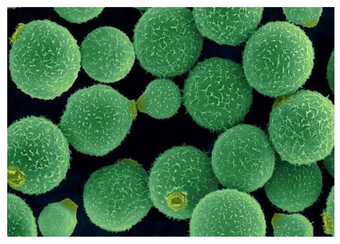
Cryptococcus

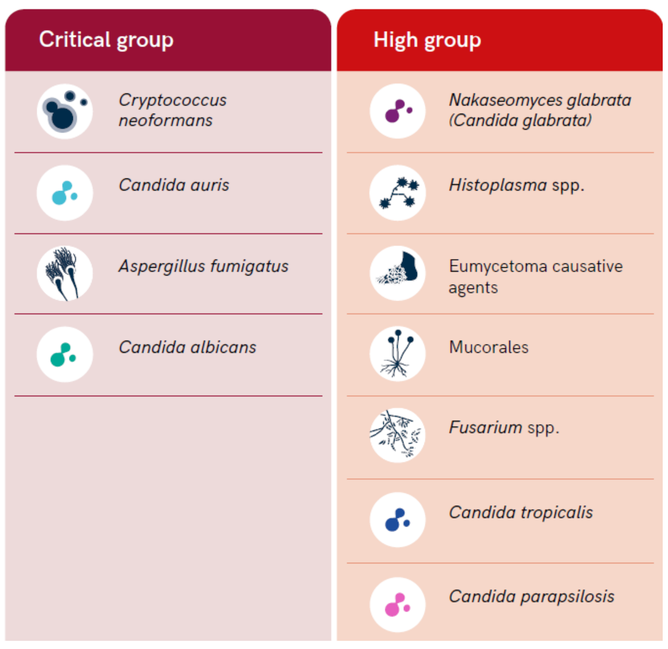

Fungal pathogens: A call for action

- The 2022 World Health Organization's report on fungal pathogens highlights the escalating issue and emphasizes the need for intensified research.
- Urges the development of novel therapeutics to combat the rising threat.

Limited treatment options and drug resistance:

- Despite the growing problem, only four FDA-approved drug classes are available for combating invasive fungal infections.

General Interest of the Hall lab:
Understand the role of kinases and phosphatases in promoting virulence of fungal pathogens and identify novel targets for antifungal drug development.

The search for antifungal targets: Cdc14 phosphatase

Cdc14 deficiency severely compromises virulence in larvae and mouse models of invasive candidiasis

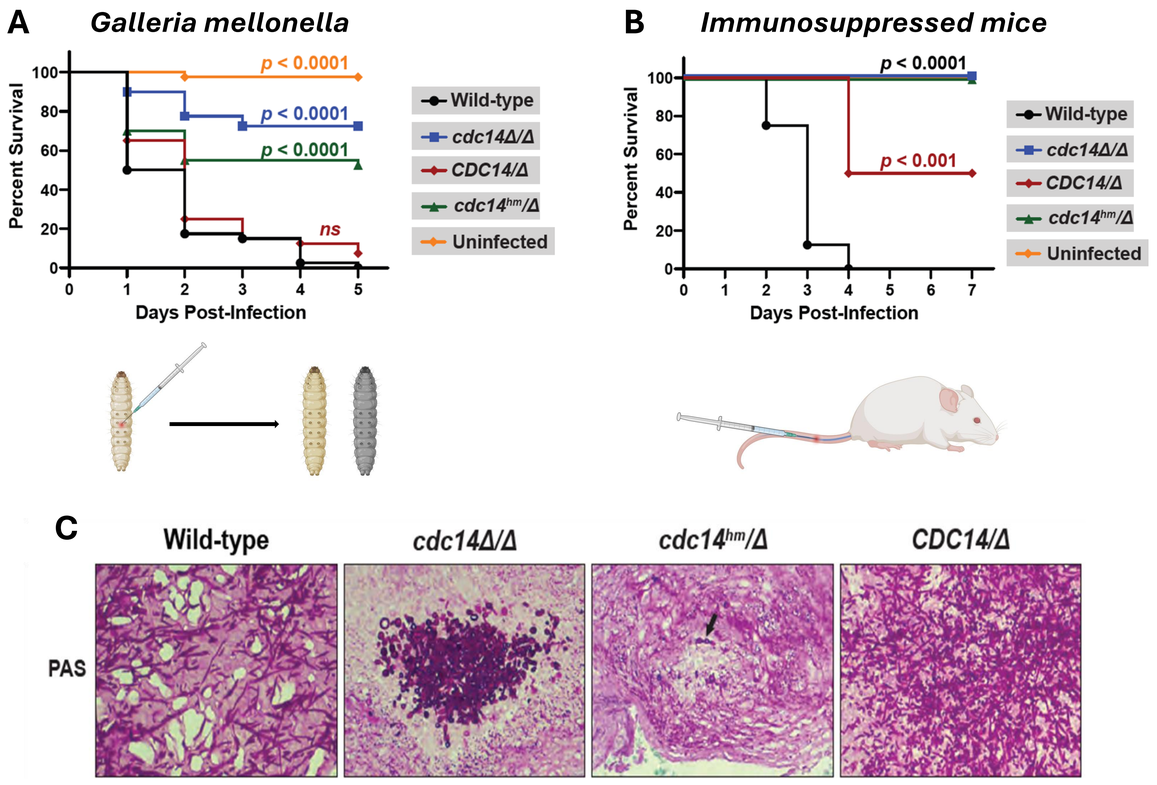

Figure 1. (A) *G. mellonella* larvae and **(B)** immunosuppressed BALB/c infection assay using Cdc14 hypomorphic and deletion strains[3]. **(C)** *Candida albicans* fails to form hyphae in infected mice when Cdc14 is deficient. PAS staining of liver sections[3].

Auxin-inducible degradation system

A powerful tool for protein characterization and drug discovery

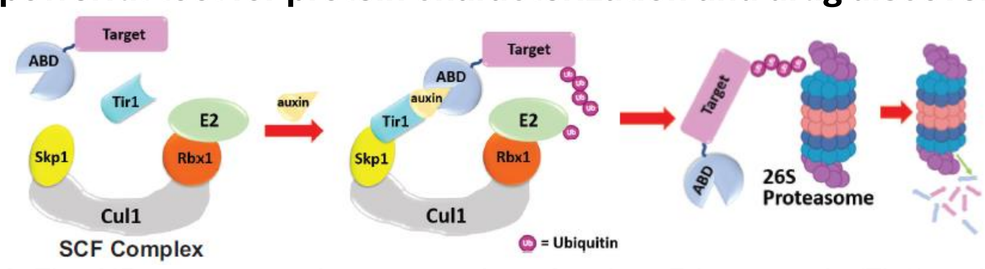

Figure 2. The AID system requires expression of a plant F-box protein (Tir1) and fusion of an auxin-binding domain (ABD) to a target gene. Upon addition of auxin, the ABD-target fusion protein physically interacts with the SCF^{Tir1} ubiquitin ligase to be polyubiquitinated and then is proteolyzed by the 26S proteasome[4].

The AID system provides rapid, efficient target degradation in *C. albicans*.

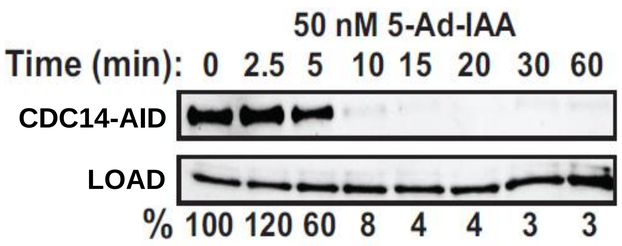

Figure 3. Cdc14-AID fusion protein is rapidly degraded in *C. albicans* cells after treatment with 50nM synthetic auxin 5-Ad-IAA[4].

The AID system effectively phenocopies loss-of-function mutations

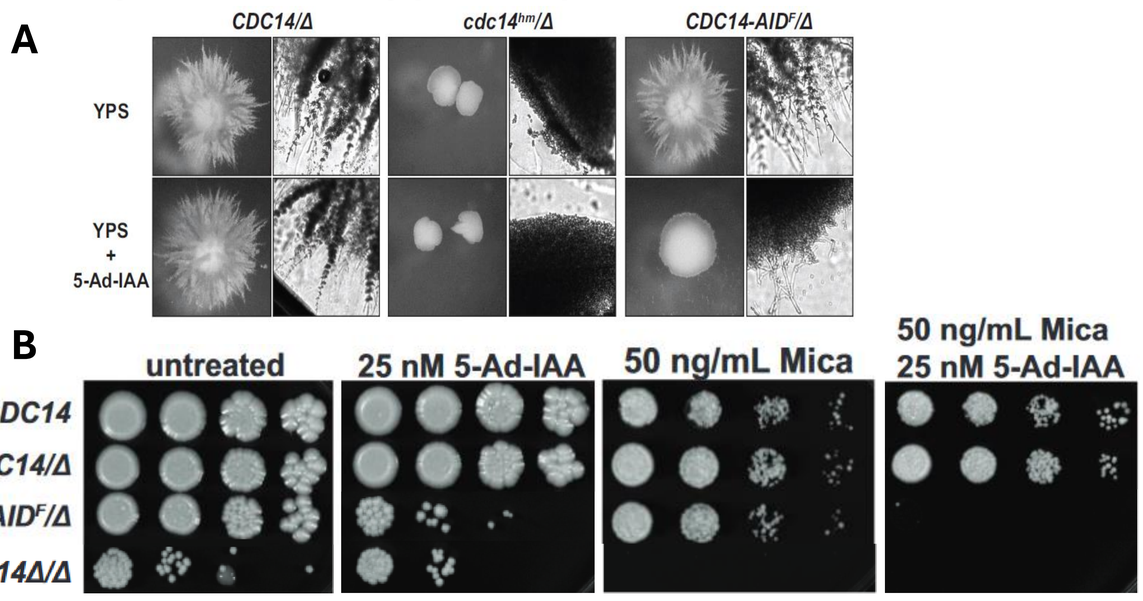

Figure 4. (A) *C. albicans* strains with the indicated genotypes grown embedded in YPS agar with or without the synthetic auxin 5-Ad-IAA. YPS induced hyphal growth only in the presence of Cdc14. **(B)** Liquid cultures of *C. albicans* strains were serially diluted and spotted on YPD agar plates supplemented with micafungin (Mica) and/or 5-Ad-IAA[4].

Applying the AID system to identify novel antifungal targets

Coupling the AID system with *in vivo* infection assays

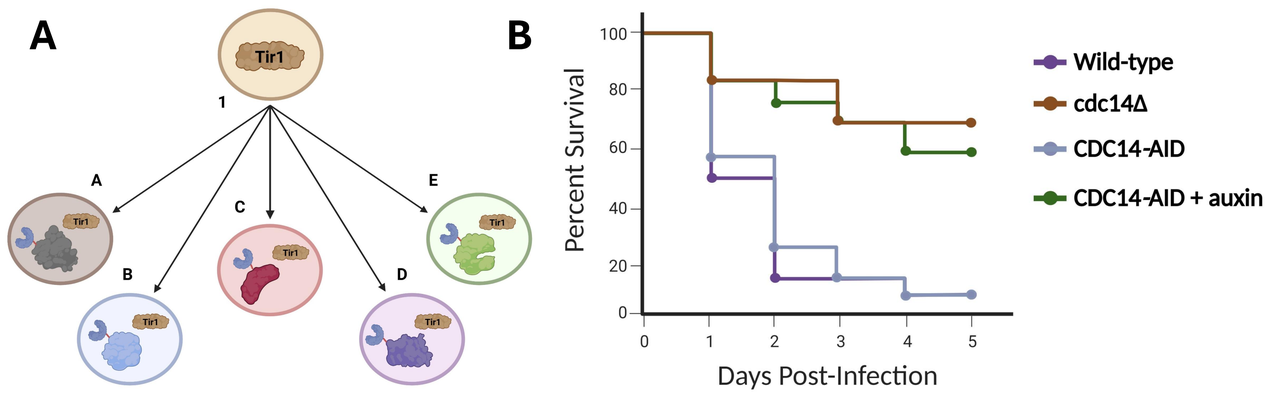

Figure 5. (A) strain library comprised of various AID fusion proteins would provide a valuable tool for the identification of novel virulence factors and antifungal targets. **1:** Generating an AID strain library requires a base strain expressing exogenous Tir1. **A-E:** Using the base Tir1 strain, a collection of yeast strains expressing both Tir1 and various AID fusion proteins could be created. **(B)** Since *CDC14-AID C. albicans* strains display the null phenotype in the presence of auxin and reduced Cdc14 function impairs virulence, we hypothesize that auxin treatment following infection will reduce virulence *in vivo*.

Future goals

- Develop the AID system in new fungal pathogens such as *C. auris* and *Coccidioides*.
- Generate AID strain libraries (i.e. kinases / phosphatases).
- Couple the AID system with *in vivo* infection assays to identify novel virulence factors and screen for antifungal targets.

Funding

National Institute of Allergy and Infectious Diseases (NIAID)
Indiana Clinical and Translational Sciences Institute

References

1. Denning 2024. *Lancet Infect Dis.*
2. Pfaller *et al.*, 2006. *Clin Infect Dis*.
3. Milholland *et al.*, 2023. *Front. Microbiol.*
4. Milholland *et al.*, 2023. *Msphere*.

Poster Number: #3

Development of digital biomarkers for vaccine induced inflammation: Exploring ECG morphology from a chest ,Äì worn wearable device

Darpit Dave

Biomedical Engineering

Background: Vaccination induces a strong response of inflammatory cytokines, which are important to study reactogenicity and immunogenicity. Wearables sensors capture physiologic signals in real-time, that provides objective evidence to vaccine induced inflammation. Inter-beat interval (IBI) derived heart rate and heart-rate variability (HRV) has been widely studied to understand these inflammatory changes. However, intra-beat information in the form of beat morphology contains valuable information but remains largely unexplored. A key challenge is that wearable ECGs are vulnerable to motion artifacts, making reliable detection of fiducial points (P, Q, S, T peaks) quite challenging.

Methods: We propose a deep-learning approach via a convolutional auto-encoder (CAE) model to study ECG ,Äì beat morphology and related inflammatory changes. The CAE model learns latent representation of beat morphology bypassing detection of individual fiducial (P, Q, S, T) points. We also use the same architecture for learning RR-interval patterns of ECG signal over a period of time. For comparison, we compute QT-intervals in studying vaccine-induced inflammatory changes. In our work we ask two key research questions: (a) Does beat-morphology show signs of vaccine-induced inflammatory response, (b) Can morphology-based approach lead to early detection of inflammatory changes? and (c) Does CAE-derived morphological representation provide improved data availability over manual computation of QT-intervals.

Results: In our preliminary experiments, with a subset of 5 patients, using CAE derived latent representation of ECG-beats detects inflammatory changes in 5/5 patients, compared to 4/5 patients with RR-intervals and 0/5 with manual computation QT-intervals. Also, compared to RR intervals, it provides early detection for 2/5 patients. CAE derived latent representations have on average 10% more data availability compared to manually computed QT-intervals, making it more robust and reliable.

Conclusions: The results indicate that ECG morphology contains valuable information that can be beneficial to study vaccine induced inflammatory changes. There is also a strong case to combine ECG morphology information and RR-intervals for improved and early detection of these changes.

Development of digital biomarkers for vaccine induced inflammation: Exploring ECG morphology from a chest – worn wearable device

Darpit Dave[1], Sarwat Amin[1], Damen Wilson[1,2], Matthew P. Ward[1,2], Steven R. Steinhubl[1]
[1]Weldon School of Biomedical Engineering
[2]IU School of Medicine

Background

- Studies have shown heart rate and heart rate variability (HRV) to correlate with vaccine-induced inflammation [1]
- However, ECG morphology remains largely unexplored
- Manual feature extraction for morphology can be unreliable given the presence of artifacts with wearable devices

Why morphology matters?

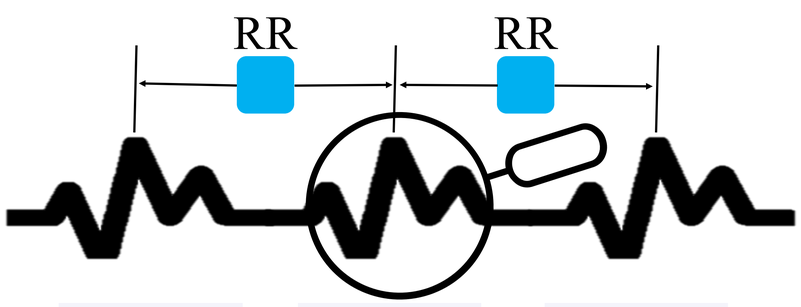

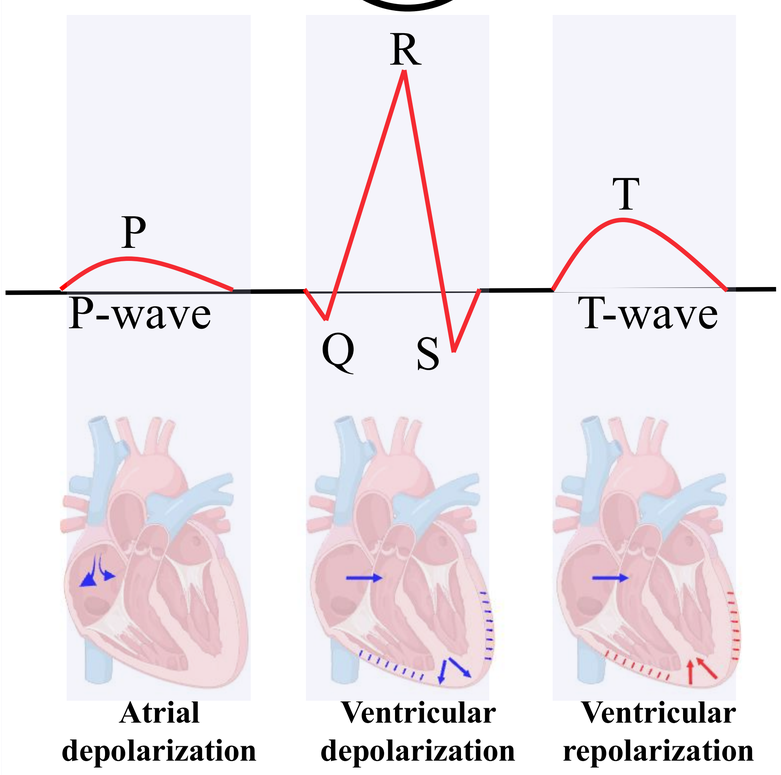

Atrial depolarization | **Ventricular depolarization** | **Ventricular repolarization**

- Research questions:
  - Does beat morphology show signs of vaccine induced inflammatory response?
  - Can morphology-based approach lead to early detection of inflammatory changes?
  - Does a deep-learning approach provide improved data availability over manual computation of features?

Wearable ECG data

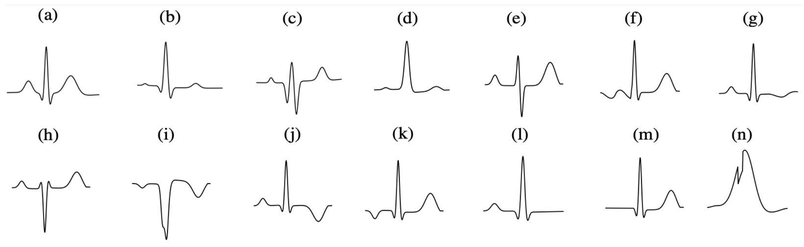

- Wearable ECG is noisy compared to 12-lead ECG used in clinical settings
- Individual beats can exist in various forms making detection of fiducial points (P, Q, R, S, T peaks) challenging [2]

Summary

- ECG morphology contains valuable information related to vaccine induced inflammation and leads to early detection
- For 5 patients, beat morphology (extracted via CAE) **detects inflammatory changes** for **5/5** patients and for **3/5** patients provides **early detection** compared to RR intervals
- Automated feature learning through autoencoders is a reliable way to extract morphological information from noisy ECG signal compared to manual feature engineering
- CAE models have on an average **10% more** data points compared to manual feature when filtered for outliers

Future Work

Combining ECG morphology and RR-interval data to effectively capture vaccine induced inflammatory responses

Methods

Data collection

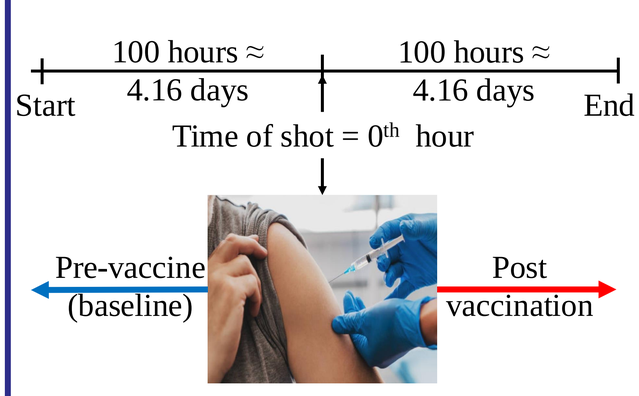

Vaccine type	Moderna and Pfizer
Patient age range	18 – 69 years old
ECG data collected	Vitalconnect patch
ECG sampling frequency	125 Hz

Modeling approach

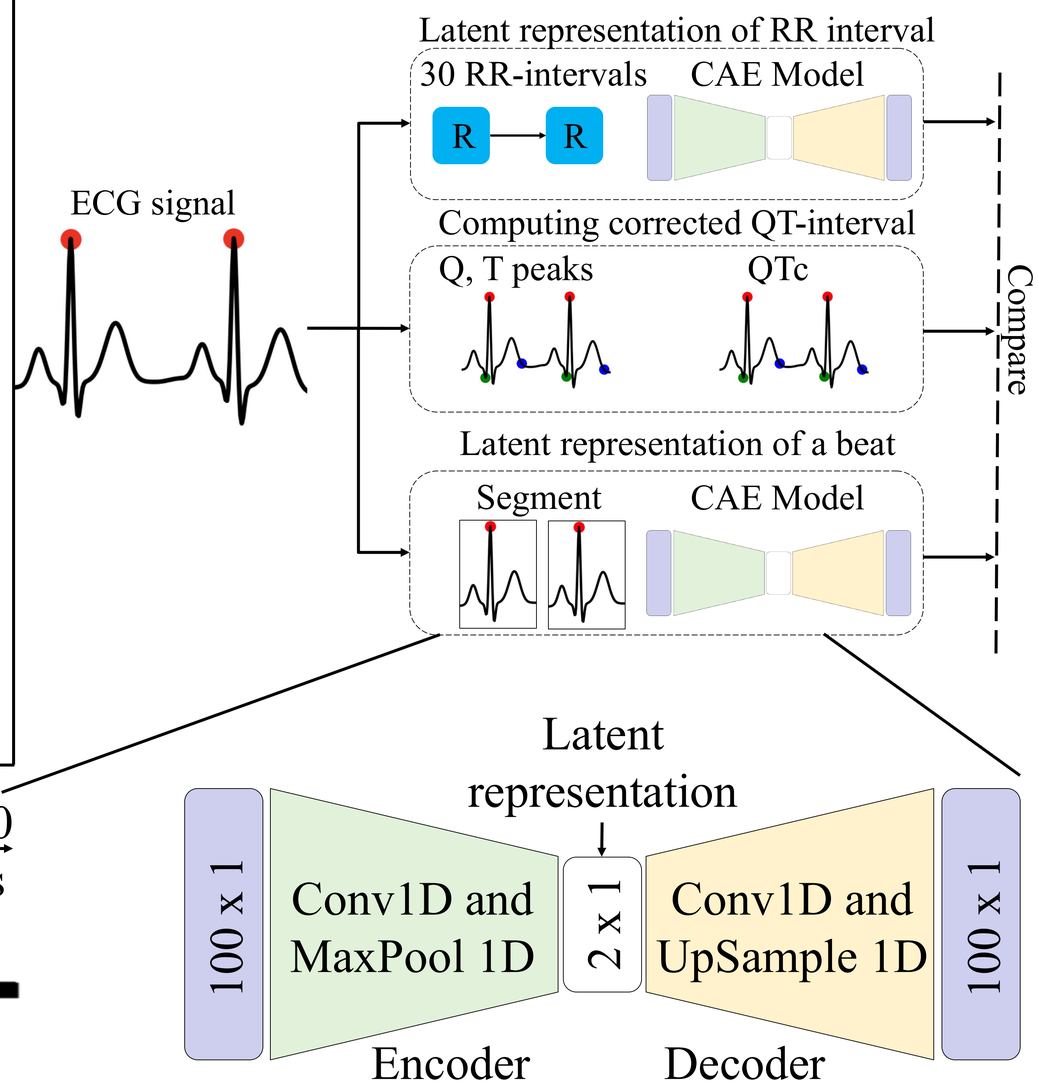

Results

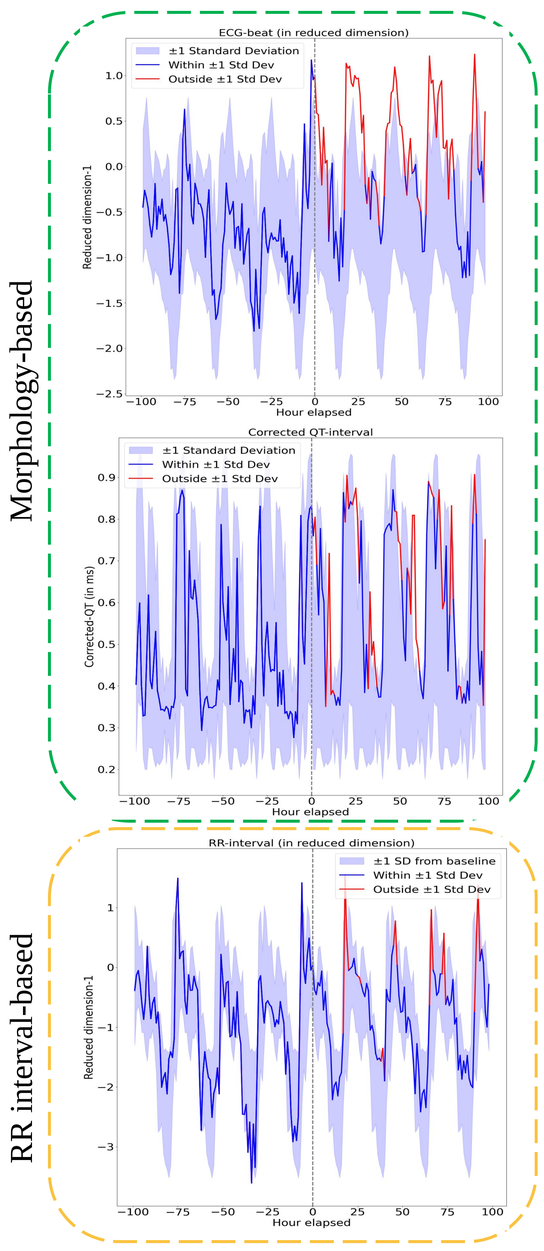

Inflammatory changes pre- vs post-vaccination through: (a) CAE based latent representation of beat, (b) Corrected QT-interval and (b) RR-interval

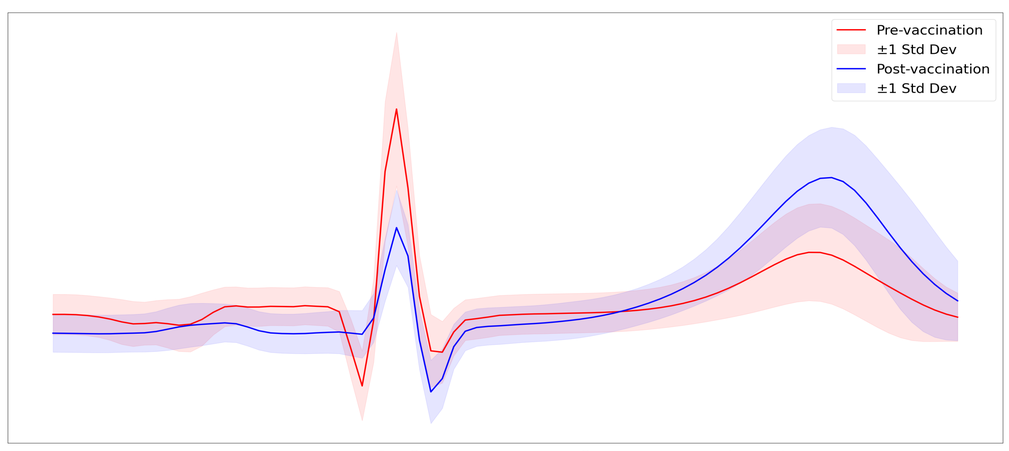

Vaccine morphology pre- and post-vaccination

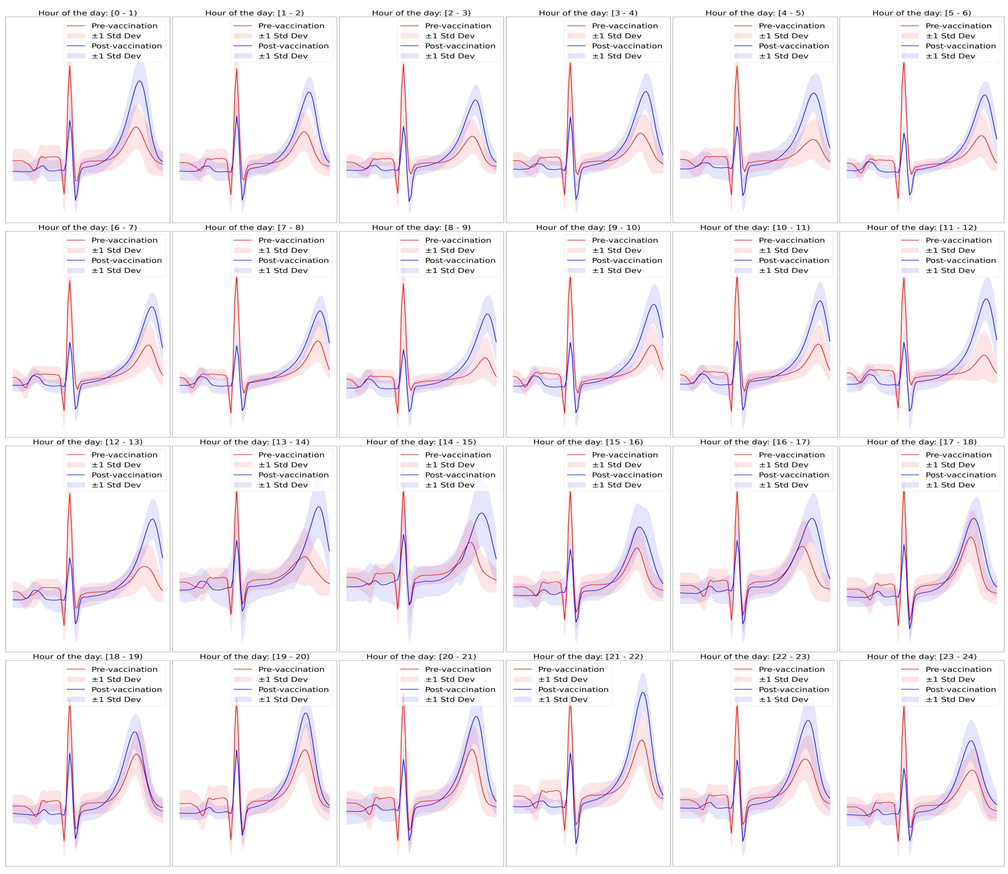

Hourly breakdown of morphological change comparison between pre-vaccination and post-vaccination ECG

References

1. Steinhubl, Steven R., Jadranka Sekaric, Maged Gendy, Huaijian Guo, Matthew P. Ward, Craig J. Goergen, Jennifer L. Anderson et al. "Wearable Sensor and Digital Twin Technology for the Development of a Personalized Digital Biomarker of Vaccine-Induced Inflammation." *medRxiv* (2024): 2024-01
2. Martínez, Arturo, Raúl Alcaraz, and José Joaquín Rieta. "Application of the phasor transform for automatic delineation of single-lead ECG fiducial points." *Physiological measurement* 31, no. 11 (2010): 1467.

Poster Number: #4

A Graphical User Interface to Monitor SARS-CoV-2 Vaccine Reactogenicity Through Continuous Digital Tracking of Autonomic Physiology

Lauryn Drager

Biomedical Engineering

Heart Rate Variability (HRV) refers to the natural variation in heart rate (HR) that is necessary for our body to adapt to stressors and to maintain homeostasis. HRV is measured in many ways and is used in conjunction with other physiological assessments to evaluate autonomic nervous system (ANS) function and cardiovascular health. The ANS coordinates the involuntary functions of peripheral organs primarily through reflexes. For example, HR and cardiac output are finely tuned by the coordinated regulation of the sympathetic (SNS) and parasympathetic (PNS) divisions of the ANS, acting to increase and decrease HR, respectively.

HR and HRV metrics exhibit circadian rhythmicity, with positive associations observed between HR, HRV metrics, and circadian rhythm markers, such as melatonin levels and core body temperature. The precise circadian rhythm may be unique to the individual. We have developed a tool that precisely and continuously tracks the unique, diurnal physiologic rhythms of anyone ‚Äì the digital Continuous Autonomic Physiologist (dCAP). dCAP maps singular HRV, combinatorial, or other physiological metrics across a 24-hour clock system, enabling visualization and simultaneous quantitative analysis of autonomic physiology with respect to an individual‚Äôs local time, daily activities (e.g., receiving a vaccine at 11 AM ET), and other data like geolocation.

Vaccines trigger an immune response within the body, and the SNS and PNS also play important roles in mediating the degree of reactogenicity (or inflammatory immune response) to the vaccine. It is therefore logical to predict that the degree of vaccine reactogenicity will positively correlate with changes in HR, HRV, and other aspects of physiology, like breathing rate and temperature. By continuously measuring the relationship between ANS activity, HRV, and other activity under autonomic regulation using dCAP, we developed a personalized framework that measures vaccine reactogenicity from characteristic changes in ANS physiological activity.

A graphical user interface was developed to illustrate dCAP and two additional modes of autonomic physiology analysis - a 3D Cartesian representation of frequency domain metrics of HRV, the 3D HRV Cartography System, and a more traditional time series representation of HRV and other parameters. Our methods provide a powerful new and personalized approach to measure and identify normal and pathological changes in health via analysis of ANS physiology over multiple time scales in and out of the clinic.

A GRAPHICAL USER INTERFACE TO MONITOR SARS-COV-2 VACCINE REACTOGENICITY THROUGH CONTINUOUS DIGITAL TRACKING OF AUTONOMIC PHYSIOLOGY

Lauryn Drager[1], Sarwat Amin[1], Damen Wilson[1], Jennifer L. Anderson[1], Jadranka Sekaric[3], Stephan Wegerich[3], Craig J. Goergen[1], Steven R. Steinhubl[1,3], Matthew P. Ward[1,2]

Background

- Vaccines induce inflammatory reactions [1], and inflammation can be mediated by parasympathetic (PNS) and sympathetic (SNS) nervous systems.
- Heart Rate Variability (HRV) is a metric for assessing the autonomic nervous system function and certain metrics can measure PNS and SNS activity [2,3].
- Heart rate and HRV demonstrate circadian variability, inflammatory response from vaccine can be influenced by inherent circadian rhythms [1].

Methods

1. The electrocardiogram, tri-axial accelerometry, and skin temperature data from healthy adults receiving the second dose of SARS-CoV-2 vaccines (Moderna and Pfizer) were captured by Vitalpatch® RTM. A set of 22 HRV metrics (from N = 35 participants) was collected, including hourly means of very low, low, and high frequency power bands, Poincare metrics, skin temperature, and heart rate.
2. MATLAB App Designer was used to create the functional Graphical User Interface (GUI) to visualize HRV metrics in temporal, 3D Cartesian, and polar cartographies.

Future Work and Applications

Future Works:

- Incorporate sunrise and sunset data into polar plots for more insights into circadian rhythms.
- Cluster data based on vaccine response in 3D Cartesian plots to assess trajectories between groups.
- Divide 3D Cartesian plots into personalized zones corresponding to physiological states.

Applications:

- Development of personalized tool to enhance medical outcomes by detecting deviations in baseline HRV data.
- Enhanced visualization of external influences on circadian rhythms.
- Identification of stress through detection of stress-induced biophysical responses.
- Tool to track recovery from sickness behavior induced by inflammation.

References

[1] Ince, L. M. et al. Influence of circadian clocks on adaptive immunity and vaccination responses. *Nat Commun* 14:476, 2023

[2] Crnko, S., B. C. Du Pré, J. P. G. Sluijter, and L. W. Van Laake. Circadian rhythms and the molecular clock in cardiovascular biology and disease. *Nat Rev Cardiol* 16:437–447, 2019

[3] Eo, Y. J., J. Park, S. Kim, K. N. Lee, S. M. Lee, D. H. Kim, C. Kim, and Y. R. Do. Estimation of melatonin level and core body temperature: heart rate and heart rate variability as circadian rhythm markers. *Biological Rhythm Research* 53:1735–1752, 2022

Suggestions

Acknowledgements

Purdue Cardiovascular Imaging Research Lab and PhysIQ Inc.

Results I: dCAP – Digital Continuous Autonomic Physiologist

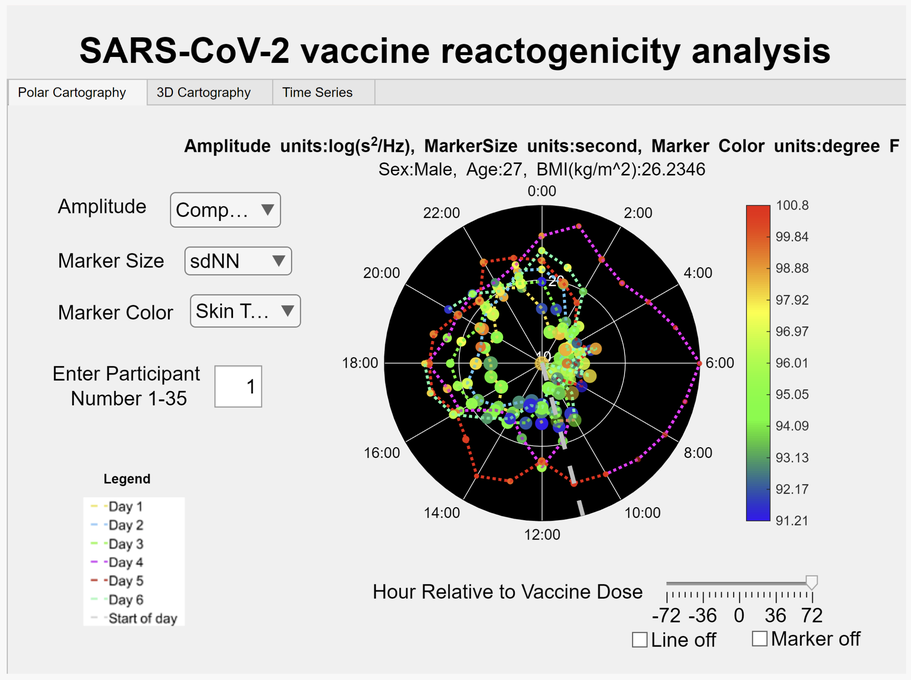

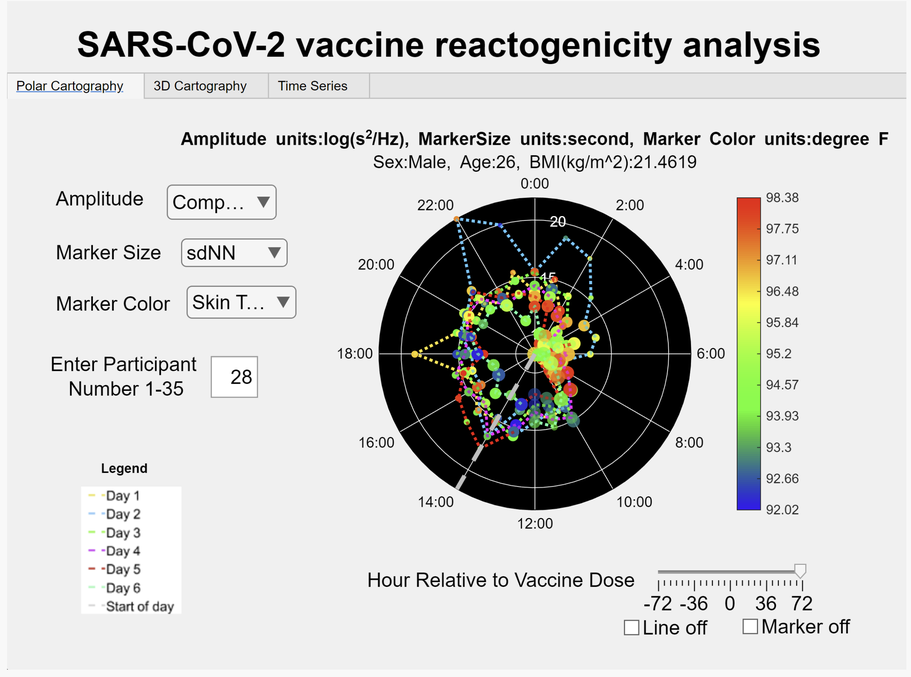

Figure 1. HRV metrics explored through dCAP. Participant 1 (left) and Participant 28 (right) both show increased skin temperature and composite LF.HF power after receiving vaccine.

Results II: Three-Dimensional HRV Cartography

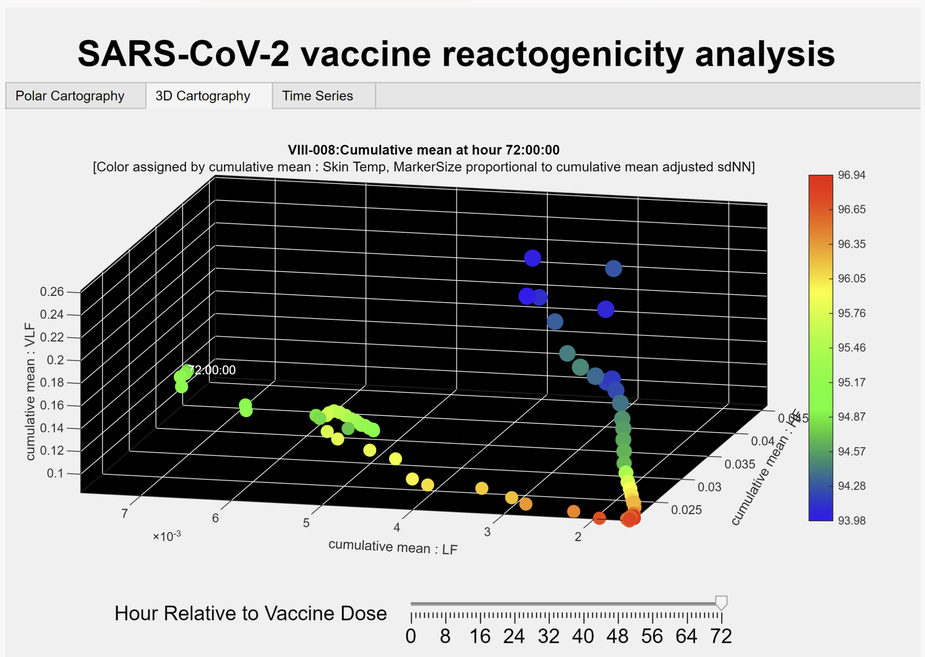

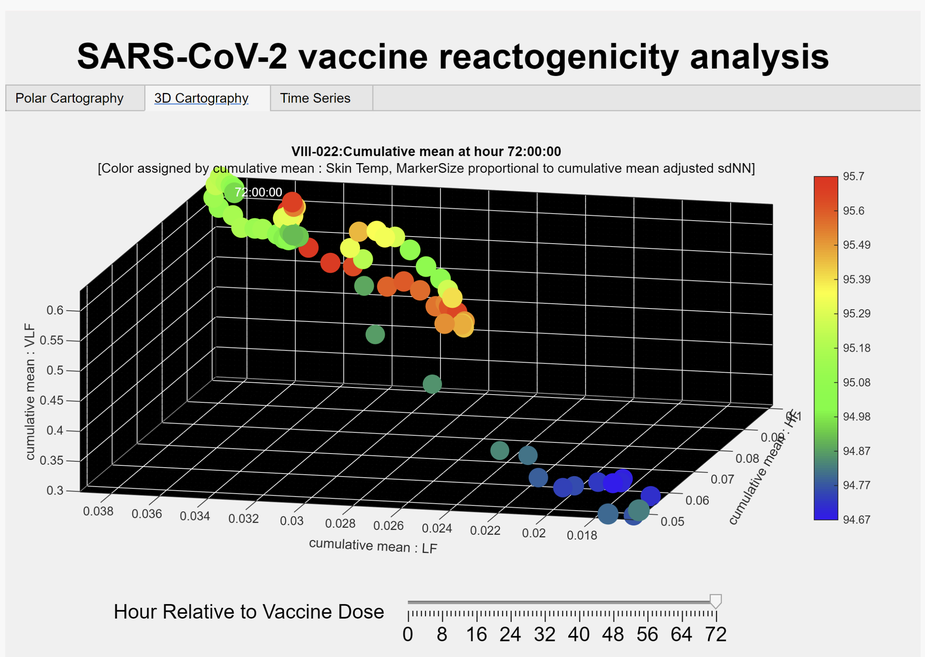

Figure 2. VLF, LF, and HF power explored using 3D HRV cartography function. Participant 1 (left) and Participant 28 (right) both show negative trajectories after receiving vaccine.

Results III: Time series representation of HRV metrics

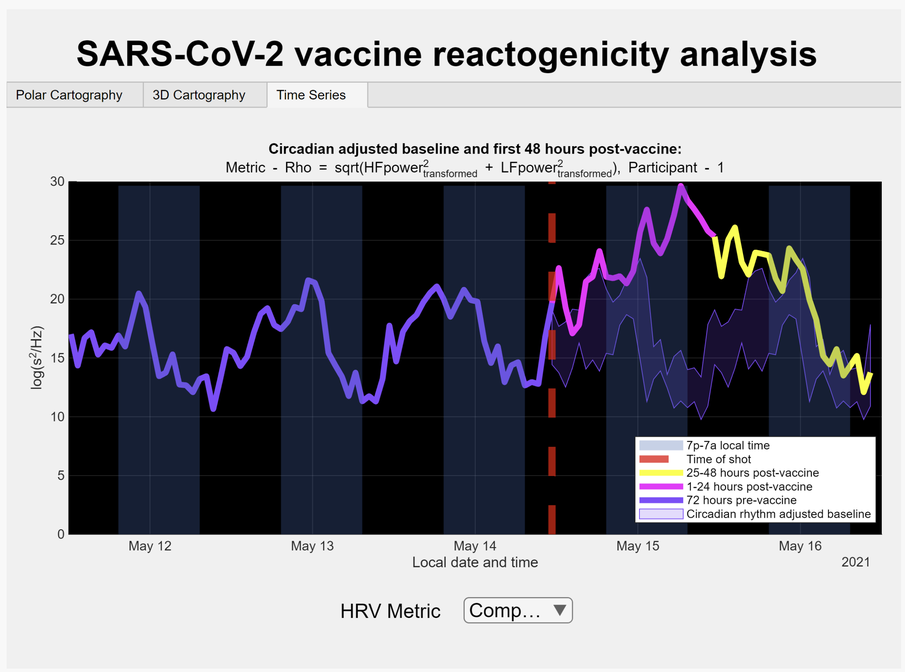

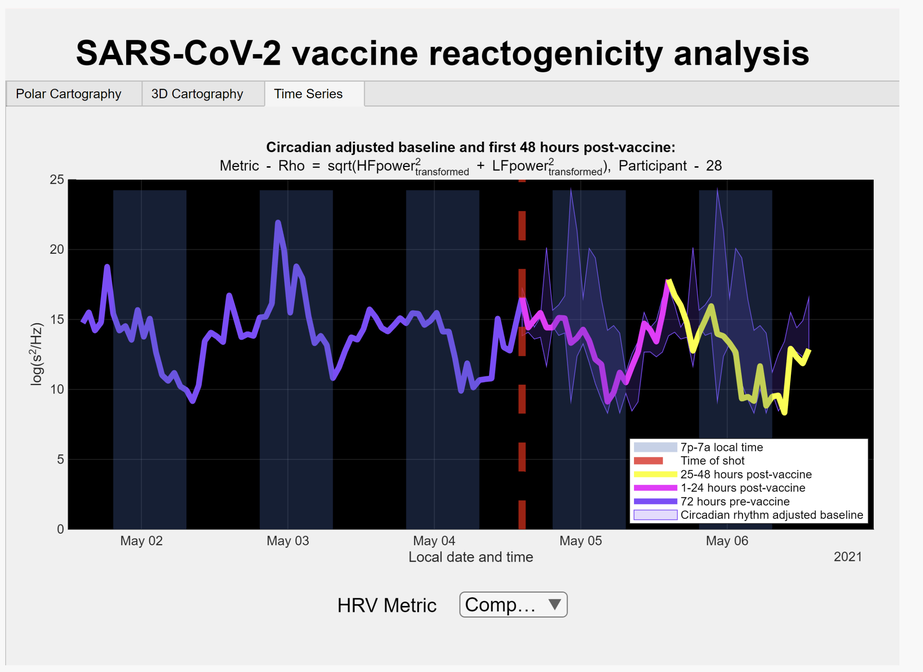

Figure 3. HRV metric explored using time series graph, showing circadian-adjusted baseline. Participant 1 (left) and Participant 28 (right) both show deviations in composite LF/HF power from respective baselines after receiving vaccine.

[1]Dept. of Biomedical Engineering, Purdue University (West Lafayette, IN)
[2]Indiana University School of Medicine (Indianapolis, IN)
[3]PhysIQ Inc. (Chicago, IL)

Contact:
Lauryn Drager - ldrager@purdue.edu
Matthew Ward, PhD - mpward@purdue.edu

PURDUE BIOCOM LAB

Poster Number: #5

Intradermal vaccination with a phytoglycogen nanoparticle and STING agonist induces cytotoxic T lymphocyte-mediated antitumor immunity

Juan Hernandez-Franco

Comparative Pathobiology

A key element in cancer vaccine development is the incorporation of potent adjuvants. This study investigated the potential of combining a cationic, plant-derived nanoparticle adjuvant (Nano-11) with the clinically validated STING agonist ADU-S100 (MIW815) to stimulate anticancer immunity through intradermal vaccination. The combination, termed NanoST, demonstrated synergistic activation of antigen-presenting cells, enhancing protein antigen cross-presentation both in vitro and in vivo. In a murine model, intradermal vaccination using ovalbumin (OVA) as a tumor antigen combined with either Nano-11 or NanoST effectively prevented the development of B16-OVA melanoma tumors. Notably, this antitumor immunity was dependent on CD8+ T cells but remained unaffected by CD4+ T cell depletion. Therapeutic vaccination with NanoST significantly improved mouse survival by suppressing B16-OVA tumor growth, an effect that was further amplified when combined with PD-1 checkpoint blockade. These findings strongly support the development of NanoST as an adjuvant for intradermal vaccination, offering a promising strategy for next-generation preventive and therapeutic cancer vaccines through targeted STING activation.

Intradermal vaccination with a phytoglycogen nanoparticle and STING agonist induces cytotoxic T lymphocyte-mediated antitumor immunity

Juan F Hernandez-Franco[1], Bennett D Elzey[2] and Harm HogenEsch[1, 2]

[1]Department of Comparative Pathobiology, Purdue University; [2]Purdue Institute for Immunology, Inflammation and Infectious Diseases (PI4D), West Lafayette, IN 47907

Introduction

The role of CD8⁺ cytotoxic T lymphocytes (CTLs) in protecting against certain infectious diseases and malignancies is critical, making them a key target for developing innovative vaccines and cancer immunotherapies. Activation of CD8⁺ T cells requires MHC I molecules to present antigenic peptides, as well as costimulatory signals provided by dendritic cells (DCs) through CD80 and CD86. However, conventional vaccines often fail to induce CD8⁺ T cell responses due to a lack of access to the MHC I pathway, a process known as antigen cross-presentation. Due to the current inefficacy of approved vaccine adjuvants in promoting cross-presentation, there is an urgent need to develop adjuvants that can initiate cross-presentation effectively.

Objective

The activation of dendritic cells (DCs) by vaccine adjuvants is critical for developing vaccination strategies and vaccine-mediated cancer immunotherapies. This study aimed to investigate the cross-presentation abilities of the combination adjuvant NanoS100, consisting of cationic plant-derived adjuvant nanoparticles (Nano-11)[1] and the synthetic STING agonist ADU-S100.

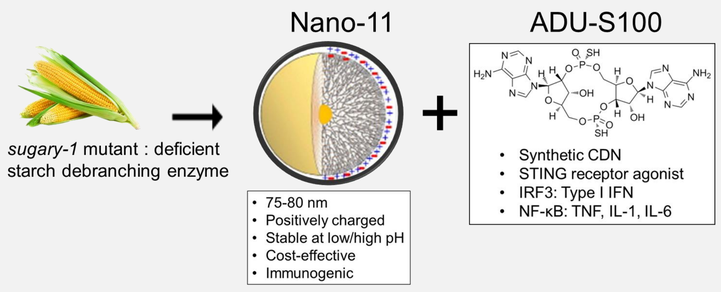

Methods

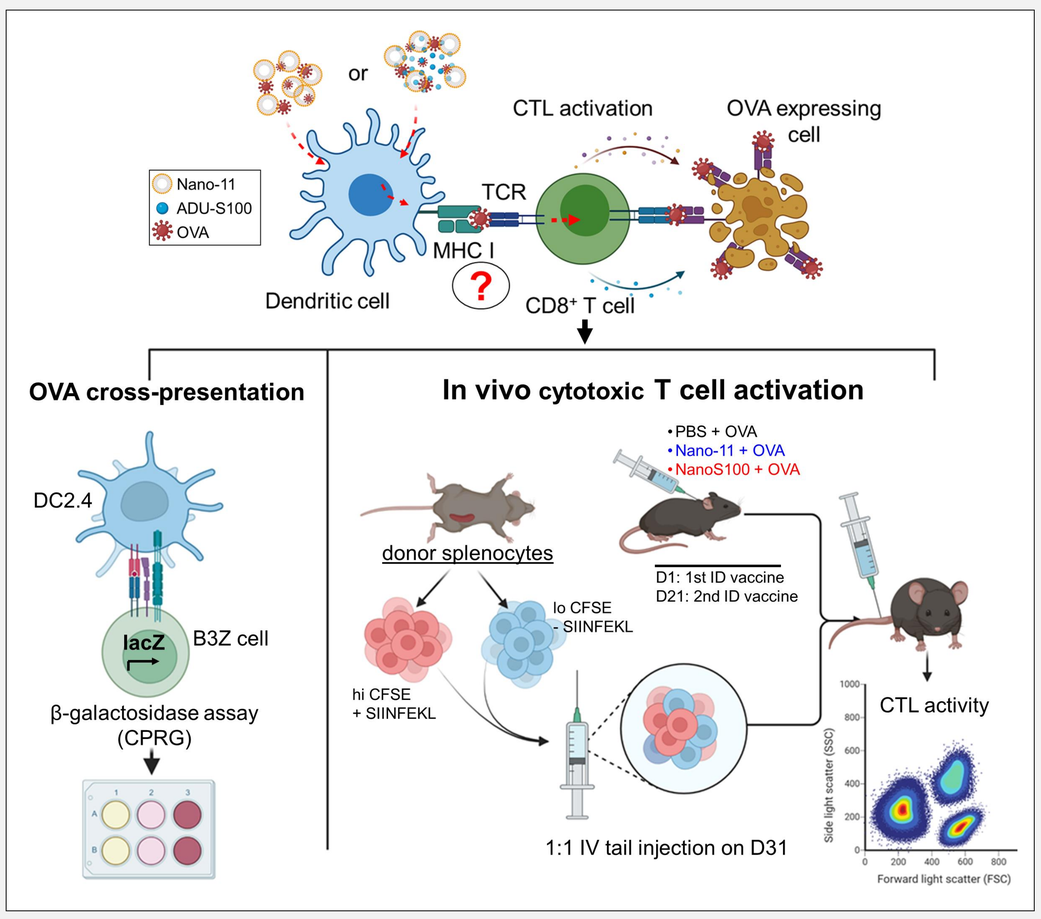

Human THP-1 cells were used to measure the expression of CD80 and CD86. Immortalized C57BL/6 DCs (DC2.4) stimulated with Nano11 ± ADU-S100 + ovalbumin (OVA) were co-cultured with a T cell hybridoma (B3Z CD8⁺ T cells) that recognize OVA (257-264) (SIINFEKL). Cross-presentation was quantified using CPRG colorimetry to measure β-galactosidase in activated B3Z co-cultures. Flow cytometry assessment of lysed donor splenocytes expressing SIINFEKL that were IV injected into mice vaccinated with NanoS100+OVA through the intradermal route revealed the SIINFEKL-specific CTL activity. Prophylactic cancer immunotherapy using NanoS100 vaccination was investigated in vivo using subcutaneous inoculation of B16 melanoma tumor cells expressing OVA in mice 10 days after an intradermal booster with NanoS100+OVA or in naive mice followed by a therapeutic vaccination with NanoS100+OVA against B16-OVA lymphoma tumor model. The percentage of tumor-free mice and mean tumor size were used to assess vaccine-mediated antitumor immunogenicity.

Results

I. Costimulatory molecules and OVA cross-presentation are induced by NanoS100

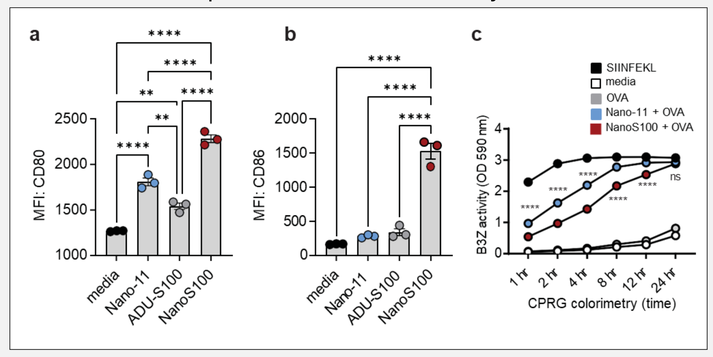

Figure 1. Nano-11 ± ADU-S100 activate DCs and induce cross-presentation of OVA in vitro. **(a)** Nano-11 and NanoS100 stimulated the expression of CD80. **(b)** Only NanoS100 promotes the expression of CD86 in DCs. **(c)** β-galactosidase in B3Z co-cultures at different times was quantified by CPRG colorimetry. *p <0.05, **p <0.01, ***p <0.001, ****p <0.0001 by one-way ANOVA with Tukey's multiple comparison test.

II. In vivo OVA-specific cytotoxic T lymphocyte assay

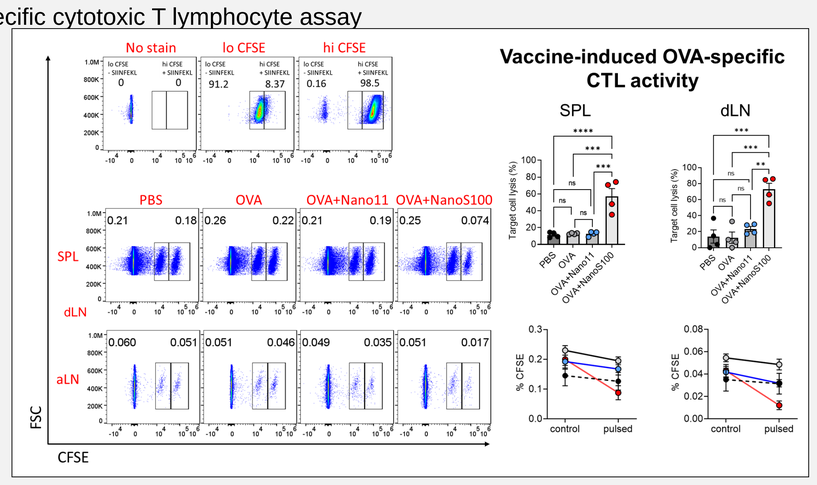

Figure 2. In vivo, NanoS100 promotes OVA cross-presentation and activation of cytotoxic T cells. Splenocytes were labeled with a low dosage of CFSE ($CFSE^{lo}$) or pulsed with SIINFEKL and labeled with $CFSE^{hi}$. A 1:1 ratio of $CFSE^{lo}$ and $CFSE^{hi}$ splenocytes was IV injected into mice immunized with Nano-11 ± ADU-S100 + OVA through the intradermal route. **p <0.01, ***p <0.001, ****p <0.0001 by one-way ANOVA with Tukey's multiple comparison test.

III. Vaccination with NanoS100 suppresses OVA-expressing B16 tumor cells

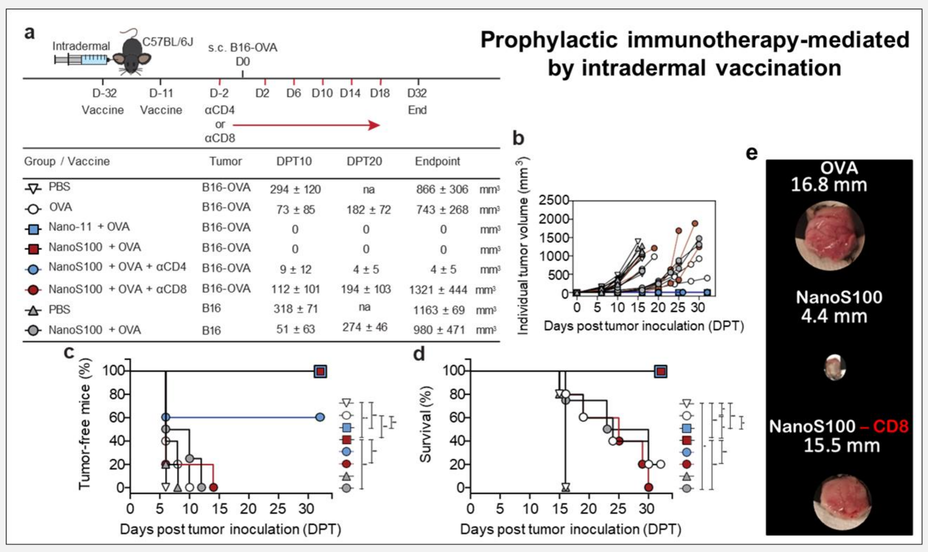

Figure 3. Tumor progression is inhibited by intradermal vaccination with Nano-11 ± ADU-S100 + OVA. **(a)** Vaccine and T cell depletion schedule, treatments, and tumor volume mean ± SEM ($n \geq 5$) at different days post tumor (DPT) inoculation with B16 or B16-OVA by subcutaneous (s.c.) injection. **(b)** Individual tumor growth curves (mm^3) in C57BL/6J mice. **(c)** Percent of mice free of tumors. **(d)** Survival rate of mice. **(e)** Tumor size comparison measured by the length of a representative sample. The log-rank (Mantel-Cox) curve comparison test was applied to determine the percentage of tumor-free mice and survival. *p < 0.05, **p < 0.01, ***p < 0.001, ****p < 0.0001.

IV. Therapeutic vaccination with NanoS100 suppresses OVA-expressing B16 cells

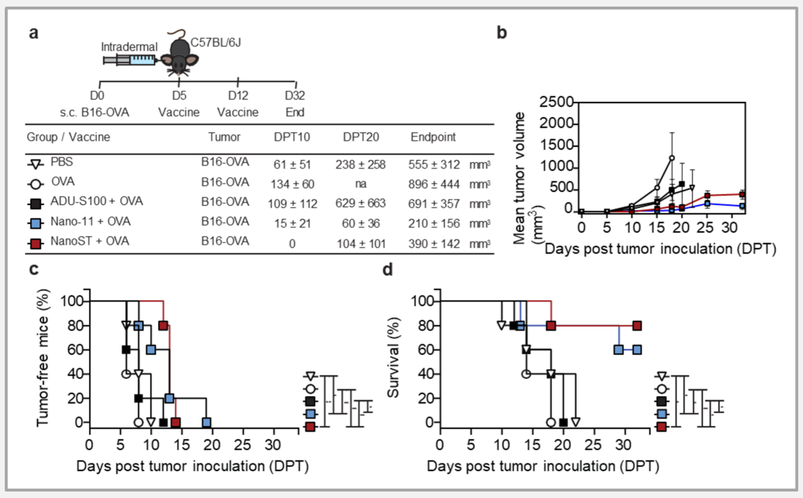

Figure 4. Nano-11 ± ADU-S100 + OVA preventative vaccination inhibits the growth of OVA-expressing B16 tumor cells in C57BL/6J mice. **(a)** Schedule of vaccinations, therapies, and tumor volume mean ± SEM ($n \geq 5$) at different days post tumor (DPT) inoculation with B16-OVA. **(b)** Individual tumor growth curves (mm^3) in mice. **(c)** Percent of mice free of tumors. **(d)** Survival rate of mice. The log-rank (Mantel-Cox) test was used to evaluate the proportion of tumor-free mice and the survival rate. *p < 0.05, **p < 0.01.

V. NanoS100 induces antigen-specific germinal center and cell-mediated responses

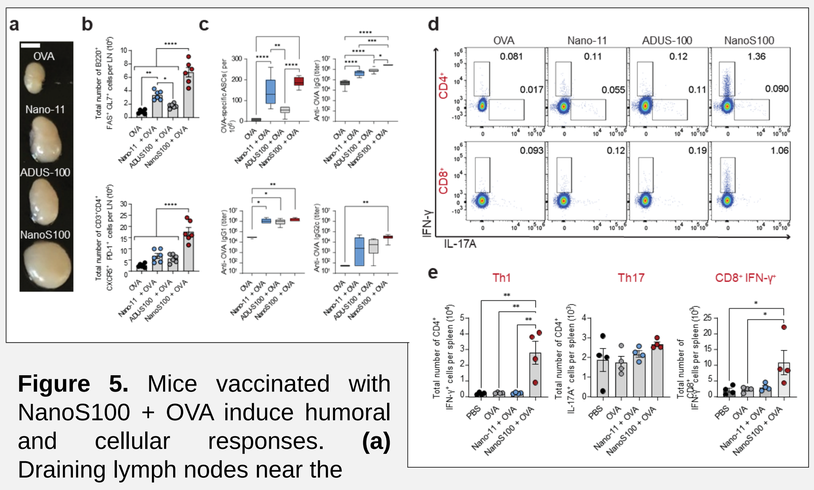

Figure 5. Mice vaccinated with NanoS100 + OVA induce humoral and cellular responses. **(a)** Draining lymph nodes near the injection site; scale bar, 2 mm. **(b)** Germinal center B cells and follicular helper T cells. **(c)** Antigen-specific plasma cells and serum IgG, IgG1, and IgG2c. **(d)** Flow cytometry plots showing OVA-specific CD4⁺ and CD8⁺ IFNγ⁺ cells from the spleens of mice immunized with Nano-11 ± ADU-S100 + OVA. **(e)** Absolute number of OVA-specific Th1, Th17 and CD8⁺ IFNγ⁺ cells. *p <0.05, **p <0.01, ***p <0.001, ****p <0.0001 by one-way ANOVA with Tukey's multiple comparison test.

Conclusions

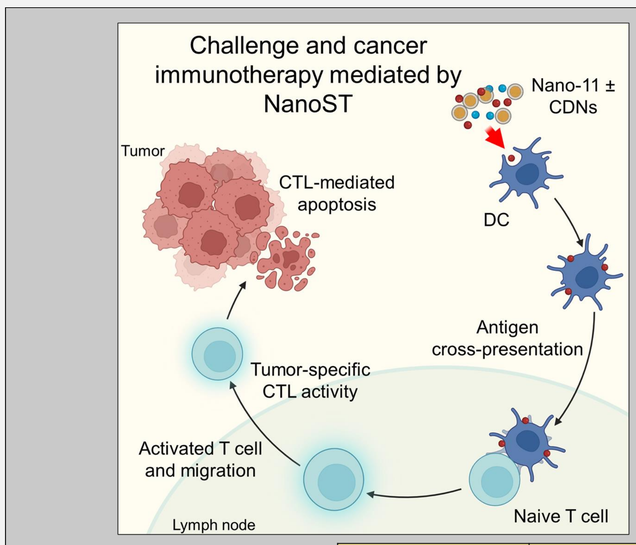

	Nano-11	NanoST
DC activation	++	+++
In vivo cross-presentation	+	+++
Immunotherapy	+++	+++

References

1. Hernandez-Franco, J.F., Jan, I.M., Elzey, B.D. et al. Intradermal vaccination with a phytoglycogen nanoparticle and STING agonist induces cytotoxic T lymphocyte-mediated antitumor immunity. *npj Vaccines* 9, 149 (2024).

Poster Number: #6

Long-Chain Polyunsaturated Fatty Acids Protect Against Muscle Atrophy Induced by Colorectal Cancer through a LOX/COX-Dependent Pathway

Xinyue Lu

Department of Nutrition Science

Colorectal cancer (CRC) is the third most prevalent and the second deadliest cancer worldwide. Over 50% of CRC patients suffer from cachexia, which is characterized by skeletal muscle wasting and loss of body weight. CRC cachexia significantly reduces chemotherapy efficiency and patient survival rates. Pharmaceutical treatments for cancer cachexia are currently limited. It is urgent to develop novel therapies to prevent and treat cachexia. Omega-3 polyunsaturated fatty acids (n-3 PUFAs) may reduce systematic inflammation and stabilize body weight in cancer patients. However, the biological mechanisms by which PUFAs may influence cachexia remain poorly understood. Prior studies have tested fish oils containing a complex mixture of eicosapentaenoic acid (EPA), docosapentaenoic acid (DPA), and docosahexaenoic acid (DHA), and human clinical trials of fish oil supplementation have generated conflicting results. We aim to investigate the roles of individual pure n-3 PUFAs EPA, DPA, and DHA, as well as the n-6 PUFAs arachidonic acid (ARA) in CRC cachexia and elucidate the biological mechanisms by which PUFAs modulate CRC cachexia. We hypothesize that PUFAs protect against CRC cachexia via conversion to anti-inflammatory lipid metabolites known as specialized pro-resolving mediators(SPMs). Using in vitro models, we found that the administration of n-3 (EPA, DHA) and n-6 (ARA) PUFAs or their downstream SPM metabolites protects against muscle cell atrophy caused by CRC cachexia. Results further show that the protective effect of LC-PUFAs against CRC cachexia depends on the lipoxygenase (LOX) and cyclooxygenase (COX) pathways. Dietary PUFAs show promise in alleviating cachexia through enzymatic metabolism to form anti-inflammatory lipid mediators (e.g., SPMs).

Long-Chain Polyunsaturated Fatty Acids Protect Against Muscle Atrophy Induced by Colorectal Cancer through a LOX/COX-Dependent Pathway

Xinyue Lu,[1,2], James F. Markworth, Ph.D.[1,2,3,4]

[1] Interdepartmental Nutrition Program (INP), Purdue University; [2]Center for Aging and the Life Course (CALC), Purdue University;
[3]Department of Animal Sciences, Purdue University; [4]Indiana Center for Musculoskeletal Health (ICMH)

ABSTRACT

Colorectal cancer (CRC) is the third most prevalent and the second deadliest cancer worldwide. Over 50% of CRC patients suffer from cachexia, which is characterized by skeletal muscle wasting and loss of body weight. CRC cachexia significantly reduces chemotherapy efficiency and patient survival rates. Pharmaceutical treatments for cancer cachexia are currently limited. It is urgent to develop novel therapies to prevent and treat cachexia. Omega-3 polyunsaturated fatty acids (n-3 PUFAs) may reduce systematic inflammation and stabilize body weight in cancer patients. However, the biological mechanisms by which PUFAs may influence cachexia remain poorly understood. Prior studies have tested fish oils containing a complex mixture of eicosapentaenoic acid (EPA), docosapentaenoic acid (DPA), and docosahexaenoic acid (DHA) and human clinical trials of fish oil supplementation have generated conflicting results. We aim to investigate the roles of individual pure n-3 PUFAs EPA, DPA, and DHA, as well as the n-6 PUFAs arachidonic acid (ARA) in CRC cachexia and elucidate the biological mechanisms by which PUFAs modulate CRC cachexia. We hypothesize that PUFAs protect against CRC cachexia via conversion to anti-inflammatory lipid metabolites known as specialized pro-resolving mediators (SPMs). Using in vitro models, we found that the administration of n-3 (EPA, DHA) and n-6 (ARA) PUFAs or their downstream SPM metabolites protects against muscle cell atrophy caused by CRC cachexia. Results further show that the protective effect of LC-PUFAs against CRC cachexia depends on the lipoxygenase (LOX) and cyclooxygenase (COX) pathways. Dietary PUFAs shows promise in alleviating cachexia through enzymatic metabolism for form anti-inflammatory lipid mediators (e.g., SPMs).

INTRODUCTION

- **Colorectal cancer (CRC):** The third most prevalent and the second deadliest cancer
  - 50% of the patients with advanced CRC are impacted by cancer cachexia
- **Cancer cachexia causes muscle wasting and reduces survival rate**
  - Tumor-derived cytokines promote the progression of cancer cachexia
  - No effective treatments developed
- **Omega-3 (n-3) polyunsaturated fatty acids (PUFA) improve cancer cachexia**
  - N-3 PUFAs and their downstream metabolites known as specialized pro-resolving lipid mediators (SPMs) reduce inflammation

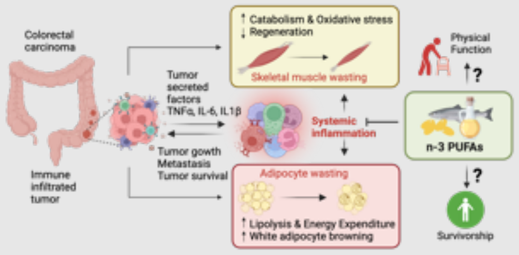

Figure 1. Tumor-secreted factors leads to systemic inflammation, causing muscle atrophy and adipocyte wasting. Fish oil rich in EPA and DHA may improve CRC muscle cachexia by resolving inflammation.

AIM & HYPOTHESIS

- In this study, we aim to investigate the role of individual PUFAs in CRC cachexia and the molecular mechanism where PUFAs affect CRC-induced muscle wasting.
- We hypothesize that individual PUFAs improve CRC-induced muscle wasting *in vitro*. It is also hypothesized that the action of PUFAs depends on the production of SPMs via COX/LOX pathway.

REFERNCES

1. Hossain, M. S., Karuniawati, H., Jairoun, A. A., Urbi, Z., Ooi, J., John, A., Lim, Y. C., Kibria, K. M. K., Mohiuddin, A. K. M., Ming, L. C., Goh, K. W., and Hadi, M. A. (2022) Colorectal Cancer: A Review of Carcinogenesis, Global Epidemiology, Current Challenges, Risk Factors, Preventive and Treatment Strategies. *Cancers (Basel)* **14**
2. Anker, M. S., Holcomb, R., Muscaritoli, M., von Haehling, S., Haverkamp, W., Jatoi, A., Morley, J. E., Strasser, F., Landmesser, U., Coats, A. J. S., and Anker, S. D. (2019) Orphan disease status of cancer cachexia in the USA and in the European Union: a systematic review. *J Cachexia Sarcopenia Muscle* **10**, 22-34
3. Kasprzak, A. (2021) The Role of Tumor Microenvironment Cells in Colorectal Cancer (CRC) Cachexia. *Int J Mol Sci* **22**
Webster, J. M., Kempen, L., Hardy, R. S., and Langen, R. C. J. (2020) Inflammation and Skeletal Muscle Wasting During Cachexia. *Front Physiol* **11**, 597675
4. Clamon, G., Byrne, M. M., and Talbert, E. E. (2022) Inflammation as a Therapeutic Target in Cancer Cachexia. *Cancers (Basel)* **14**
5. Buckley, C. D., Gilroy, D. W., and Serhan, C. N. (2014) Proresolving lipid mediators and mechanisms in the resolution of acute inflammation. *Immunity* **40**, 315-327
6. Murff HJ, Shrubsole MJ, Cai Q, Su T, Dooley JH, Cai SS, Zheng W, Dai Q: N-3 Long Chain Fatty Acids Supplementation, Fatty Acids Desaturase Activity, and Colorectal Cancer Risk: A Randomized Controlled Trial. *Nutr Cancer* 2022, **74**(4):1388-1398.
7. Tojjari A, Choucair K, Sadeghipour A, Saeed A, Saeed A: Anti-inflammatory and Immune Properties of Polyunsaturated Fatty Acids (PUFAs) and Their Impact on Colorectal Cancer (CRC) Prevention and Treatment. *Cancers (Basel)* **15**(17).
8. Yeh KY et al.: Omega-3 Fatty acid-, Micronutrient-, and Probiotic-enriched Nutrition Helps Body Weight Stabilization in Head and Neck Cancer Cachexia. *Oral Surg Oral Med Oral Pathol Oral Radiol* **116**:41-48.
9. Van Blarigan EL et al.: Marine omega-3 Polyunsaturated Fatty Acid and Fish Intake after Colon Cancer Diagnosis and Survival: CALGB 89803 (Alliance). *Cancer Epidemiol Biomarkers Prev*, **27**:438-445.

METHODS

Model 1: Muscle wasting induced by cancer conditioned media

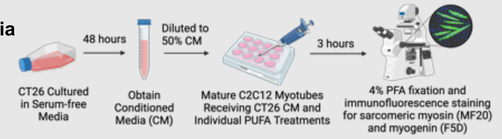

Figure 2. In-vitro design for cancer conditioned media model. C2C12 muscle cells were differentiated for 72 hours and exposed to CT26 conditioned media containing tumor-secreted factors. At the same time, C2C12 myotubes receive individual PUFA treatments including arachidonic acids (ARA), eicosapentaenoic acid (EPA), docosahexaenoic acid (DHA), and docosapentaenoic acid (DPA) (25 μM).

Model 2: Muscle wasting induced by a muscle-cancer cell co-culture model

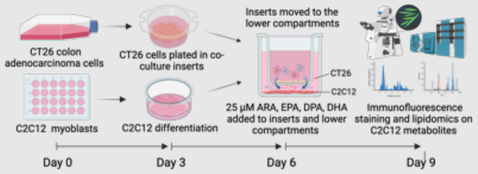

Figure 3. Experimental design for *in vitro* co-culture model. The co-culture design allows for the crosstalk between muscle cells and cancer cells through a semi-permeable membrane. C2C12 cells were induced to differentiate for 72 hours and then co-cultured with CT26 cancer cells to induce cachexic muscle wasting. Murine C2C12 muscle cells are exposed to secretomes continuously produced by murine CT26 colorectal carcinoma cells. Both cell lines received individual PUFA treatments (25 μM) for 72 hours. Myotubes were visualized by immunofluorescent staining for myosin (MyHC, stained by MF20) and the differentiation marker myogenin (MyoG, stained by F5D). Cell nuclei were counterstained with DAPI. Conditioned media was collected from the lower compartments and lipid profile was analyzed by targeted LC-MS/MS to detect the change in lipid metabolites composition.

RESULTS

N-3/n-6 PUFAs Improve Muscle Wasting In CT26 Co-culture Model

In the co-culture model, the cross-talk between CT26 cancer cells and C2C12 muscle cells led to significant muscle wasting. All the individual PUFAs improved cachexic muscle wasting by increasing myotube diameter (Figure 4). However, PUFAs did not fully rescue the muscle wasting, partly due to the potent effect of continuous secretion interaction between muscle and cancer cells in the co-culture model.

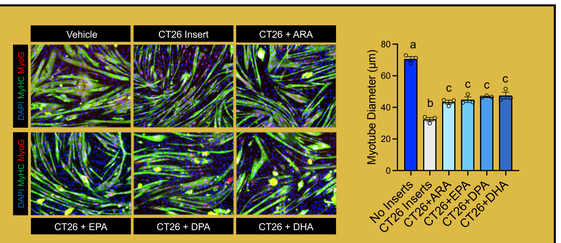

Figure 4. N-3 and n-6 LC-PUFAs improve muscle wasting when muscle cells are indirectly co-cultured with caner cells. Continuous interaction with CT26 cells reduced myotube diameter by 50%. Individual LC-PUFAs were found to increase the myotube diameter at least by 20%. Groups with different letters indicate a significant difference with p<0.05.

The Benefit of PUFAs on CRC-induced Muscle Wasting Depends on the Activation of LOX/COX Pathway

While CT26 cancer conditioned media significantly reduced C2C12 myotube diameter, all the individual PUFAs (ARA, EPA, DHA, and DPA) protected against muscle atrophy induced by CT26 conditioned media containing tumor-secreted soluble factors (Figure 5A).

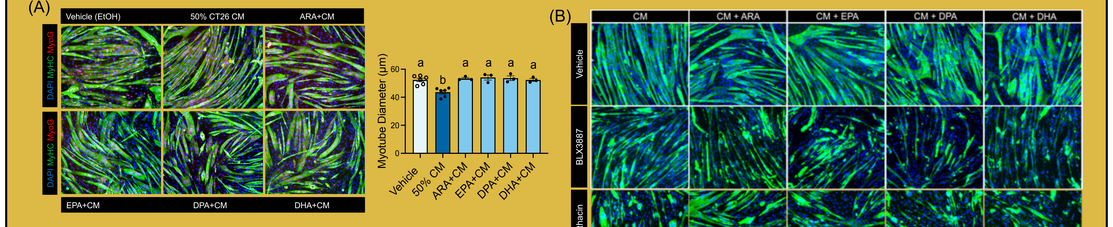

Lipoxygenase (LOX) and cyclooxygenase (COX) are the important enzymes catalyzing the endogenous metabolism of PUFAs, which makes them essential for the endogenous production of specialized pro-resolving mediators (SPMs). Since we hypothesize that PUFAs improve CRC cachexia by producing SPMs, we blocked the activity of 15-LOX and COX using BLX3887 and indomethacin, respectively. It was found that all the PUFAs (ARA, EPA, DHA, and DPA) lost their rescuing ability when 15-LOX pathway was inhibited. However, only DHA and DPA failed to improve muscle wasting when COX pathway was inhibited (Figure 5B). The results indicate that PUFAs improve CRC-induced muscle wasting through a 15-LOX dependent pathway, and the effects of ARA and EPA might be independent of COX pathway. In addition, the difference in COX dependence may suggest a possible difference in molecular mechanisms where DPA and DHA take effect in CRC cachexia.

Figure 5. Protective effects of n-3 and n-6 LC-PUFAs against muscle wasting in conditioned media model depends on the activation of 15-LOX and COX . (A) C2C12 myoblasts were induced to differentiate for 72 h and exposed to 50% CT26 adenocarcinoma cell conditioned media. All the individual LC-PUFAs including ARA, EPA, DPA, or DHA (25 μM) reversed the atrophic effect of CT26 conditioned media. Groups with different letters indicate a significant difference with p<0.05. (B) Differentiated C2C12 myoblasts were treated for 72 h with CT26 cancer conditioned media with or without the individual LC-PUFA species, the COX inhibitor indomethacin or the 15-LOX specific inhibitor BLX3887. *p<0.05 for effect of PUFA treatment. #p<0.05 for effect of LOX inhibitor.

Production of SPMs in Response to PUFA Treatments

Liquid chromatography-tandem mass spectrometry analysis on conditioned media from C2C12-CT26 co-culture model shows that individual PUFAs elevated the production of corresponding intermediate metabolites and SPMs. In response to ARA and EPA, the production of lipoxin A4 (LXA4) and resolvin E1 (RvE1) were largely increased, respectively. Resolvin D1 (RvD1), protectin D1 (PD1), and maresin 2 (MaR2) were elevated upon DHA treatment, and DPA increased the production of n-3 DPA-derived resolvin D5 (RvD5) (Figure 6).

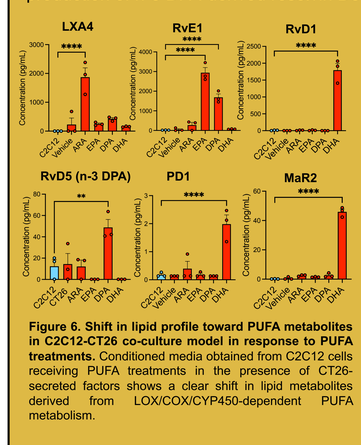

Figure 6. Shift in lipid profile toward PUFA metabolites in C2C12-CT26 co-culture model in response to PUFA treatments. Conditioned media obtained from C2C12 cells receiving PUFA treatments in the presence of CT26-secreted factors shows a clear shift in lipid metabolites derived from LOX/COX/CYP450-dependent PUFA metabolism.

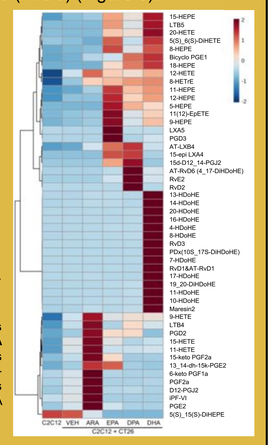

SPMs Directly Improve TNF-induced Muscle Wasting

SPMs, the downstream bioactive lipid mediators produced by the LOX/COX-dependent metabolism of PUFAs, are found to improve muscle wasting induced by tumor-secreted factor TNFα to different levels. Resolvin D1 derived from n-3 DHA shows the greatest ability to increase myotube diameter. RvE1 derived from EPA, protectin D1 (PD1), maresin 1 (MaR1), and LXA4 also show beneficial effects on myotube diameter, indicating a promising role of SPMs on alleviating muscle wasting induced by tumor-derived cytokines.

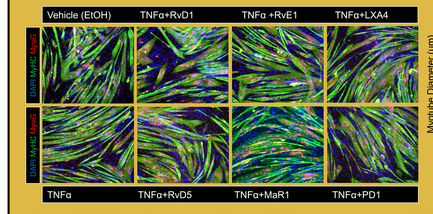

Figure 7. SPMs derived from different PUFA sources alleviate TNFα-induced muscle wasting. Confluent C2C12 myoblasts were induced to differentiate in the presence of TNFα (100ng/ml) and individual SPM treatment (100 nM) for 72 hours. Groups with different letters indicate a significant difference with p<0.05.

CONCLUSIONS

- N-6 PUFA (ARA) and n-3 PUFA (EPA, DPA, DHA) protect murine skeletal muscle cells against the atrophic effect of CT26 (colon adenocarcinoma) secreted factors.
- The protective effects of PUFAs rely on the enzymatic activity of the LOX and COX pathways.
- Endogenous metabolites of PUFAs such as the SPMs may be important in mediating the protective role of PUFA in cancer cachexia.

Poster Number: #7

Age-dependent changes in the molecular signatures of mouse brain elucidated by multi-protease proteomic and phosphoproteomic analyses

Rodrigo Mohallem Ferreira

Comparative Pathobiology

With the growing elderly population, aging and age-related diseases are at the forefront of the medical challenges faced in the 21st century. The prevalence of age-related diseases, particularly neurodegenerative illnesses, is now at an all-time high. It is estimated that one fourth of Americans over the age of 55 suffer from a mental disorder, and worldwide one person is diagnosed with dementia in every 3 seconds. Despite the increasing numbers of patients suffering from dementia, there are currently no treatments or therapeutic strategies available. In fact, the process of neurodegeneration remains poorly understood, and the mechanisms underlying the pathobiology of aging brains are complex yet not fully explored. In this study, we focus on unveiling the changes in the proteome, kinome and phosphoproteome of aging mice brains to elucidate the molecular signatures of age-related neurodegenerative processes. Using a multi-enzyme proteolysis approach, our proteomics results showed differential regulation of 446 proteins in an age-dependent fashion. Gene set analyses revealed a marked increase in proteins associated with neuroinflammation, synaptic function, and protein folding among proteins upregulated in aged mice. These pathways are known to contribute to neurodegeneration and declining synaptic function "Post-translational protein phosphorylation" also emerged as a top upregulated pathway in aged mice, prompting us to investigate age-related changes in the kinome and phosphoproteome. Multi-protease digestion revealed the identification of over 2000 additional phosphosites relative to trypsin alone, highlighting a significant advantage of this approach for comprehensively capturing phosphorylation events relevant to aging. Furthermore, we were able to map 751 phosphosites for which there was no information available in the literature, including key proteins involved in the onset of neurogenerative diseases, such as Tau S147 and S148. Tau (Mapt) was hyperphosphorylated in old mice and phosphorylation of Tau is known to derive protein aggregation and development of Alzheimer,Äôs Disease. Kinome prediction using upregulated phosphosites indicated the activation of PI3K-AKT-mTOR-p53 signaling pathway. This finding was further corroborated with hyperphosphorylation of several proteins, including key proteins in the onset of Alzheimer,Äôs and Parkinson,Äôs diseases, such as Mapt and Dpysl2. Interestingly when comparing wild-type mice and PD susceptible A53T aSyn mice, we observed 160 proteins that are only dysregulated in the aged brain of mutant mice. Together with proteins such as Alpha-1-B Glycoprotein, a plasma glycoprotein that is only upregulated in PD susceptible mice, our dataset also provides potentially important biomarkers for the onset of PD during aging.

Age-dependent changes in the molecular signatures of mouse brain elucidated by multi-protease proteomic and phosphoproteomic analyses

ARYAL LAB

Rodrigo Mohallem[1,2,*] Allison Schaser[3] & Uma K Aryal[1,2,#]

[1]Department of Comparative Pathobiology, Purdue University, USA; [2]Bindley Bioscience Center, Purdue University, USA; [3]Department of Speech, Language, and Hearing Sciences, Purdue University, West Lafayette, IN 47909, USA.

PURDUE UNIVERSITY

Introduction & Abstract

Aging is one of the main risk factors of Neurodegeneration

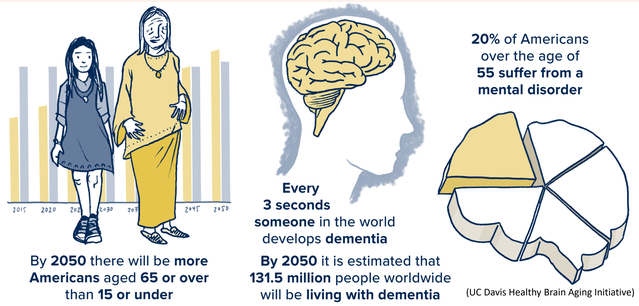

Neurodegeneration is among the main risk factors accompanying aging. It is estimated that 1/5 of all Americans above the age of 55 live with some form of dementia. Furthermore, as the word's aging population increases, so does the number of patients suffering from cognitive decline. To date, there are no treatments to mitigate, let alone cure, neurodegenerative diseases. One of the main reasons behind the lack of strategies to combat dementia is the complexity of the molecular signatures that contribute to aging-associated neurodegeneration. Therefore, it is paramount that we understand the mechanisms governing neurodegeneration in a holistic way.

Our Work

Our analysis showed differential regulation of 446 proteins in an age-dependent fashion. Gene set analyses revealed a marked increase in proteins associated with neuroinflammation, synaptic function, and protein folding among proteins upregulated in aged mice. We also found that several proteins involved in Glutamatergic Signaling, Neuroinflammation, and cytokine signaling had an increase in their phosphorylation status in old mice. These findings are corroborated with our observations suggesting a reorganization on the mouse kinome. Kinase enrichment analysis using upregulated phosphosites indicated the activation of PI3K-AKT-mTOR signaling pathway, that, taken together with the hyperphosphorylation of several proteins, including key proteins in the onset of Alzheimer's and Parkinson's diseases, such as Mapt and Dpysl2, sheds light on novel (phospho)proteins and pathways that play a role in age-dependent neurodegeneration.

Experiment Workflow

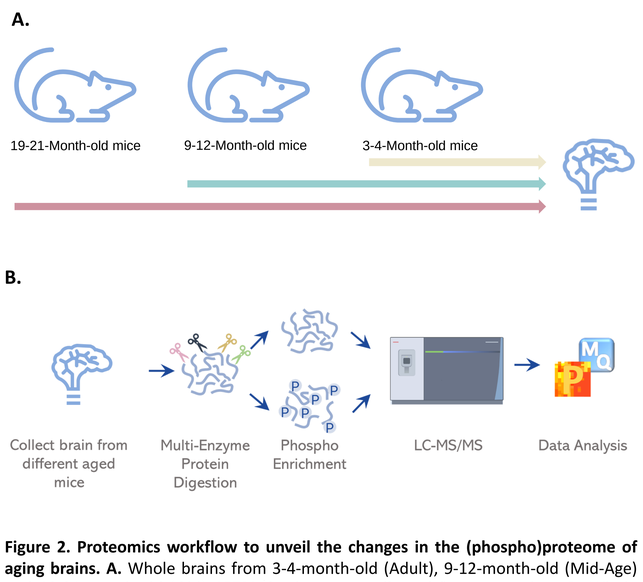

Figure 2. Proteomics workflow to unveil the changes in the (phospho)proteome of aging brains. A. Whole brains from 3-4-month-old (Adult), 9-12-month-old (Mid-Age) and 19-21-month-old (Old) C57BL/6 mice were collected for proteomics. **B.** Whole brains were homogenized, proteins were extracted, reduced, alkylated, digested with Trypsin, Chymotrypsin, AspN or GluC, and desalted using pierce C18 columns. Phosphopeptides were then enriched with PolyMac spin tips. Peptides and phosphopeptides were analyzed by LC-MS/MS in a Fusion Orbitrap Lumos. Raw data were analyzed using the MaxQuant and Perseus software.

Results

Proteome landscape of mice brain drastically changes during aging

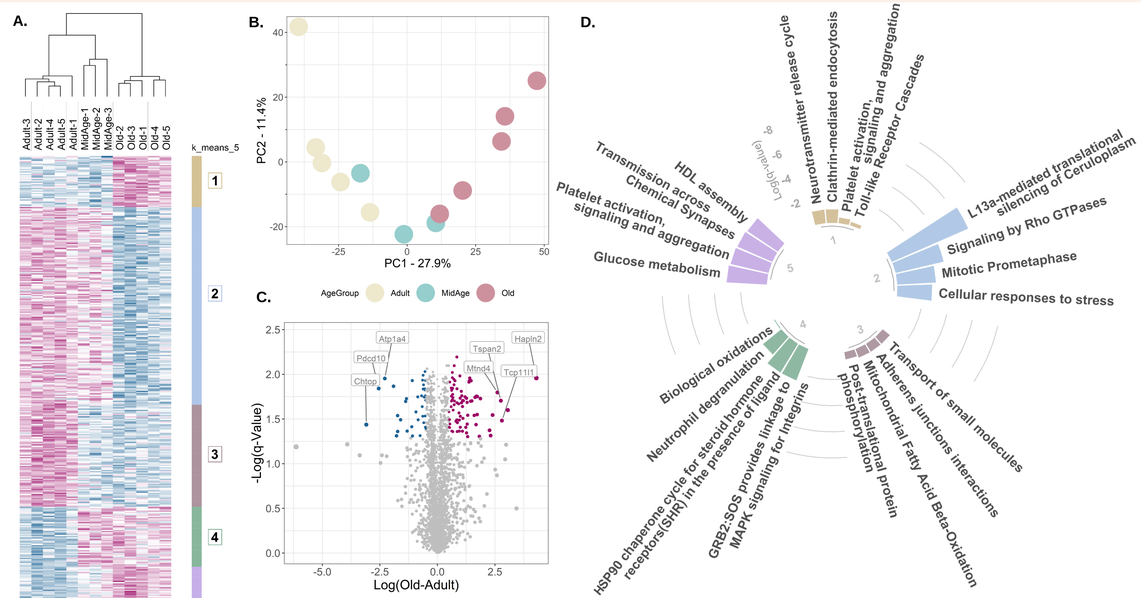

Figure 3. Proteome landscape of mice brain drastically changes during aging. A. Heatmap representation of all significantly changing (q<0.05) proteins in our analysis. Hue represents the Z-score normalized Log2(LFQ) values. Red hue indicates upregulated proteins and blue represents downregulated proteins. Proteins were clustered into 6 cluster by k-means. **B.** PCA plot of all brain samples analyzed in the global proteomics. Mice age groups are indicated by color. **C.** Volcano plot analysis of all quantified proteins. Significantly regulated (q<0.05 & FC >|0.5|) proteins are color coded, and top regulated proteins are labeled. **F.** Cluster-wise Reactome Gene Set enrichment analysis of significantly regulated proteins. Colors and numbers indicate the k-means cluster (Fig. 3A) for which the Gene Sets were enriched.

Aging is accompanied by extensive dysregulation of the brain's phosphoproteome

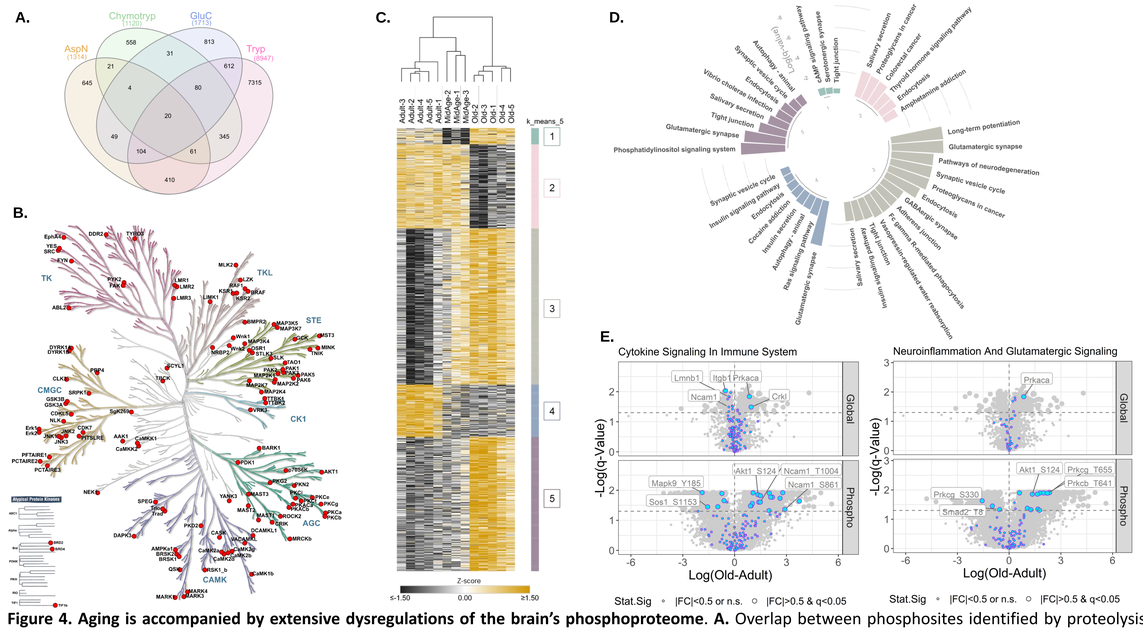

Figure 4. Aging is accompanied by extensive dysregulations of the brain's phosphoproteome. A. Overlap between phosphosites identified by proteolysis with Trypsin, Chymotrypsin, GluC and AspN. **B.** Kinase tree depicting all phosphorylated kinases that could be mapped using our multi-enzyme digestion strategy. Illustration reproduced courtesy of Cell Signaling Technology, Inc. **C.** Heatmap representation of all significantly changing (q<0.05) phosphosite proteins in our analysis. Hue represents the Z-score normalized Log2(LFQ) values. Yellow hue indicates upregulated phosphosites and back represents downregulated phosphosites. Proteins were clustered into 5 cluster by k-means **D.** Cluster-wise Reactome Gene Set enrichment analysis of significantly regulated proteins. Colors and numbers indicate the k-means cluster (Fig. 3A) for which the Gene Sets were enriched. **E.** Volcano plot representations of proteins and phosphosites involved in Cytokine Signaling in the Immune System and **F.** Neuroinflammation and Glutamatergic Signaling.

Results

The brain kinome suffers extensive changes during aging

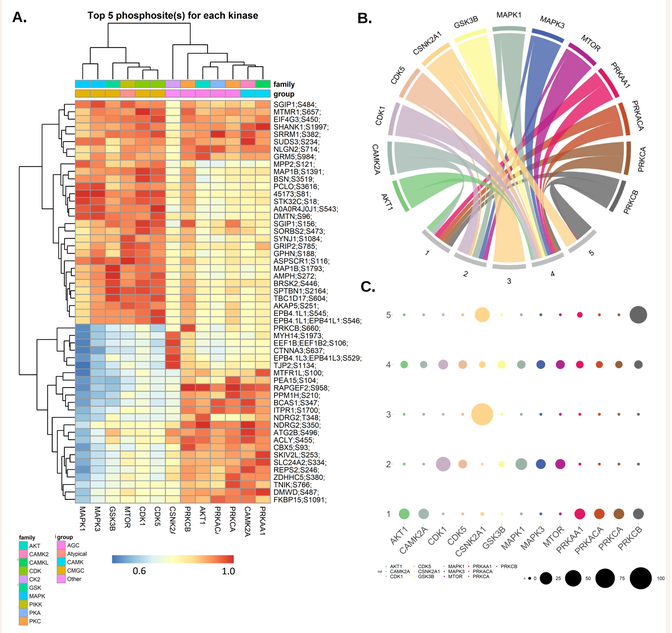

Figure 5. The brain kinome suffers extensive changes during aging. A. Kinase activation enrichment analysis. Red hue indicates higher kinase enrichment scores **C.** & **D.** Enriched kinases can be categorized into 5 clusters, that are composed by distinct target phosphosites

Conclusions & Future Directions

Concluding remarks

- Aging underlies an extensive reprograming of the brain proteome, phosphoproteome, and kinome, with the dysregulation of several signaling pathways
- There is a preferential enrichment of Neuroinflammation and other inflammation-related pathways, observed on both global and phosphoproteomic analyses, indicating a correlation between aging, inflammation and neurodegeneration
- We also observed a predominant activation of the PI3K-AKT-mTOR-signaling axis, highlighting its involvement in neuronal aging
- We shed light into several neurodegeneration biomarkers, both at protein and phosphorylation levels

Future work

- Specific roles of the PI3K-AKT-mTOR-signaling axis in neuronal aging

Acknowledgements

- All MS experiments were performed at the Purdue Proteomics Facility, at the Bindley Bioscience Center. This project was partially supported by the Showalter Trust and the Indiana CTSI.

Contact

*ferreir@purdue.edu; #uaryal@purdue.edu

Poster Number: #8

Analysis of the effect of single amino acid mutations in the budding and cell membrane localization of the Ebola virus matrix protein VP40.

Andres Felipe Monsalve Arango

Borch Department of Medicinal Chemistry and Molecular Pharmacology

Ebola virus is the name given to six species of filovirus, four of which are known to cause a severe and sometimes fatal viral hemorrhagic fever. These viruses are characterized by having a negative-strand RNA genome and a lipid envelope. The Ebola virus genome encodes a 326-residue and ~40 kDa protein called VP40, which is critical in regulating the budding and assembly process in the virus lifecycle. The expression of VP40 in mammalian cells is sufficient to induce the formation of virus-like particles (VLPs) in the absence of other Ebola virus proteins, making it possible to study VP40 cellular behaviors in the absence of the viral genome and high containment facilities. VP40 is a peripheral binding protein that is found as a dimer and can form larger oligomers that form a shell below the plasma membrane prior to budding and subsequently in virions. VP40 mutations have been used to examine the mechanisms of VP40 interactions with the plasma membrane to regulate viral assembly and budding by changing the membrane-binding capabilities of the protein.

Analysis of the effect of single amino acid mutations in the budding and cell membrane localization of the Ebola virus matrix protein VP40.

Andres F Monsalve[1], Hannah M Woods[1], Robert V. Stahelin[1]
[1]Borch Department of Medicinal Chemistry & Molecular Pharmacology, Purdue University, West Lafayette, IN 47906

Abstract/Background

Ebola virus is the name given to six species of filovirus, four of which are known to cause a severe and sometimes fatal viral hemorrhagic fever. These viruses are characterized by having a negative-strand RNA genome and a lipid envelope. The Ebola virus genome encodes a 326-residue and ~40 kDa protein called VP40, which is critical in regulating the budding and assembly process in the virus lifecycle. The expression of VP40 in mammalian cells is sufficient to induce the formation of virus-like particles (VLPs) in the absence of other Ebola virus proteins, making it possible to study VP40 cellular behaviors in the absence of the viral genome and high containment facilities. VP40 is a peripheral binding protein that is found as a dimer and can form larger oligomers that form a shell below the plasma membrane prior to budding and subsequently in virions. VP40 mutations have been used to examine the mechanisms of VP40 interactions with the plasma membrane to regulate viral assembly and budding by changing the membrane-binding capabilities of the protein.

VP40

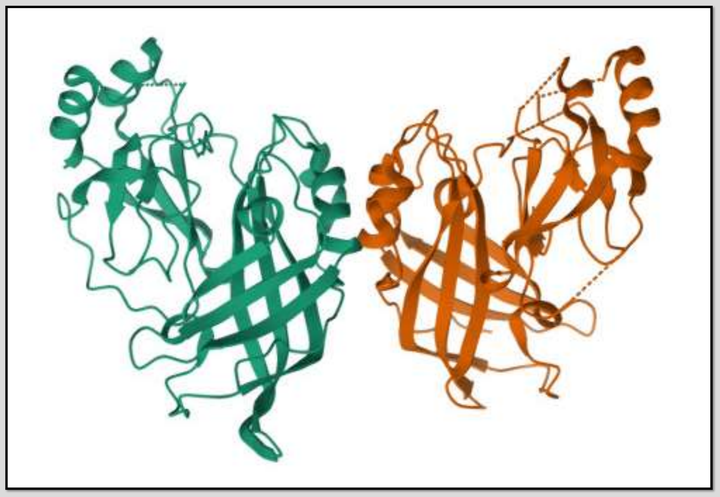

VP40 dimer

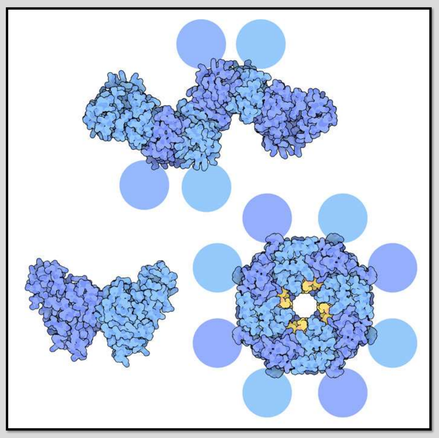

VP40 structures

- Peripheral protein that contains 326 amino acids.
- Weighs ~40 kDa.
- N-terminal domain mediates dimerization and oligomerization.
- C-terminal domain mediates membrane binding.
- Can adopt different structures that undergo various functions in the virus replication cycle.

Ebola Virus budding process

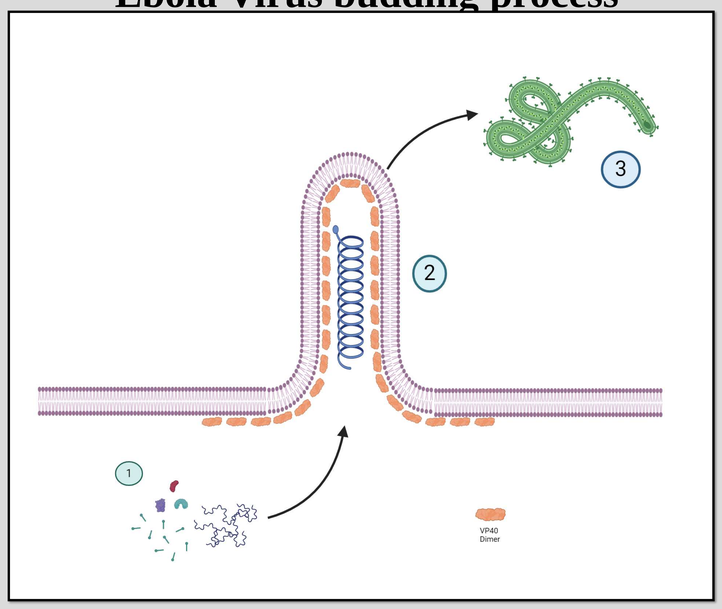

1. **Viral genome and proteins.**
2. **VP40 interacts with the lipids in the inner leaflet of the cell membrane to develop the budding and assembly process.**
3. **Virions are released from the host cell.**

Methodology:

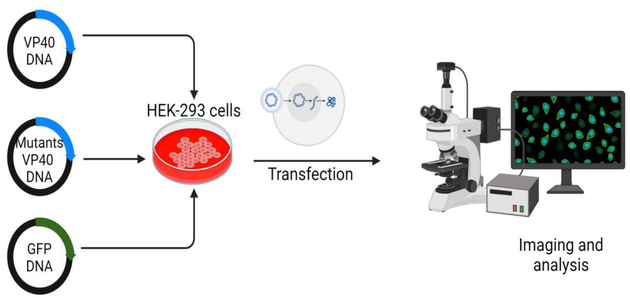

Human embryonic kidney cells (HEK-293) were transfected with plasmids encoding VP40 and VP40 mutants (G226R, S228N, S228G). Then, cells were stained with Hoechst 33342 and WGA for analysis with confocal microscopy.

Virus-like particles (VLPs) are a BSL-2 compatible model of select viral lifecycle processes. Ebola VLPs will self-assemble at the inner leaflet of the plasma membrane when the viral matrix protein VP40 is transiently expressed in mammalian cells.

Using confocal microscopy to study cell membrane localization of VP40

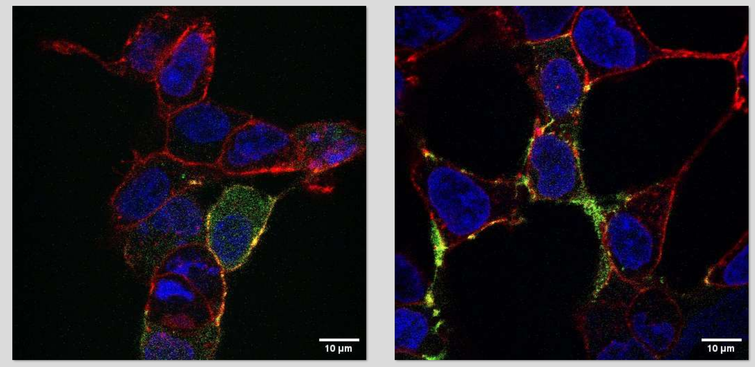

Wild type VP40 G226R

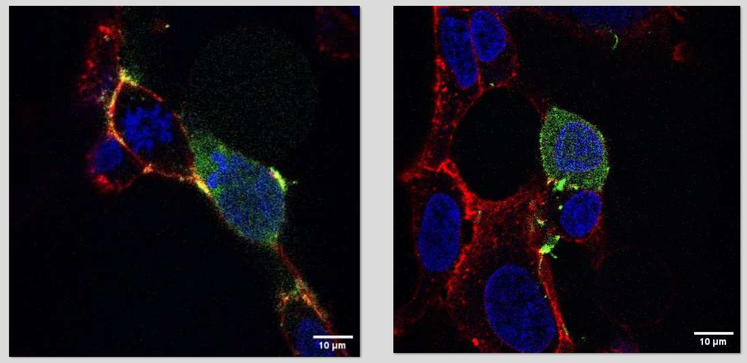

S228G S228N

By comparing cell membrane localization between WT VP40 and mutants, it is posible to confirm that those mutations that increase the positive net charge within the C-terminal domain enhance the cell membrane localization. This can be due to the more favorable interactions with the negatively charged lipids in the membrane. This may explain why G226R appears to be more localized at the cell membrane than wild type VP40.

Future Directions

- Determine how exactly this mutations affect the cell membrane localization of VP40 by carrying out quantitative analysis of cell membrane localization.
- Collect and quantify the virus like particles to study how the budding process is affected by the mutations.

References

- Breiden, B., & Sandhoff, K. (2019).
- Crystal Structure of Ebola Virus VP40 Dimer. 2013. https://doi.org/10.2210/PDB4LDB/PDB.
- Goodsell, D. S. Ebola Virus Proteins. *RCSB Protein Data Bank* 2014. https://doi.org/10.2210/RCSB_PDB/MOM_2014_10.
- Motsa, B. B.; Stahelin, R. V. Lipid–Protein Interactions in Virus Assembly and Budding from the Host Cell Plasma Membrane. *Biochem Soc Trans* 2021, *49* (4), 1633–1641. https://doi.org/10.1042/BST20200854.
- Motsa, B. B.; Sharma, T.; Cioffi, M. D.; Chapagain, P. P.; Stahelin, R. V. Minor Electrostatic Changes Robustly Increase VP40 Membrane Binding, Assembly, and Budding of Ebola Virus Matrix Protein Derived Virus-like Particles. *J Biol Chem* 2024, *300* (5), 107213. https://doi.org/10.1016/J.JBC.2024.107213.
- Narkhede, Y.; Saxena, R.; Sharma, T.; Conarty, J. P.; Ramirez, V. T.; Motsa, B. B.; Amiar, S.; Li, S.; Chapagain, P. P.; Wiest, O.; Stahelin, R. V. Computational and Experimental Identification of Keystone Interactions in Ebola Virus Matrix Protein VP40 Dimer Formation. *Protein Science* **2024**, *33* (5), e4978. https://doi.org/10.1002/PRO.4978.

NIH National Institutes of Health Turning Discovery Into Health

Funding Source
R01AI158220

Poster Number: #9

Activation of the Innate Immune System to Eliminate RSV Infection Using a Bispecific Small Molecule Targeting Ligand

Jeffery Nielsen

Department of Chemistry

Human respiratory syncytial virus (RSV) is the primary viral cause of lower respiratory tract infections (LRTIs) in newborns, young children, and the elderly. Roughly 70% of infants will become infected with RSV within their first year of life, while ~90% of all children will become infected with RSV within their first two years. Overall, RSV has been shown to cause nearly 34 million cases of LRTI in children younger than 5 years of age, resulting in 3.4 million hospitalizations. Despite this, no effective therapeutic is available for severe RSV infection in children, and the two vailable vaccines have only been approved for use in individuals >60 years of age. There exists a substantial need to develop antiviral therapeutics to treat RSV infection in all age groups. Previously, we have produced a novel, bifunctional small molecule capable of targeting and eliminating severe influenza infection in animals via activation of the host‚Äôs innate immune system after only a single dose. As such, we have adapted this platform technology to successfully target the RSV Fusion (F) protein, the primary immunogenic protein of RSV particles. A library F protein targeting ligands were linked to two distinct hapten molecules, each capable of binding to two different, naturally occurring antibodies found in humans. Once recruited to the F protein by the linked targeting ligand, these antibodies engage the innate immune effector cells to simultaneously kill the infectious virus particles and/or virus-infected cells. Preclinical in vitro and in vivo experiments are currently being performed to evaluate the efficacy, safety, and pharmacokinetics of the targeted ligand complex. Ultimately, this dual targeting tactic demonstrates a unique approach for the rapid and effective treatment of severe RSV infections for all age groups.

Activation of the Innate Immune System to Eliminate RSV Infection Using a Bispecific Small Molecule Targeting Ligand

PURDUE UNIVERSITY

Purdue Institute of Inflammation, Immunology and Infectious Disease

Conrrad Nicholls, PhD, Jeffery Nielsen, PhD, Charity Campbell, Joshua Ramsey, Magdalena Alvis, McLayne Houin, Jeramiah Budd, Ian Alford, Imrul Shariar, PhD, Philip Low, PhD
Eradivir Inc., West Lafayette, IN 47907

PURDUE CHEMISTRY

ERADIVIR

Abstract

Human respiratory syncytial virus (RSV) is the primary viral cause of lower respiratory tract infections (LRTIs) in newborns, young children, and the elderly. Roughly 70% of infants will become infected with RSV within their first year of life, while ~90% of all children will become infected with RSV within their first two years. Overall, RSV has been shown to cause nearly 34 million cases of LRTI in children younger than 5 years of age, resulting in 3.4 million hospitalizations. Despite this, no effective therapeutic is available for severe RSV infection in children, and the two available vaccines have only been approved for use in individuals >60 years of age. There exists a substantial need to develop antiviral therapeutics to treat RSV infection in all age groups. Previously, we have produced a novel, bifunctional small molecule capable of targeting and eliminating severe influenza infection in animals via activation of the host's innate immune system after only a single dose. As such, we have adapted this platform technology to successfully target the RSV Fusion (F) protein, the primary immunogenic protein of RSV particles. A library F protein targeting ligands were linked to two distinct hapten molecules, each capable of binding to two different, naturally occurring antibodies found in humans. Once recruited to the F protein by the linked targeting ligand, these antibodies engage the innate immune effector cells to simultaneously kill the infectious virus particles and/or virus-infected cells. Preclinical in vitro and in vivo experiments are currently being performed to evaluate the efficacy, safety, and pharmacokinetics of the targeted ligand complex. Ultimately, this dual targeting tactic demonstrates a unique approach for the rapid and effective treatment of severe RSV infections for all age groups.

Background

Platform Technology:

BAiT™
Bispecific Antigenic immuno-Therapy

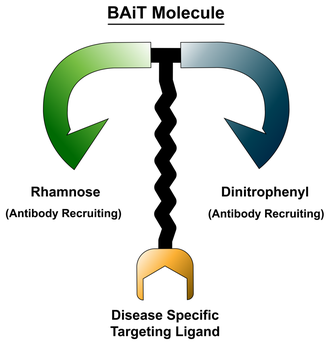

Figure 1 - Bispecific Antigenic Immuno-Therapy (BAiT) molecule general structure: The BAiT molecule is a highly modular tool capable of being altered to meet the demand of a wide variety of diseases.

Mechanism:

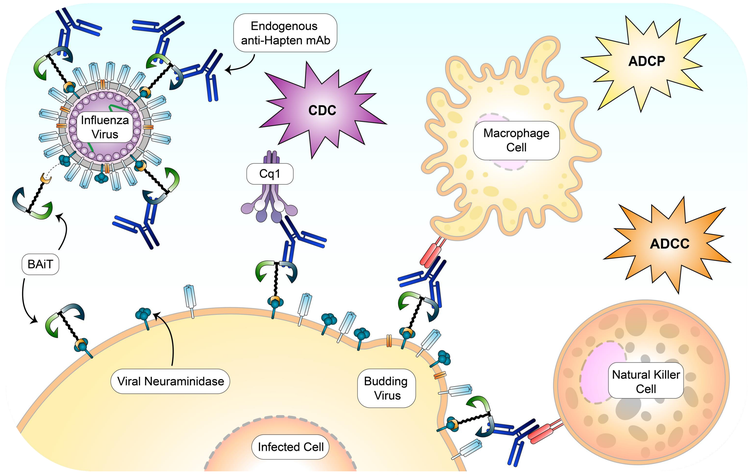

Figure 2 - Mechanism of Action of the BAiT Platform: Relying on the high binding affinity of disease specific targeting ligands, BAiT molecules link proteins of interest to endogenously produced anti-Hapten antibodies abundant in all humans. The tethering of these antibodies to disease specific proteins via BAiT molecules recruits complement proteins, macrophages, and even natural killer cells to sites of infection, effectively eliminating infected cells and removing virus particles.

Foundation in Influenza:

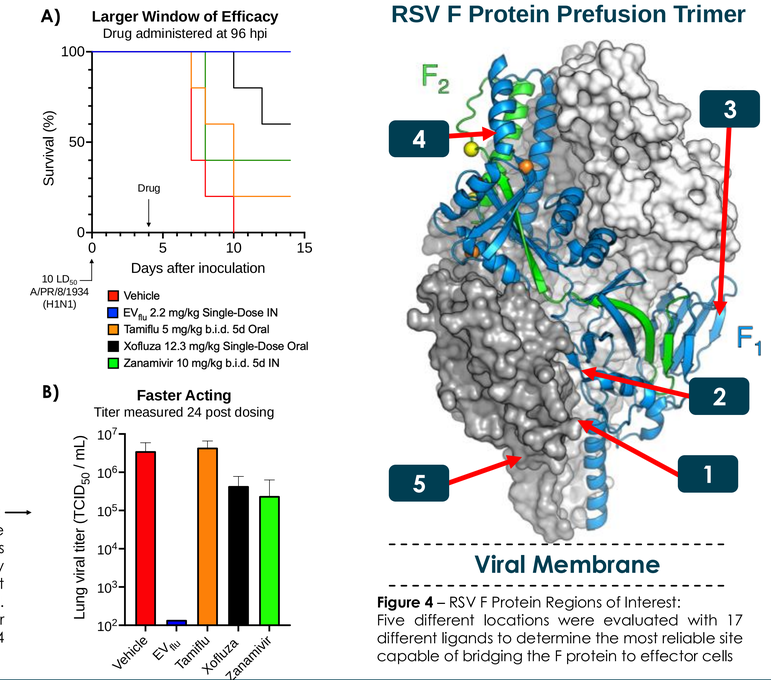

Figure 3 – Proof of concept in influenza: **A)** EVflu, our lead molecule for the treatment of influenza infection, has demonstrated robust antiviral efficacy when administered out to 96 hours post infection, protecting all mice treated. **B)** EVflu was shown to reduce viral titer to limit of quantification after only 24 hours post treatment.

Experimental Design

Target of Interest:
RSV F Protein Prefusion Trimer

Figure 4 – RSV F Protein Regions of Interest: Five different locations were evaluated with 17 different ligands to determine the most reliable site capable of bridging the F protein to effector cells

Results

Direct Antiviral Efficacy Screen of Compounds

Compound	IC_{50}	CC_{50}	SI
EV38	1.58 µM	>100 µM	63..29
EV39	1.98 µM	>100 µM	50.51
EV54	No Effect	>100 µM	N/A
EV68	186 nM	>100 µM	537.63
EV73	168 nM	>100 µM	595.24
EV74	707 nM	>100 µM	141.44
EV109	1.12 µM	>100 µM	89.29
EV110	258 nM	>100 µM	387.60

Table 1 – Direct antiviral efficacy and cellular cytotoxicity of currently tested compounds: For cellular cytotoxicity, cells were incubated with various dilutions of compounds for 5 days, then cell viability was determined via MTS assay. For direct antiviral efficacy, compounds were diluted in media and added to cells, then, RSV Long strain was added to the cells at an MOI of 0.1. Cell viability was determined via MTS assay and compared to untreated, virus infected cells to identify the baseline of virus-imposed cell death.

EV68 Specifically Binds to RSV F

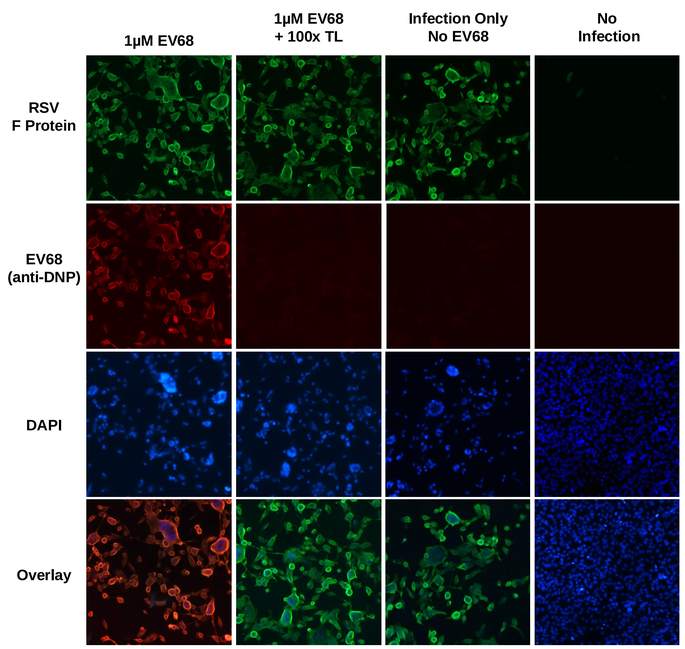

Figure 5 – Immunofluorescence assay of RSV infected cells: Hep2 cells were infected with RSV Long strain at an MOI of 3. After letting the infection run for 36 hours, cells were fixed. EV68 was then incubated with the cells at a concentration of 1 µM with or without 100x targeting ligand (TL) for 1 hour. Cells were washed, and RSV F protein antibody Palivizumab (mouse), and anti-DNP antibody (rabbit) were incubated with the cells for 1 hour. Secondary antibodies G-α-M Alexa Fluor 488 and G-α-R Alexa fluor 594 were then incubated with the cells for 1 hour. Cells were stained with DAPI and imaged using a fluorescent microscope. EV68 binding was shown to be out-competed by 100x free TL.

Complete Immunological Profile - EV68

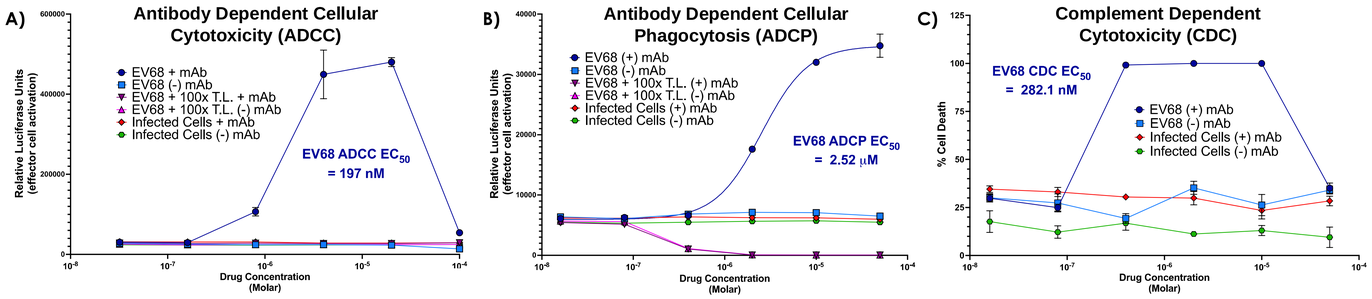

Figure 6 – Complete immunological activation panel of EV68: Hep 2 cells were infected with an MOI of 3, and ADCC, ADCP or CDC assays were performed 24 hours post infection to determine the ability of EV68 to activate effector cells (ADCC or ADCP) or to kill cells in the presence of completement system proteins (CDC), confirming our mechanism of action. **A)** ADCC EC_{50} is 197 nM. **B)** ADCP EC_{50} is 2.52 µM. **C)** CDC EC_{50} is 282.1 nM. All EC_{50} values were determined via Absolute EC50 quantification using GraphPad Prism.

Preclinical In Vivo Efficacy - EV68

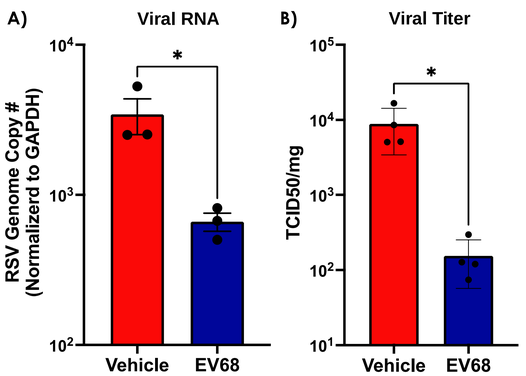

Figure 7 – In vivo efficacy of EV68:

Eight-week-old female Cotton Rats (n = 4 / group) were infected with 1x10⁶ $TCID_{50}$ / ml of RSV Long strain intranasally. After 24 hpi - mice were administered a single dose of 1.5 µM / kg of EV68 intranasally. Mice were sacrificed 2 days post infection (24 hours after treatment) and their lungs were harvested, the lobes were separated, weighed, and one lobe was flash frozen in liquid nitrogen for TCID50 analysis and the other was stored in RNA lysis buffer for qRT-PCR analysis.
A) Relative qRT-PCR was performed on extracted RNA to quantify the viral RNA normalized to GAPDH (* = P value of 0.0401). **B)** Viral titer was determined via TCID50/mg lung weight (* = P value of 0.0186).

Conclusions

Initial results indicate that our bispecific molecules protect against RSV infection in vitro. This suggests that our targeting ligands are still able to bind to RSV particles, disrupting some early stage of virus entry or fusion. In addition, effector cell activation suggests that the binding is specific, and the haptens linked to our targeting ligands are still accessible to antibodies. Lastly, positive in-vivo data suggest that our mechanism of action is effective at reducing viral load in the cotton rat model.

Acknowledgements

I would like to thank Eradivir Inc for allowing me to present this work and a special thank you to Dr. Jeffery Nielsen for his continued guidance as VP of R&D Research. Lastly, I would like to thank Dr. Phil Low for his continued support of our company as our academic partner at Purdue University.

Poster Number: #10

Insight into Dengue Virus Nonstructural Protein 1(NS1) Interaction with Apolipoprotein A1

Mercy Orukpe Moses

Biological Sciences

Flaviviruses, primarily transmitted by arthropods, have seen a significant rise in global spread and epidemic transmission over the past six decades, with the dengue virus alone estimated to infect up to 400 million individuals annually. This virus, characterized by its small, enveloped, single-stranded RNA genome, encodes several structural and nonstructural proteins, including the critical nonstructural protein 1 (NS1), which plays essential roles in viral replication and immune evasion. Recent studies have highlighted the interaction between NS1 and high-density lipoprotein (HDL), specifically its major protein component, apolipoprotein A1 (Apo A1). This interaction may disrupt HDL's anti-inflammatory functions, exacerbating dengue pathogenesis. Notably, cholesterol-rich domains in cell membranes are crucial for dengue virus entry and replication, and depletion of these lipid rafts has been shown to inhibit infection. Furthermore, decreased serum levels of Apo A1 have been observed in dengue-infected patients, suggesting a complex interplay between NS1 and lipoproteins that may trigger pro-inflammatory signals. This study aims to investigate the molecular determinants of the interaction between NS1 and Apo A1, hypothesizing that NS1 interaction with Apo A1 via its hydrophobic regions, inhibits dengue virus infectivity. Understanding these interactions is vital for elucidating the mechanisms of dengue virus pathogenesis and could inform the development of novel antiviral strategies. Protein-protein interactions (pull down assay and immunofluorescence assay) were carried out to check for interaction, and plaque assays to study the overall effect of Apo A1 in dengue virus infection. The results I have so far show that there is a potential interaction between NS1, and Apo A1 but individual deletions of the hydrophobic regions did not alter this interaction. Also, preincubating HEK293T cells with increasing concentration of Apo A1 increased NS1 attachment to the cells suggesting that Apo A1 may be upregulating SR-BI receptors for NS1 attachment. Co-transfection and preincubation of NS1 and Apo A1 followed by Dengue virus transfection into Vero cells showed a reduction in the number of plaques formed, suggesting a reduction in dengue virus infectivity. Going forward, cryo-electron microscopy will be utilized to ascertain the sites of interaction between NS1 and Apo A1. Infection of dengue virus into preincubated cells with NS1 and/or Apo A1 will also be done to eliminate the toxic effect of transfecting reagent on the cells. NS1 is highly conserved within the flavivirus family, so other flavivirus NS1 will be investigated for interaction with Apo A1 and its overall effect in the infection cycle.

Insight into Dengue Virus Nonstructural Protein 1(NS1) Interaction with Apolipoprotein A1

Mercy Orukpe Moses[1], Prateek Kumar[1], Richard Kuhn[1,2]

[1]Department of Biological Science, Purdue University, West Lafayette, IN 47907

[2]Purdue Institute of Inflammation, Immunology and Infectious Disease, Purdue University, West Lafayette, IN, 47907

Department of Biological Sciences

Introduction

Flaviviruses, particularly the dengue virus, are single-stranded RNA viruses transmitted by arthropods, causing severe health complications worldwide. The dengue virus infects approximately 400 million people annually, with significant hospitalization rates[1]. Characterized by a small, enveloped structure, the dengue virus encodes various proteins, including the nonstructural protein 1 (NS1), which is crucial for viral replication and immune evasion[2]. Recent studies indicate that NS1 interacts with high-density lipoprotein (HDL) and its major component, apolipoprotein A1 (Apo A1), potentially disrupting HDL's anti-inflammatory functions and exacerbating dengue pathogenesis[3].

Cholesterol-rich domains in cell membranes are essential for dengue virus entry, and depletion of these lipid rafts inhibits infection[4]. Notably, decreased serum levels of Apo A1 have been observed in dengue-infected patients, suggesting a complex interplay between NS1 and lipoproteins that may trigger pro-inflammatory signals[5]. This research aims to elucidate the molecular determinants of the interaction between NS1 and Apo A1, hypothesizing that NS1 interaction with Apo A1 via its hydrophobic regions, inhibits dengue virus infectivity. Understanding these interactions is vital for elucidating dengue virus pathogenesis and could inform the development of novel antiviral strategies to combat this global health threat.

Objectives

- Determining the molecular interactions between NSI and Apo Al in vitro, by mutagenesis studies; research shows that detergents reduced the binding affinity of NS1-Apo A1 suggesting this interaction may be occurring in the nonpolar regions of the proteins. Individual deletions in the hydrophobic regions of NS1 were made to check for interaction with Apo A1.

- Studying the functional roles of NS1-Apo A1 Interaction in dengue virus infection; previous report has showed that Apo A1 inhibits NS1-induced Dengue virus attachment to cells, we aim to understand the overall effect of Apo A1 in dengue virus infectivity and the attachment factors involved.

Methodology

- A. The structure of Dengue NS1 was docked unto the full-length Apo A1 (UNIPROT P02647) using Schrodinger's biologics (Glide module). The residues in ball and sticks are sites of interaction from the docking that are within the hydrophobic domains of NS1. B. Individual deletions were made in the hydrophobic regions of NS1 (β-roll, Flexible loop and Greasy finger)[6].

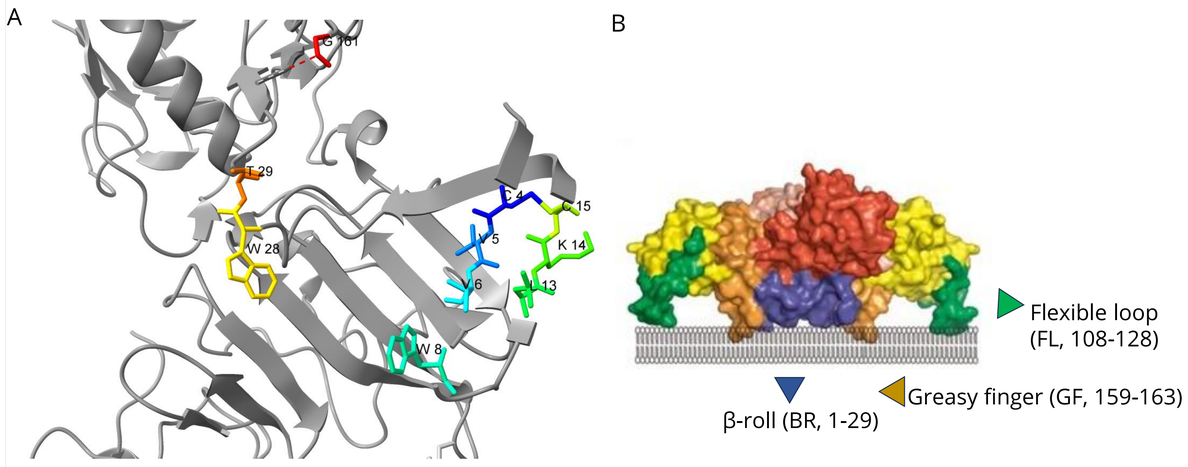

- The intracellular trafficking of NS1 (WT/Deletions) were examined using the HiBiT Nanoluciferase assay by cloning the HiBiT tag to the C-terminus of NS1 and addition of the substrate to give luminescence.

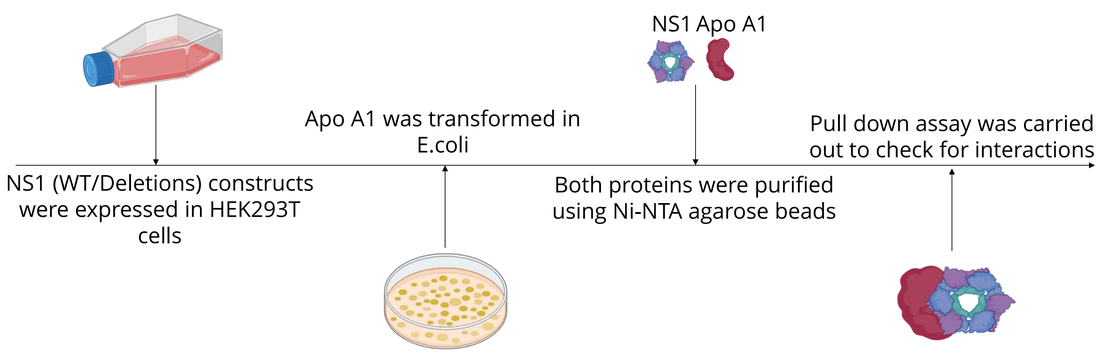

- NS1 and/or Apo A1 plasmids/proteins were cotransfected/preincubated into HEK293T cells, respectively. After 24 hours, 2ug of invitro transcribed dengue virus serotype 2 was transfected into the same wells, overlayed with agarose and plaques counted.

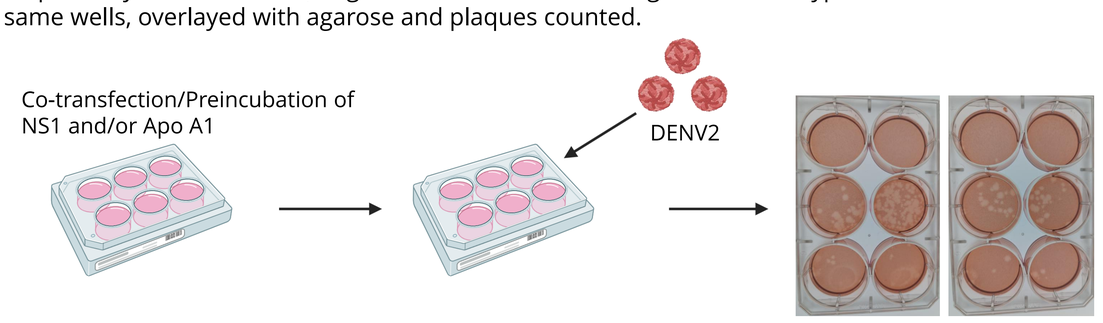

- HiBiT Nanoluciferase was used to carry out the attachment assay. The luminescence measured corresponds to the amount of NS1 present in the cells. The cells were incubated for 1 hour at 4°C, washed to remove any unbound NS1, and luminescence measured.

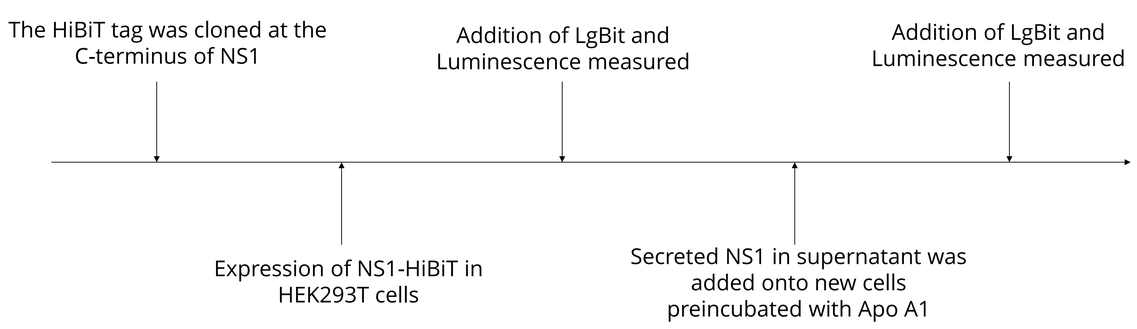

Results

- Luminescence of the supernatants (secreted NS1) and lysates (intracellular NS1) after 72 hours of transfection showed a significant difference between the WT and the different deletions.

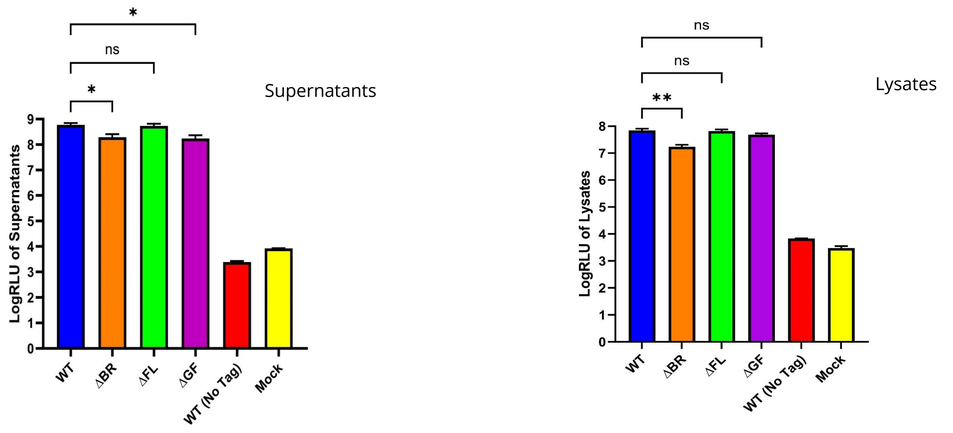

- Western blot showing A. Purified NS1 (WT/Deletions) B. Purified Apo A1, TEV cleaved. C&D. The elute of NS1 (monomer and dimer) and Apo A1 after pull-down assay. B. The elute of NS1 deletions and Apo A1 after the pull-down assay.

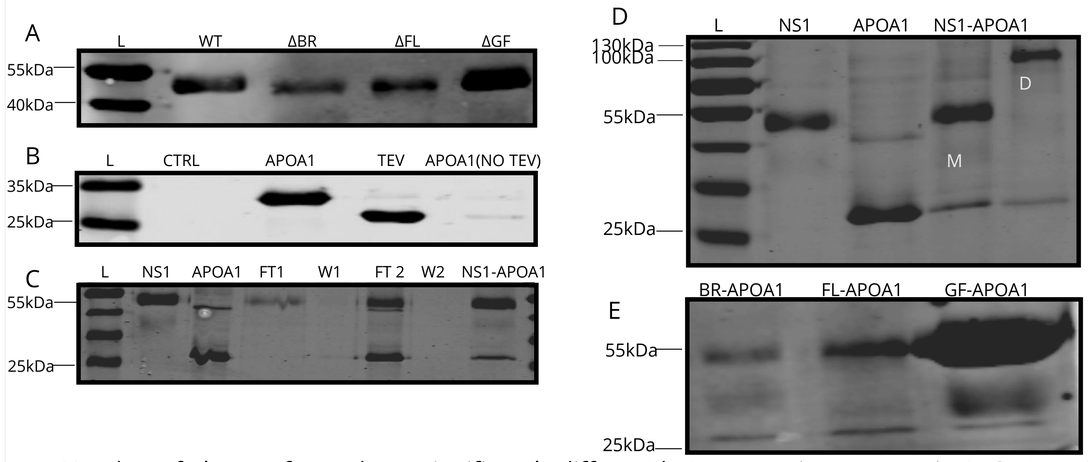

- Number of plaques formed was significantly different between various groups in A. Co-transfection of NS1-Apo A1 and subsequent transfection of Dengue virus RNA. B. Preincubation of purified NS1 and Apo A1 and Dengue virus RNA transfection.

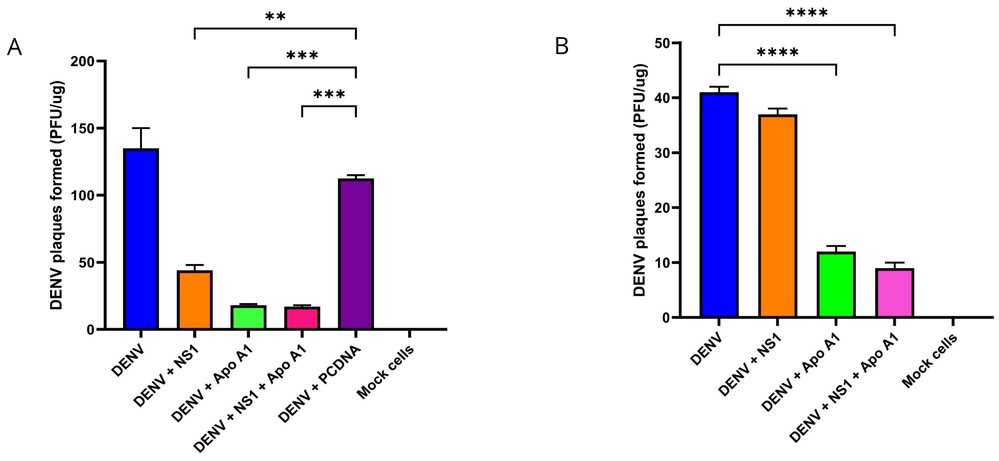

- Attachment assay showing A. %Attached WT NS1 varied when compared to that of the deletions in HEK 293T cells. B. Preincubated cells with increasing concentration of Apo A1 increased the % of attached NS1 to cells

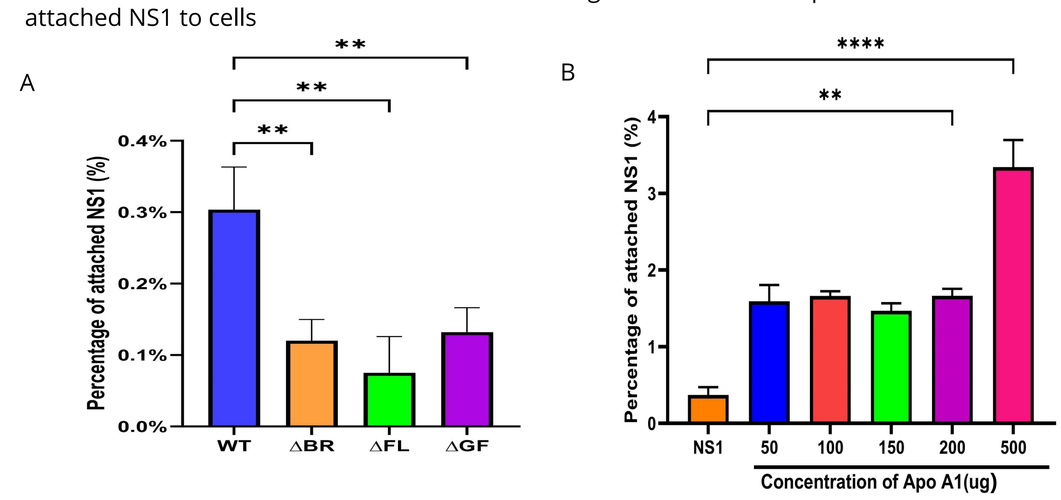

Conclusion

- Individual /single deletion of the hydrophobic domain of NS1 does not impact its interaction with Apo A1
- Endogenous expression of Apo A1 in the presence of transfected dengue virus reduces infectivity.
- Upregulation of SR-B1 receptors by Apo A1 increases NS1 attachment to HEK293T cells.

Future Directions

- Cryo-EM analysis of NS1-Apo A1 interaction
- Protein-protein interaction assay of other flaviviruses NS1 interaction with Apo A1
- Attachment assay for NS1-Apo A1 during Dengue virus infection by blocking SR-B1 receptor.
- Infection instead of transfection of Dengue virus after preincubation of purified proteins.

Acknowledgements

Special thanks to my advisor Dr. Richard Kuhn for his great support and guidance on this project. I also appreciate the members of the Kuhn Lab.

References
1. S. Bhatt., et al 2013, The global distribution and burden of dengue. Nature 496, 50A507 (2013)
2. D. A. Muller, P. R. Young, 2013. The flavivirus NSI protein: Molecular and structural biology, immunology, role in pathogenesis and application as a diagnostic biomarker. Antiviral Res.98, 192—208
3. Coelho DR, et al., 2021. ApoA1 neutralizes proinflammatory effects of dengue virus NSI protein and modulates viral immune evasion. J Virol 95:eOI 974-20.
4. Lee Y-R., et al, 2008. Autophagic machinery activated by dengue virus enhances virus replication. J.Virology 374:240—248.
5. Benfrid S, et al., 2022. Dengue virus NSI protein conveys proinflammatory signals by docking onto high-density lipoproteins. EMBO Rep. 5;23(7):e53600.
6. D. L. Akey, et al., 2015. Structure-guided insights on the role of nsl in flavivirus infection, Bioessays, vol. 37,no. 5, pp. 489—494.

Poster Number: #11

Age-dependent changes in mouse brain and liver lipidomes

Punyatoya Panda

Comparative Pathobiology

Background: Aging is a major risk factor for various diseases such as cancer and neurological disorders including Alzheimer‚Äôs disease. However, the mechanisms of aging are complex and remain elusive. Like genes and proteins, lipids play key structural, regulatory, and signaling roles within the cells. Therefore, characterizing lipids in various organs provides useful information for understanding their functions under different physiological or disease states. However, relatively very little is known about the composition and age-dependent changes of lipids in the brain and liver, the two most lipid-rich organs after adipose tissues. In this work, we characterized the brain and liver lipidome using two complementary analytical approaches: targeted profiling using Multiple Reaction Monitoring(MRM) and untargeted Liquid Chromatography-tandem mass spectrometry (LC-MS/MS), and the spatial mapping of lipids using Desorption Electrospray Ionisation(DESI).

Methods: The brain and liver tissues collected from three age groups of mice-young adult(3‚Äì5-month-old), middle-aged(10‚Äì12-month-old) and old-aged mice(19‚Äì21-month-old) were homogenized and lipids were extracted by Bligh-Dyer method. For MRM-profiling, these were administered into an Agilent QqQ 6410 and samples were screened for specific ion transitions corresponding to different lipid classes and fatty acid composition based on LIPID-MAPS database. For untargeted lipidomics, samples were analyzed using an Agilent 6545 Q-TOF MS coupled with Agilent 1290 Infinity II UPLC System. The untargeted LC-MS/MS-data were searched against MONA-database for lipid identification and relative quantitation. For DESI Imaging, the tissue sections were subjected to ambient mass spectrometry in Waters Synapt XS. Statistical analysis of identified lipid species or classes was performed by Perseus using ANOVA to identify the significantly changing lipids.

Results:
Using MRM profiling, the samples were screened for 3246 MRMs comprising of 24 different lipid classes and fatty acid composition including different phospholipid classes like phosphatidylcholines(PCs), phosphatidylethanolamines(PEs), ceramides, di- and tri-acylglycerols. In the brain, phosphatidylcholines(PCs), phosphatidylethanolamines(PEs) and free-fatty-acids (FFAs) were among the most abundant classes of lipids, while in the liver, tri- and di-acylglycerols were among the most abundant ones, apart from PCs and FFAs. Statistical analysis revealed age-dependent changes in sphingomyelins, TGs and FFA in the brain, and TGs, DGs, and phospholipids classes in the liver.

Conclusions:
In conclusion, the MRM profiling enables simpler, faster, sensitive, and cost-effective exploratory lipid analysis workflow for characterizing the lipidome in diverse biological samples. Understanding age-dependent changes in lipid composition using this MRM method can shed light on potential biomarkers and mechanisms associated with aging.

Age-dependent changes in mouse brain and liver lipidomes

Punyatoya Panda[1], Christina R. Ferreira[2], Bruce R. Cooper[2], Allison Schaser[3], Uma K. Aryal[1,2]

[1]Department of Comparative Pathobiology, Purdue University, West Lafayette, IN. [2]Bindley Bioscience Center, Purdue University, West Lafayette, IN.
[3]Department of Speech, Language, and Hearing Sciences, Purdue University

PURDUE UNIVERSITY College of Veterinary Medicine

ARYAL LAB

INTRODUCTION

Like genes and proteins, lipids play key structural, regulatory, and signaling roles. Thus, profiling lipids in different organs provides useful information for understanding the complex biological processes under various physiological or disease states. However, very little is known about the composition and age-dependent changes of lipids in the brain and liver, two most lipid-rich organs after adipose tissues. In this study, we performed exploratory lipidomic analysis of mice brain and liver at different ages via Multiple Reaction Monitoring Mass Spectrometry (MRM-MS) to determine changes in different classes of lipids and correlate the differences in lipid profiles with the age groups. The MRM-MS analysis was performed using ion transitions based on precursor (Prec) and neutral loss (NL) scans obtained from LIPID MAPS database for screening each sample independently for 24 different classes of lipids including different phospholipid classes such as phosphatidylcholines (PCs), phosphatidylethanolamines (PEs), ceramides, di- and tri-acylglycerols, and acylcarnitine.

EXPERIMENTAL WORKFLOW

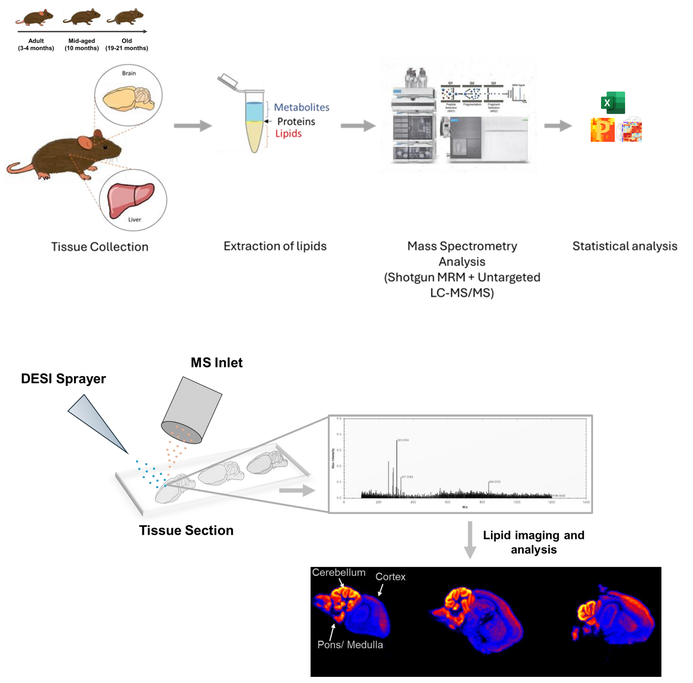

Figure 1: Experimental workflow. Mice from three different age groups were sacrificed. Their brain and liver were collected and homogenized, and the lipidome was extracted by Bligh-Dyer method. These were subjected to MRM spectrometry, and statistical analysis and interpretation was done by Perseus and OriginPro.

RESULTS

SCREENING OF LIPIDS BY CLASS IN BRAIN AND LIVER

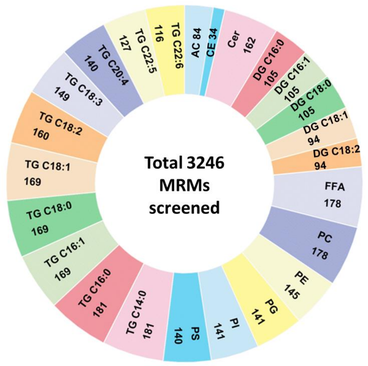

Abbreviation	Lipid
PC	Phosphatidylcholine
PE	Phosphatidylethanolamine
PG	Phosphatidylglycerol
PI	Phosphatidylinositol
PS	Phosphatidylserine
AC	Acylcarnitine
CE	Choline Esters
Cer	Ceramides
FFA	Free fatty acids
DG	Diacylglycerols
TG	Triacylglycerols

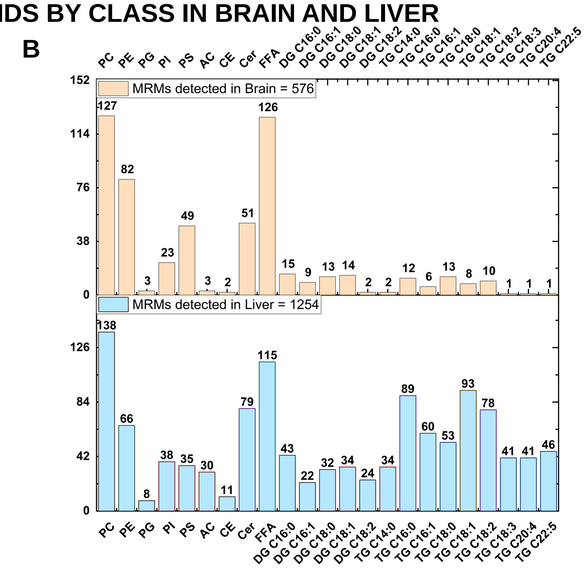

Figure 2: A. Screening of MRMs by class. A total of 3246 MRMs were screened [A] that included 24 classes of lipids. **B.** Distribution and coverage of MRMs across Brain and Liver. 576 were detected in the brain and 1254 were detected in the liver [B].

AGE INDUCED BRAIN AND LIVER PERTUBATIONS AND THEIR LIPIDOMIC COMPOSITION

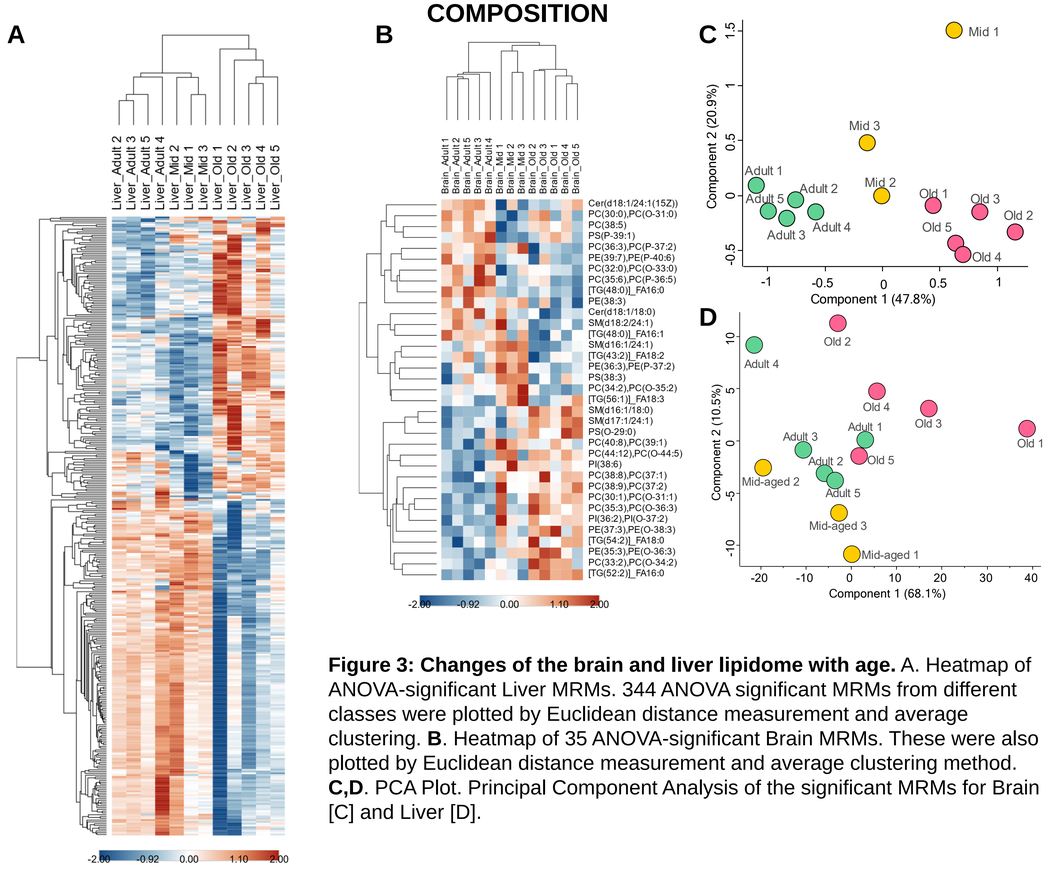

Figure 3: Changes of the brain and liver lipidome with age. A. Heatmap of ANOVA-significant Liver MRMs. 344 ANOVA significant MRMs from different classes were plotted by Euclidean distance measurement and average clustering. **B**. Heatmap of 35 ANOVA-significant Brain MRMs. These were also plotted by Euclidean distance measurement and average clustering method. **C,D**. PCA Plot. Principal Component Analysis of the significant MRMs for Brain [C] and Liver [D].

RESULTS

LIPID IDENTIFICATION: DESI-MS VS. TARGETED AND/OR UNTARGETED LC-MS/MS ANALYSES

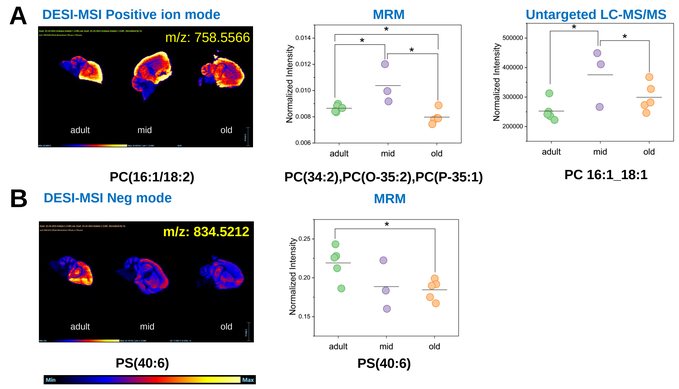

Figure 4:. Examples of lipids changing in the brain that were identified in more than one analyses (Desorption Electrospray Mass Spectrometry Imaging (DESI MSI), MRM, Untargeted LC-MS/MS). Scatter plots display top lipids that show increasing and decreasing pattern with age in the brain and were validated with more than one technique.

SUMMARY

- We screened for a total of 3246 MRMs covering 24 lipid classes for both the liver and the brain.
- Of 576 MRMs detected in the brain, we found 35 significant lipid MRMs that varied across the different age groups.
- Of 1254 MRMs detected in the liver, we found 344 significant lipid MRMs that varied across the age groups.
- Liver is a metabolically a very active organ and is the site of oxidation of triacylglycerols (TG) for energy production. Our data suggests that the energy homeostasis is disrupted with age, as most of the TGs and DGs are changing in aging mice.
- Aging mice brain showed changing lipid profiles of free fatty acids, ceramides and phospholipids.
- Triacylglycerols, that lead to impairment of cognitive function are upregulated with age in brain.
- Increased sphingomyelin concentrations have been reported in neurodegenerative diseases, which is also implicated by our results.

FUTURE DIRECTIONS

- Validation of MRM-MS data with targeted LC-MS/MS analysis using available lipid standards.
- Perform spatial lipidomics to profile brain-region resolved mouse brain lipidome.
- Perform brain-region resolved lipidome profiling using senescence and Alzheimer's disease mice models.
- Correlate lipidome data with the proteome and phosphoproteome data for mapping specific cellular pathways impacted by aging or age-related diseases.

ACKNOWLEDGEMENTS

This study was supported in part by Bindley Fellow program sponsored by the Bindley Bioscience Center to Uma K. Aryal. All the data were collected at the Metabolite Profiling Facility of Bindley Bioscience Center.

For more information, contact: uaryal@purdue.edu (Uma K. Aryal)

Poster Number: #12

Kiharalab EMSuite Server for Structure Modeling, Validation and Refinement of Cryo-EM Maps

Joon Hong Park

Department of Computer Sciences

Cryo-electron microscopy (cryo-EM) is a recent experimental method for determining molecular structures, providing critical insights into their functions and mechanisms. However, accurate interpretation of these maps requires sophisticated computational tools to model accurate atomic structures. The EMSuite Server, available at https://em.kiharalab.org, incorporates advanced algorithms developed at Kihara Lab, providing researchers with an efficient and user-friendly solution for processing cryo-EM data. This prsentation highlights the server‚Äôs key functionalities and demonstrates how its algorithms can be effectively utilized to generate accurate structural models with multiple examples. By leveraging these tools, researchers can generate high-quality structural models that enhance the understanding of molecular functions and mechanisms.

Kiharalab EMSuite Server for Structure Modeling, Validation and Refinement of Cryo-EM Maps

Han Zhu, Joon Hong Park, Javad Baghirov, Xiao Wang, Pranav Punuru, Genki Terashi, Yuki Kagaya, Kai Ling, Shu Li, Yuanyuan Zhang, & Daisuke Kihara

Department of Biological Sciences, Department of Computer Science

Purdue University, West Lafayette, IN 47907

Department of Biological Sciences

https://em.kiharalab.org

Introduction

The Kihara Lab EMSuite Server (https://em.kiharalab.org) is designed to provide easy access to advanced algorithms for computational biology research. Its primary goal is to enable researchers to use powerful tools for analyzing protein structures, molecular modeling, and functional annotations without the need for complex installations or high-performance computing resources.

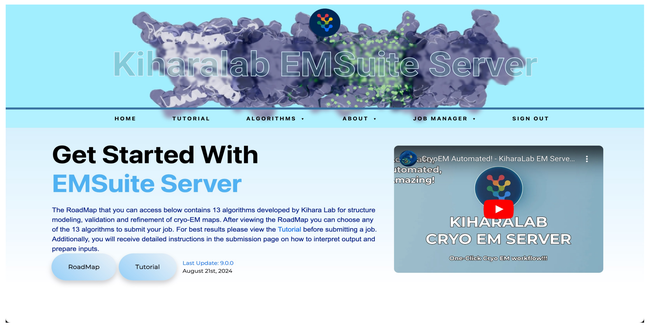

Job Manager

The job Manager page allows users to track and manage all their submitted jobs in one place. It provides an overview of each job's Id, algorithm, status, and start and end times. Users can quickly access the results of completed jobs by clicking "View". Additionally, the page includes a job filtering feature, enabling users to sort and filter their jobs based on different criteria for easier management.

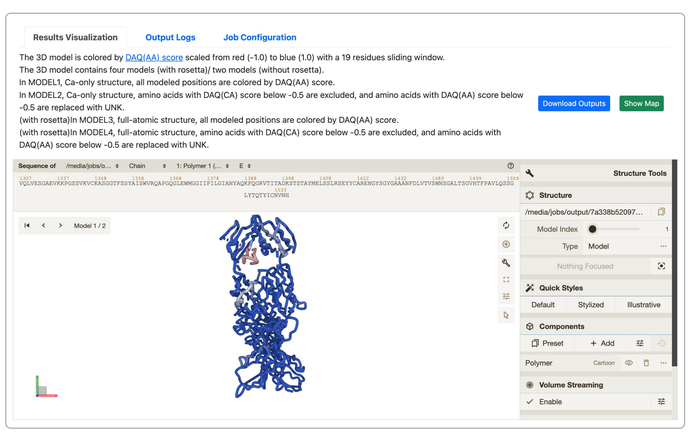

Algorithms

Protein Modeling from Cryo-EM maps - DeepMainmast

DeepMainmast [1] is a new de novo protein main-chain tracing method that uses deep learning to identify the positions of Cα atoms and the types of amino acids. To enhance the modeling performance, AlphaFold2 [2] models can be used as input data.

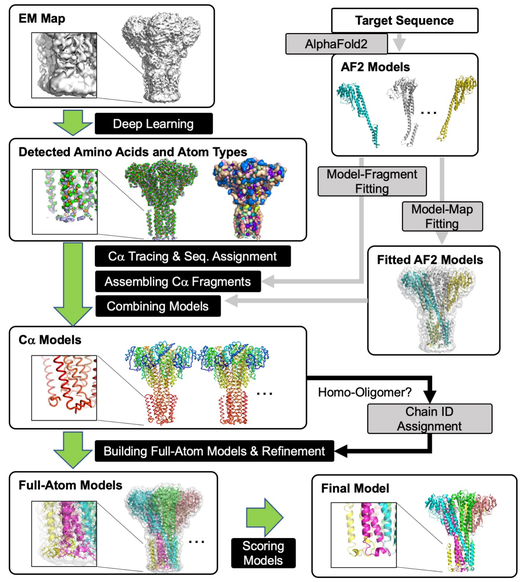

DNA/RNA Modeling from Cryo-EM maps - CryoREAD

CryoREAD [3] is a deep learning-based fully automated *de novo* DNA/RNA atomic structure modeling method. It can identify phosphate, sugar, and base positions in a cryo-EM map using deep learning, which are traced and modeled into a 3D structure.

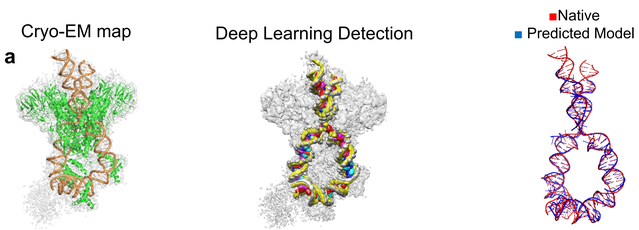

Protein Structure Validation with CryoEM maps – DAQ-score

DAQ [4] is a deep learning tool for assessing protein models from cryo-EM maps. It estimates residue quality by analyzing probabilities of amino acid, atom, and secondary structure types. Log-odds scores are calculated using average probabilities across the model to assign residue-wise scores for the structure model.

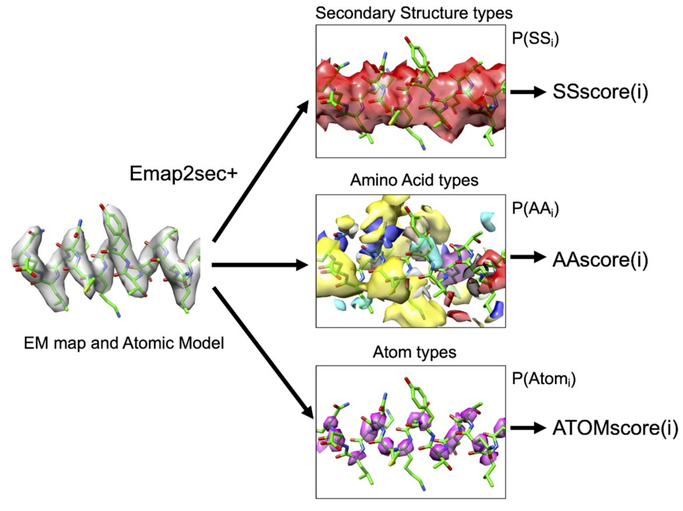

Job Review

If a job fails or produces unexpected results, users can easily submit the issue for review using the Job Review section, located at the bottom of the job page. By describing the problem and submitting the job for review, users can seek clarification or assistance. When a job is submitted for review, the developer team quickly investigates the issue and provides feedback

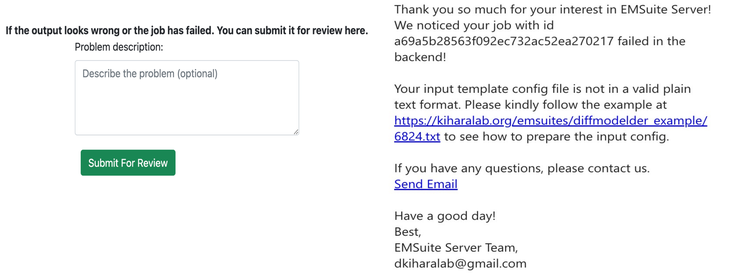

References

1. Terashi, Genki, et al. "DeepMainmast: integrated protocol of protein structure modeling for cryo-EM with deep learning and structure prediction." ***Nature Methods*** 21 (2024): 122-131.
2. Jumper, John, et al. "Highly accurate protein structure prediction with AlphaFold." ***Nature*** 596.7873 (2021): 583-589.
3. Wang, Xiao, Genki Terashi, and Daisuke Kihara. "CryoREAD: de novo structure modeling for nucleic acids in cryo-EM maps using deep learning." ***Nature Methods*** 20.11 (2023): 1739-1747.
4. Terashi, G., Wang, X., Maddhuri Venkata Subramaniya, S.R. et al. Residue-wise local quality estimation for protein models from cryo-EM maps. ***Nat Methods*** 19, 1116–1125 (2022).

Poster Number: #13

Targeting N formyl peptide receptor 2 to resolve inflammation and stimulate skeletal muscle regeneration in Duchenne muscular dystrophy

Hamood Ur Rehman

Animal Sciences

Duchenne muscular dystrophy (DMD) is a genetic disorder caused by mutations in the dystrophin gene, affecting about 1 in 3,500 male births, with no known cure. Treatments, such as the glucocorticoid deflazacort, aim to slow disease progression by targeting inflammation, though they often have significant side effects. The beneficial effects of glucocorticoids in DMD are not fully understood, limiting the development of safer alternatives. Annexin A1 (ANXA1) is a protein that mediates the anti-inflammatory effects of glucocorticoids, and drugs mimicking ANXA1 (e.g., Ac2-26) are under development for inflammatory diseases.

In this study, ANXA1 was found to be highly expressed in dystrophic muscle tissue of mdx mice, primarily in infiltrating immune cells rather than muscle cells. Experiments revealed that deflazacort boosts ANXA1 expression in muscle cells (C2C12 cells) and promotes their differentiation, an effect blocked by an FPR2 inhibitor, suggesting ANXA1's role in muscle regeneration. Similarly, deflazacort-treated macrophages produced ANXA1 and promoted myogenesis-inducing factors. Additionally, the ANXA1 mimetic Ac2-26 also stimulated muscle cell differentiation via FPR2 signaling. Together, these findings indicate that deflazacort activates ANXA1/FPR2 signaling, which may facilitate inflammation resolution and muscle repair in DMD. Ongoing research is further investigating ANXA1/FPR2,Äôs therapeutic potential in DMD using Ac2-26 in vivo.

Targeting N-formyl peptide receptor 2 to resolve inflammation and stimulate skeletal muscle regeneration in Duchenne muscular dystrophy

Hamood Ur Rehman[1], Binayok Sharma[1], Xinyue Lu[1], James F. Markworth[1]
[1]Department of Animal Sciences, Purdue University, West Lafayette, IN, 47906, USA

INTRODUCTION

- Duchenne muscular dystrophy (DMD) is an X-linked recessive disorder caused by mutations in the dystrophin gene. The absence of dystrophin in DMD renders muscle cells more vulnerable to mechanical stress, leading to persistent myofiber damage and chronic inflammation.
- DMD affects approximately 1 in 3,500 live male births globally. Currently, there is no cure for DMD.
- Glucocorticoids are commonly prescribed to reduce muscle inflammation in DMD patients due to their anti-inflammatory and immunomodulatory properties.
- Deflazacort, a synthetic glucocorticoid, was approved by the FDA in 2017 for DMD treatment.
- The precise mechanism by which glucocorticoids exert their therapeutic effects upon dystrophic muscle remains unclear.
- We hypothesize that these therapeutic effects of glucocorticoids in DMD are mediated through production of annexin A1 (ANXA1) a protein that signals via N-Formyl Peptide Receptor 2 (FPR2).

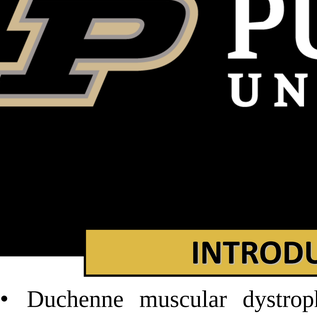

Fig. 1: Glucocorticoids activate the translation and excretion of ANXA1 protein which binds to FPR2 receptors, present on the surface of cells, to suppress the prostaglandins synthesis, and thereby reduce inflammation. GCR: Glucocorticoids Receptors, GRE: Glucocorticoid Elements, ARA: Arachidonic acid, NSAIDS: Non-Steroid anti-inflammatory drugs, COX: Cyclooxygenase, PLA2: Phospholipase A2

MATERIALS AND METHODS

- Tibialis anterior (TA) muscles from *mdx* mice were collected, frozen, and analyzed via immunohistochemistry.
- Muscle injury was induced by injection of 1.2% barium chloride ($BaCl_2$) in TA muscles of C57BL/6J mice, with tissues collected on days 1, 3, and 5 post-injury. Immunohistochemistry was performed on tissue sections.
- Skeletal muscle cells (C2C12 myotubes) were treated with glucocorticoids, Ac2-26 (an annexin A1 mimetic), and FPR2 inhibitors (Boc-2, WRW4). Cells and media were collected for PCR and western blot.
- Bone marrow cells were isolated, polarized into M1 and M2 macrophages, and treated with glucocorticoids, Ac2-26, and FPR2 inhibitors. Conditioned media was collected and applied to C2C12 cells to assess myogenesis.

RESULTS AND DISCUSSION

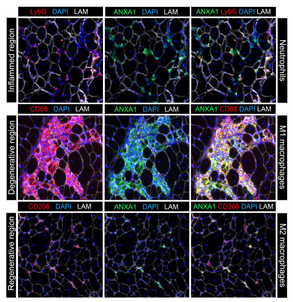

Fig. 2: Expression of ANXA1 by immune cells in the TA muscle of *mdx* mice. Neutrophils (Ly6G, red) during the inflamed stage, Pro-inflammatory M1-like macrophages (CD68, red) during the degenerative stage, Anti-inflammatory M2-like macrophages (CD206, red) during the regenerative stage are expressing ANXA1. DAPI (blue) labels nuclei, and LAM (white) marks laminin.

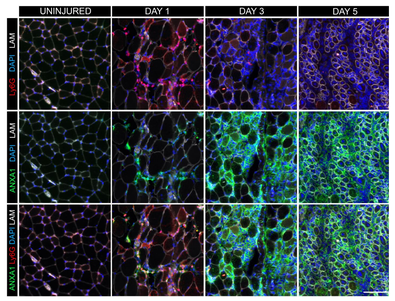

Fig. 3: Expression of ANXA1 by neutrophils in the TA muscle of C57BL/6J mice in response to injury induced by injection of 1.2% $BaCl_2$. On Day 1, the injured area is densely infiltrated with neutrophils (Ly6G, red), which are expressing ANXA1. By Day 3 and Day 5, the number of neutrophils has decreased, but ANXA1 expression remains elevated, suggesting that other cell types may also be contributing to ANXA1 production at these later stages of injury.

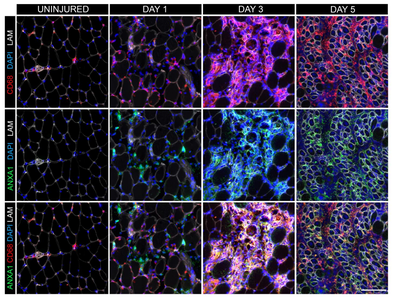

Fig. 4: Expression of ANXA1 by macrophages in the TA muscle of C57BL/6J mice at various time points following injury induced by injection of 1.2% $BaCl_2$. On Day 1, macrophages have not yet infiltrated the injury site, and ANXA1 expression is primarily observed in neutrophils. By Day 3, macrophages have infiltrated the tissue heavily and are expressing high levels of ANXA1. By Day 5, the regenerative process has begun, and ANXA1 expression remains elevated, suggesting ongoing involvement in tissue repair.

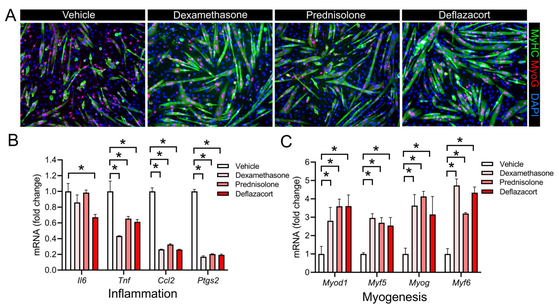

Fig. 5: Glucocorticoids directly enhance myogenesis. (A) Immunohistochemistry shows that glucocorticoids stimulate myotube formation and myogenin protein expression (B): RT-qPCR analysis reveals that glucocorticoids reduce inflammatory gene expression while increasing myogenic gene expression, supporting muscle differentiation and regeneration.

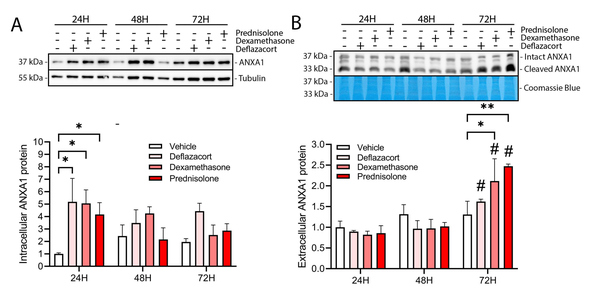

Fig. 6: Western Blot analysis of the effect of glucocorticoids on production and secretion of ANXA1: (A): Intracellular ANXA1 levels as determined by western bblot significantly increase after 24 hours of treatment. (B): Extracellular Annexin A1 levels significantly rise after 72 hours, indicating enhanced extracellular secretion.

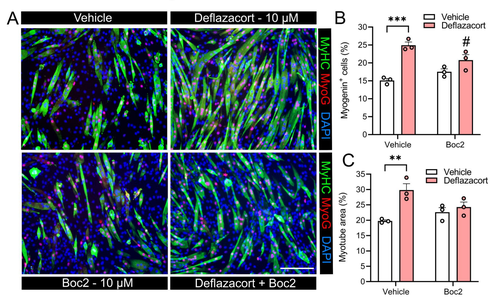

Fig. 7: Deflazacort promotes muscle cell growth via FPR2. Immunohistochemistry analysis shows that deflazacort enhances myogenesis. This effect is reversed by the FPR2 inhibitor Boc2.

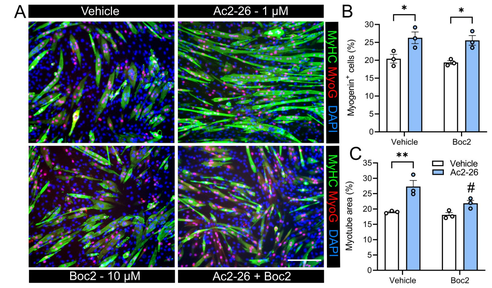

Fig. 8: Ac2-26 promotes muscle cell growth via FPR2. Immunohistochemistry analysis show that ANXA1 mimetic peptide Ac2-26 enhances myogenesis. This effect is reversed by the FPR2 inhibitor Boc2.

RESULTS AND DISCUSSION

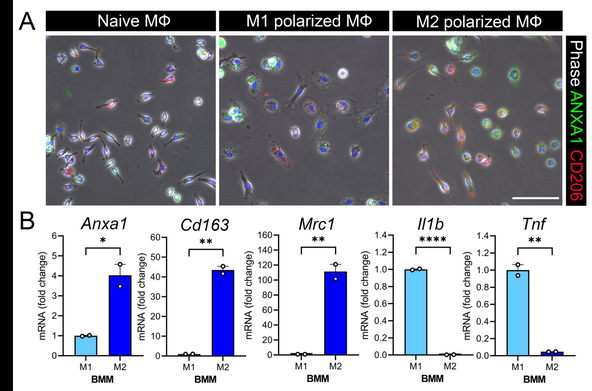

Fig. 9: ANXA1 is produced by M2-polarized macrophages. (A): M2 macrophage polarization increases ANXA1 protein expression and CD206 (M2 marker) levels, as visualized by fluorescent microscopy. **(B):** RT-qPCR analysis shows upregulation of M2-like markers (*Anxa1*, *Cd163*, *Mrc1*) and downregulation of M1-like markers (*Il1b*, *Tnf*) in M2-polarized BMMs.

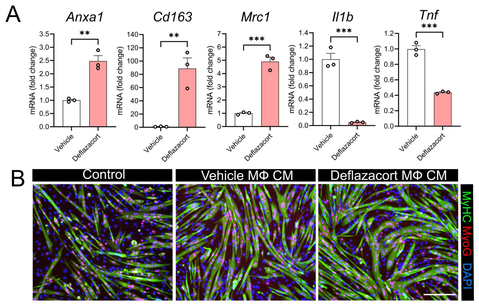

Fig. 10: Macrophage-derived ANXA1 drives myogenesis via immune-muscle cross-talk: (A): Deflazacort skews macrophages towards an anti-inflammatory regenerative subset, as shown by upregulation of M2-like marker (*Anxa1, Cd163, Mrc1*) and downregulation of M1-like markers (*Il1b, Tnf*) in RT-qPCR analysis of BMMs. **(B):** Conditioned media from deflazacort-treated BMMs enhances myotube differentiation in C2C12 cells, as evidenced by increased MyHC and MyoG expression.

SUMMARY/CONCLUSION

- Immune cells express ANXA1 at sites of inflammation in acutely injured and dystrophic skeletal muscle tissue.
- Glucocorticoids enhance ANXA1 expression by both resident muscle cells and infiltrating macrophages
- Upregulation of ANXA1 helps resolve inflammation via FPR2 receptors by suppressing pro-inflammatory gene expression and promoting anti-inflammatory gene expression, thus shifting the environment towards an anti-inflammatory state.
- Deflazacort-mediated ANXA1 expression directly contributes to increased myogenesis in skeletal muscle tissue.

Poster Number: #14

Optimization of Diphyllin-Derived Broad-Spectrum Antivirals

Laura Sanford

Borch Department of Medicinal Chemistry and Molecular Pharmacology

Diphyllin is a naturally occurring compound with a variety of biological activities, including antiviral activity. The core of its antiviral activity comes from its function as a vacuolar-ATPase inhibitor, a host protein that helps facilitate viral entry. To maximize diphyllin‚Äôs utility as a viral entry inhibitor, work has been done to increase potency through derivatization. Although derivatization has significantly improved potency, most diphyllin derivatives undergo rapid metabolism. To maximize diphyllin derivatives‚Äô effect as antivirals, their metabolic stability must be improved to ensure there is a high amount of drug available for as long as possible. Metabolically labile sites on the diphyllin scaffold were predicted computationally to provide a starting point for optimization. Deuterium and fluorine substitutions were employed to rule out stable sites and identify which parts of diphyllin contribute most to metabolism. Deuterium substitution ruled out four hypothesized sites of metabolism. Fluorine substitution on the scaffold successfully stabilizes the diphyllin. This fluorinated diphyllin was further derivatized, resulting in potent compounds with improved metabolic stability. Further investigation includes broad spectrum antiviral testing as well as synthesis of more soluble derivatives to improve drug-like properties and potentially reduce toxicity.

OPTIMIZATION OF DIPHYLLIN-DERIVED BROAD-SPECTRUM ANTIVIRALS

[1]Laura Sanford, [2]Patrick Keiser, [1]Naoaki Fujii, [3]Monica Xu, [1]Liying Che, [1]Robert Stahelin, [3]Greg Knipp, [2]Robert Davey, [1]V. Jo Davisson

[1]Borch Department of Medicinal Chemistry and Molecular Pharmacology, Purdue University
[2]Department of Microbiology, Boston University
[3]Department of Industrial and Molecular Pharmaceutics, Purdue University

PURDUE UNIVERSITY

Borch Department of Medicinal Chemistry and Molecular Pharmacology

Overview:

Diphyllin is a natural product that inhibits vacuolar ATPase (V-ATPase), a host cell proton pump implicated in pH-sensitive viral entry. Although optimization is taking place in the context of Ebola virus, a deadly virus with no small molecule therapeutics available, these compounds should be broad-spectrum for viruses that undergo pH-sensitive entry. Derivatization of the phenol improves potency and permeability. Fluorine substitution can improve metabolic stability. These studies show dramatic improvements to diphyllin. Future optimization includes solubility improvements and further studies in alternate viral models.

pH -Sensitive Viral Entry

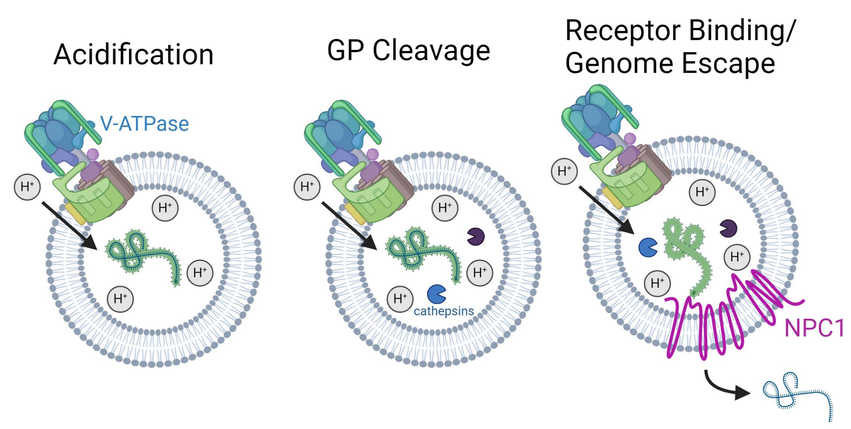

Figure 1[a]. Ebola enters the cell through macropinocytosis, resulting in endosomal containment. V-ATPase, an ATP-driven proton pump, is responsible for endosomal acidification in normal endo-lysosomal trafficking. However, this results in activation of cathepsins (cysteine proteases) which cleave the glycoprotein. This, paired with a conformational change due to the acidity, allows the remnant of the glycoprotein to bind to the NPC1 receptor, fuse to the membrane, and release its genome into the cytoplasm

Viral Entry Assay

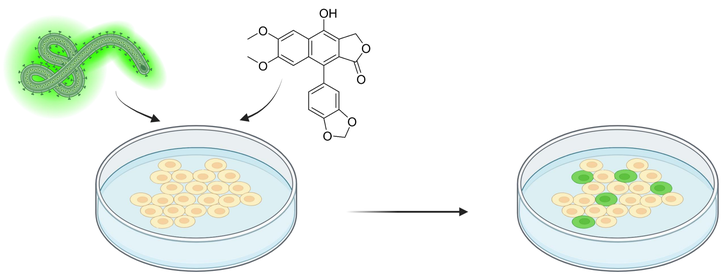

Figure 2. Cells were treated with a dose response of diphyllin derivatives for 1h before infection. Cells were then infected with EBOV-GFP at an MOI of 0.2. After 24-48 hours, cells were fixed and imaged to calculate infection efficiency relative to no treatment.

Diphyllin

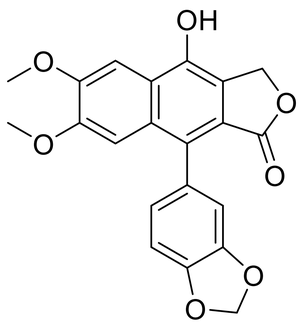

- Selectivity: Good
- Potency (EBOV Entry): 1.1 μM
- Permeability: Low
- Tolerance[b]: ≥ 100 mg/kg PO
- Fraction Unbound: 7%

Figure 3. Structure of diphyllin and relevant properties.

Derivatization

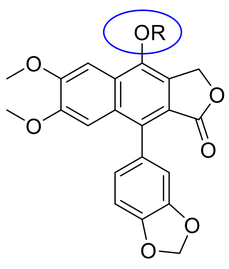

★ Changing the dimethoxy substitution on the A-ring reduced potency

★ Changing the lactone ring to a lactam with substitutions reduced potency

R	EBOV EC_{50} (nM)	ID
	1086 ± 23	Diphyllin
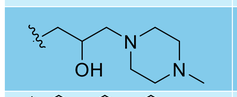	54 ± 14	3COH01[c]
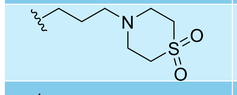	177 ± 44	3C41
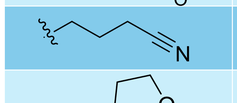	37 ± 2^7	3C24
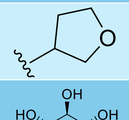	40 ± 1	cyc2O
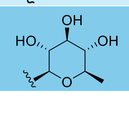	428 ± 78	Patentiflorin A

Table 1. Selected derivatives of diphyllin and their potencies in an Ebola virus entry assay.

Metabolism and Permeability

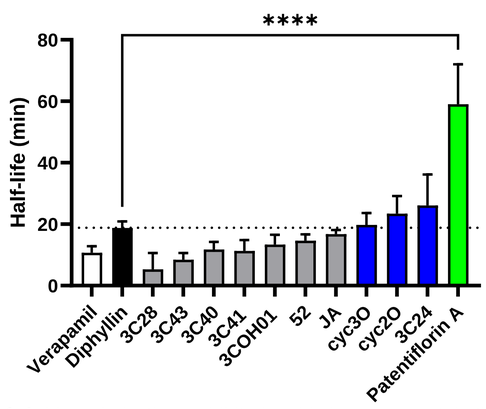

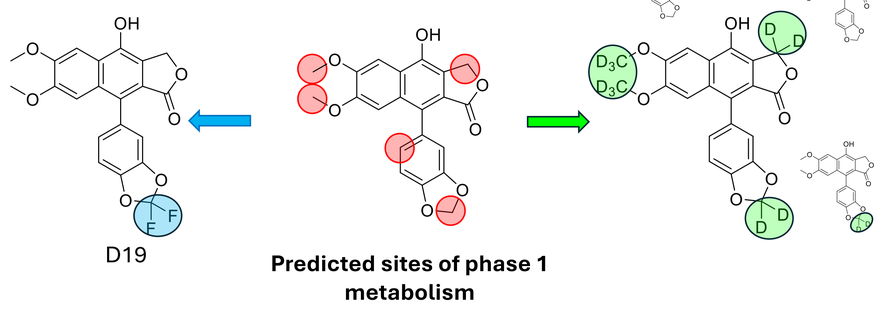

Figure 4. **A**. Many derivatives exhibited rapid phase one metabolism in mouse liver microsome assays. Only one derivative was able to significantly slow the metabolism. This may mean the diphyllin scaffold itself is the major source of metabolism. **B**. Using Schrodinger software, the metabolic sites of diphyllin for CYP3A4 enzymes were predicted. These results led to deuterium and fluorine substitutions to reduce metabolism at these sites.

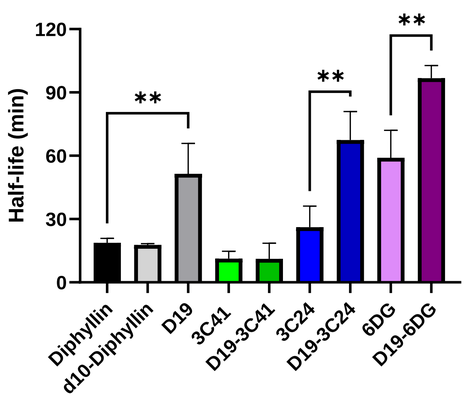

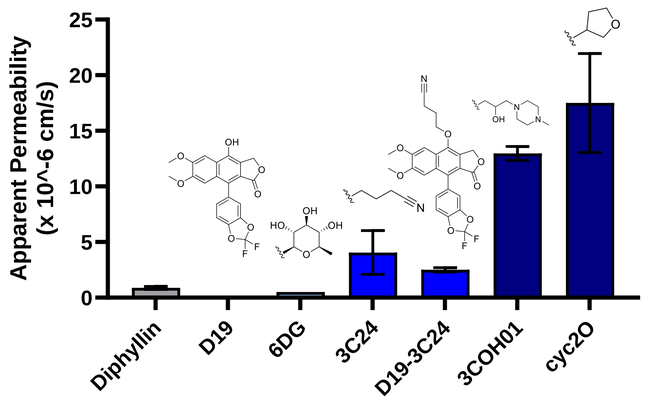

Figure 5. **A**. None of the deuterated structures improved half-life (d10, which contains 10 deuterium atoms, is shown in gray). D19, fluorinated diphyllin, was able to significantly improve half-life. Derivatives that have sufficient metabolic stability also gain a significant increase in half-life when added to the fluorinated scaffold. **B**. Candidates from previous assays were tested in a Caco-2 permeability assay to determine their likelihood for oral bioavailability.

Pharmacokinetics

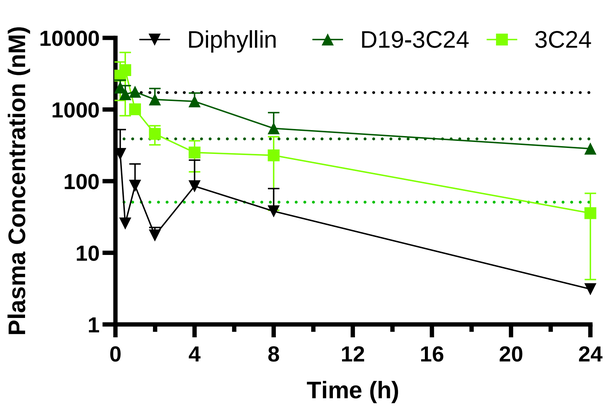

Compound	Half-Life (h)	AUC (nmol · h · L^{-1})
Diphyllin	4.25	822
3C24	6.4	6861
D19-3C24	9	16173

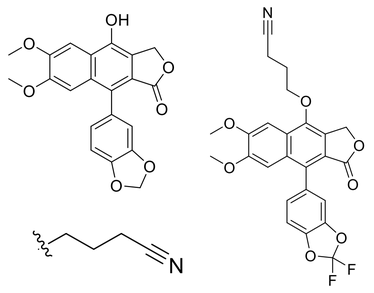

Figure 6. Derivatization produces improved pharmacokinetic profiles. Dotted lines on the pharmacokinetic plot indicate EC_{90} from EBOV entry assay, which is the threshold to stay above for activity. Pharmacokinetic studies were run in mice at approximately 50 mg/kg and normalized. As predicted in the microsome assays, the half-life of D19-3C24 was an improvement upon 3C24.

Broad-Spectrum Activity

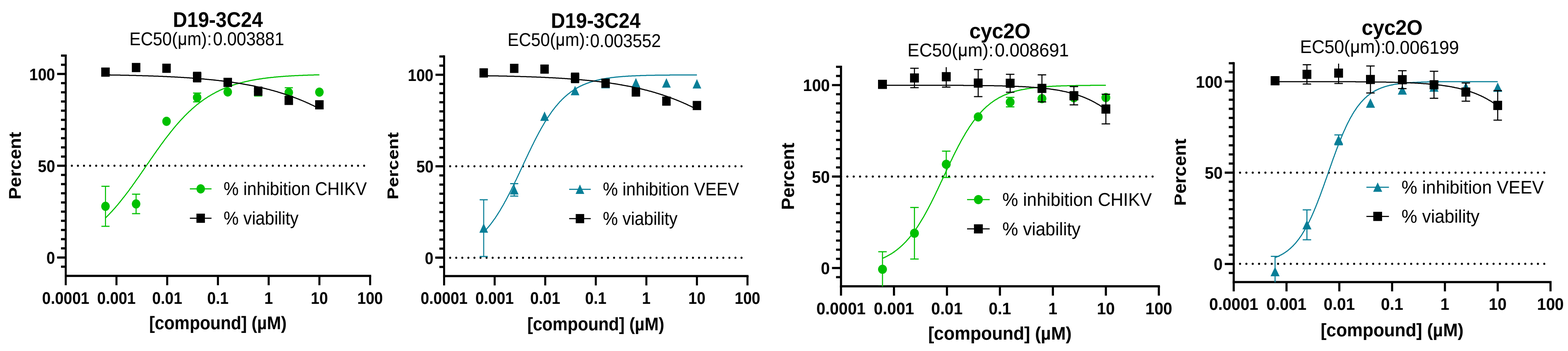

Figure 7. Viability assays were run with Chikungunya and Venezuelan Equine Encephalitis Viruses at UNC Chapel Hill. Efficacious concentrations in the single-digit nanomolar range were achieved for many compounds.

Future Directions

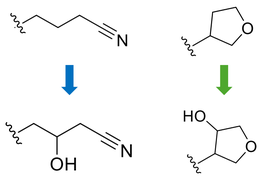

Addition of hydroxyl group improves solubility significantly

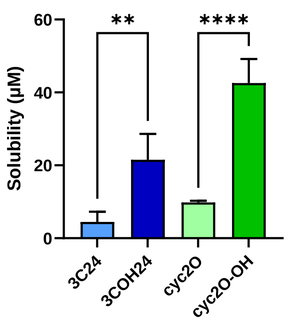

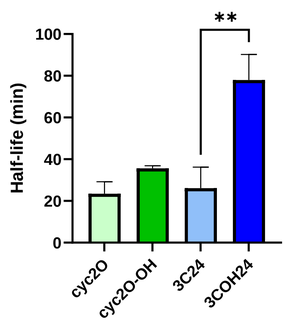

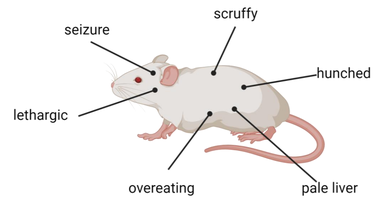

Figure 8. A. We are experimenting with creating more soluble side chains for diphyllin. Addition of a hydroxyl group can significantly improve solubility. The metabolic stability of these compounds also changes, sometimes significantly. In addition to solubility, we beginning to investigate the cause of toxicity at maximum tolerated doses.

References

[a]Sanford, Keiser, et al. *Eur J Med Chem*, 2024, 275, 116537.
[b]Duan et al. *Front Endocrinol (Lausanne)*, 2020, 11, 592818.
[c]Martinez-Lopez et al. *Ebiomedicine*, 2019, 47, 269-283.
[d]Plescia et al. *ACS Infec Dis*, 2022, 8(5), 942-957.

Acknowledgements

Funding from NIH Grant R01AI128364
University of North Carolina, Chapel Hill for VEEV and CHIKV testing
Robyn McCain and the Purdue Translational Pharmacology Core
NIH T32 for Drug Discovery in Infectious Disease 5T32AI148103 - 05

Poster Number: #15

Role of Mammalian Lipoxygenases (LOX) in the Resolution of Skeletal Muscle Inflammation.

Binayok Sharma

Animal Sciences

Mammalian lipoxygenase (LOX) enzymes are important in the regulation of inflammation and its active resolution by oxidizing polyunsaturated fatty acids (PUFAs) such as omega-6 arachidonic acid (ARA) and omega-3 docosahexaenoic acid (DHA) to produce bioactive lipid mediators. Early in the acute inflammatory response the 5-lipoxygenase (5-LOX) pathway produces pro-inflammatory eicosanoids (e.g., leukotrienes) that are essential for promoting leukocyte recruitment to the site of injury. On the other hand, the 15-LOX pathway plays an important role in the resolution phase of the acute inflammatory response by catalyzing the initial step in biosynthesis of specialized pro-resolving lipid mediators (SPMs) (e.g., lipoxins, resolvins, protectins, and maresins). Here we explored how whole-body knockout of the Alox15 gene, encoding the murine leukocyte type 12/15-LOX enzyme, impacts skeletal muscle inflammation and regeneration in mice. Alox15-/- mice displayed an overall similar muscle phenotype as wild type (WT) control mice in the absence of an inflammatory stimuli. Nevertheless, following sterile skeletal muscle injury induced by intramuscular injection of barium chloride (BaCl2, 1.2%) Alox15-/- mice displayed greater monocyte/macrophage infiltration (Cd68 and Adgre1 mRNA) and blunted induction of myogenic genes (e.g., Myog). Intramuscular concentrations of pro-inflammatory eicosanoids including thromboxane B2 (TXB2), prostaglandin (PG) D2 (PGD2), PGE2), and PGI2 (measured as 6-keto-PGF1Œ±) were also markedly elevated in Alox15-/- mice. At day 14 post-injury, Alox15-/- mice displayed striking deficits in both the number and size of regenerating myofibers as well as shifts in muscle fiber type profile indicative of poor tissue regenerative ability. Surprisingly, we found that resident muscle stem cells (satellite cells) obtained from Alox15-/- mice also exhibited distinct behaviors when cultured in-vitro even in the absence of an intact host immune system. The proliferation rate of primary myoblasts obtained from Alox15-/- mice was higher, but their myogenic differentiation and fusion capabilities were lower when compared to WT myoblasts. These deleterious effects of a lack of Alox15 on in-vitro myogenesis could be mimicked by treatment of WT myoblasts with pharmacological LOX inhibitors including the pan LOX inhibitor nordihydroguaiaretic acid (NDGA), the dual 12/15-LOX inhibitor baicalein, and the 15-LOX specific inhibitors BLX-3887 and 9c(i472). Overall, these findings demonstrate the importance of Alox15 in regulating acute inflammation and facilitating muscle regeneration. Targeting the 15-LOX pathway might be a novel therapeutic approach to improve muscle recovery following injury. This could be a potential alternative to traditional anti-inflammatory therapies for the management of muscle injuries through modulating inflammation and facilitating of tissue repair.

Keywords: 15-Lipoxygenase, Skeletal muscle, Injury, Inflammation, Resolution

Role of Mammalian Lipoxygenases (LOX) in the Resolution of Skeletal Muscle Inflammation

Binayok Sharma[1], Xinyue Lu[1,2], Hamood Ur Rehman[1], James F. Markworth[1,2]

[1]Department of Animal Sciences, Purdue University, West Lafayette, IN. [2]Interdepartmental Nutrition Program (INP), Purdue University, West Lafayette, IN

Introduction

- Mammalian lipoxygenase (LOX) enzymes catalyze the oxidation of polyunsaturated fatty acids (PUFAs), such as omega-6 arachidonic acid (ARA) and omega-3 docosahexaenoic acid (DHA) to produce bioactive lipid mediators[1].
- LOX enzymes are central to various physiological and pathological processes, working with cyclooxygenase (COX) and cytochrome p450 (CYP) pathways to generate pro- and anti-inflammatory compounds, crucial for inflammation, its active resolution, and tissue regeneration[2,3].
- 15-LOX mediates the body's response to injury by first promoting inflammation through 15-HETE, then triggering the resolution phase via biosynthesis of anti-inflammatory lipoxins, resolvins, and protectins making it a potential therapeutic target to promote regeneration[4].

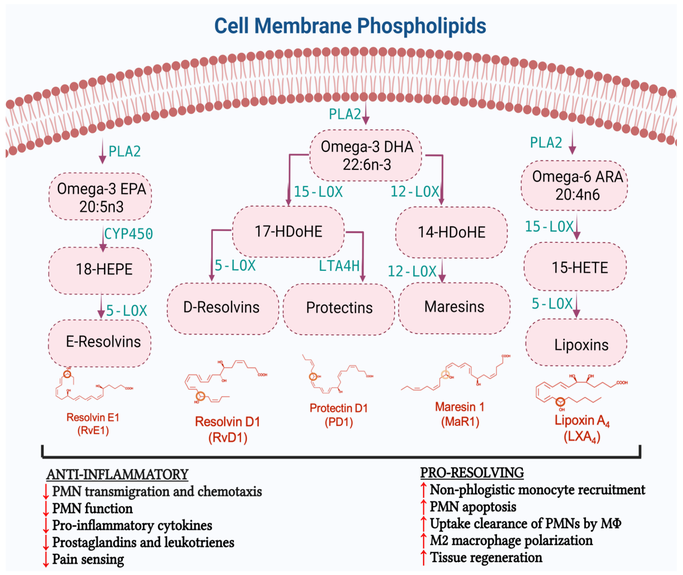

Research goals

- To determine the effect of whole-body knockout of the *Alox15* gene encoding the 12/15-LOX enzyme on skeletal muscle inflammation.
- To investigate the role of the 12/15-LOX enzyme in skeletal muscle regeneration following whole-body *Alox15* knockout.

Experimental design

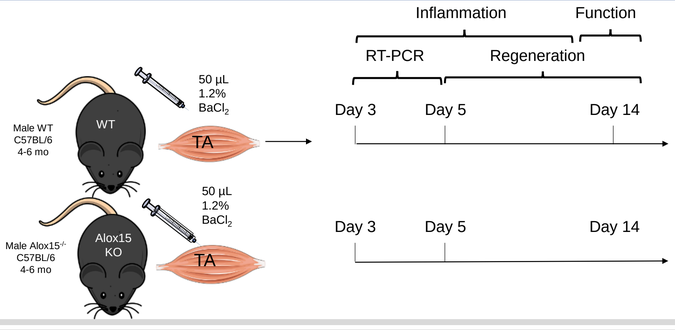

References

1. R. K. Saini and Y.-S. Keum, "Omega-3 and omega-6 polyunsaturated fatty acids: Dietary sources, metabolism, and significance — A review," *Life Sciences*, vol. 203, pp. 255-267, 2018-06-15 2018, doi: 10.1016/j.lfs.2018.04.049.

2. J. F. Markworth, K. R. Maddipati, and D. Cameron-Smith, "Emerging roles of pro-resolving lipid mediators in immunological and adaptive responses to exercise-induced muscle injury," (in en), 2016 2016.

3. B. Wang et al., "Metabolism pathways of arachidonic acids: mechanisms and potential therapeutic targets," (in en), Signal Transduction and Targeted Therapy, vol. 6, no. 1, pp. 1-30, 2021-02-26 2021, doi: 10.1038/s41392-020-00443-w.

4. K. Gronert, N. Maheshwari, N. Khan, I. R. Hassan, M. Dunn, and M. Laniado Schwartzman, "A role for the mouse 12/15-lipoxygenase pathway in promoting epithelial wound healing and host defense," (in eng), *The Journal of Biological Chemistry*, vol. 280, no. 15, pp. 15267-15278, 2005-04-15 2005, doi: 10.1074/jbc.M410638200.

Figure 1

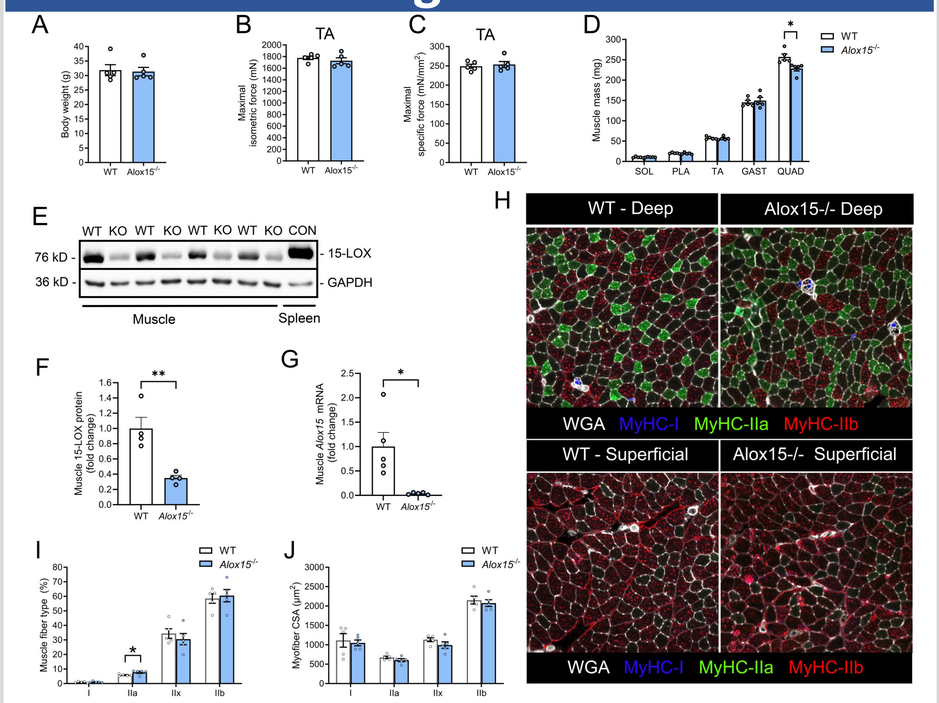

Figure 1: Characterization of the skeletal muscle phenotype of leukocyte type 12/15-lipoxygenase (15-LOX) deficient mice. A: Body weights of Wild Type (WT) and *Alox15* knockout (*Alox15*$^{-/-}$) mice. B: Maximal isometric force of tibialis anterior (TA) muscle. C: Specific isometric force (sPO) in mN/mm^2. D: Absolute muscle mass of soleus (SOL), plantaris (PLA), TA, gastrocnemius (GAST), and quadriceps (QUAD). E-F: Western blot and quantification of 15-LOX protein in TA muscle. G: *Alox15* mRNA expression in TA muscle by RT-qPCR. H: TA muscle fiber type analysis by myosin heavy chain (MyHC) staining. I: Muscle fiber type composition quantified by MuscleJ software. J: Cross-sectional area (CSA) of TA muscle fibers.

Figure 2

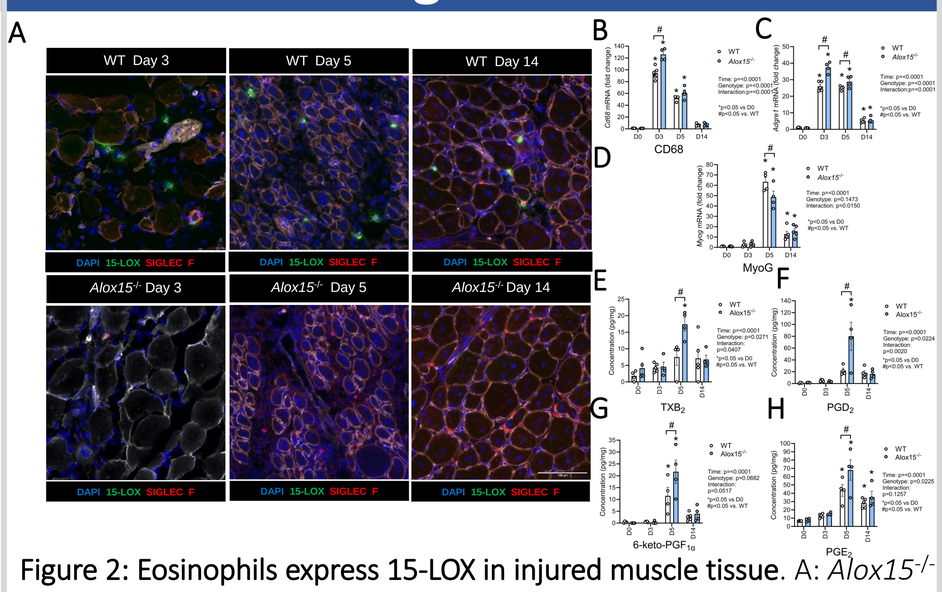

Figure 2: Eosinophils express 15-LOX in injured muscle tissue. A: *Alox15*$^{-/-}$ eosinophils lack 15-LOX protein expression. B-D: Effect of *Alox15* deficiency on muscle mRNA expression. E-H: Effect of *Alox15* deficiency on the muscle lipid mediator response to injury.

Figure 3

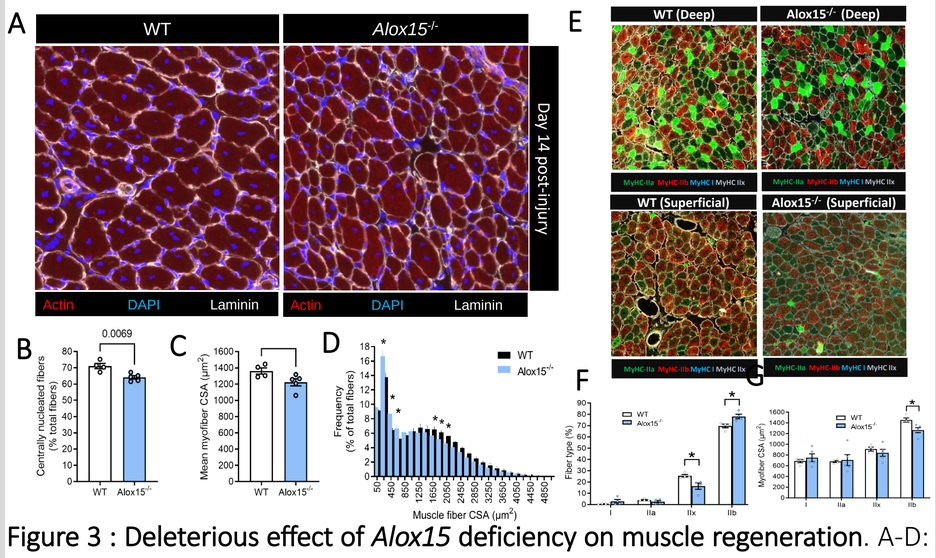

Figure 3 : Deleterious effect of *Alox15* deficiency on muscle regeneration. A-D: At day 14 post-injury, WT mice show a higher number of centrally nucleated myofibers. E-F *Alox15*$^{-/-}$ mice exhibit smaller muscle cross-sectional areas, indicating reduced myofiber size, particularly in type IIb fibers.

Figure 4

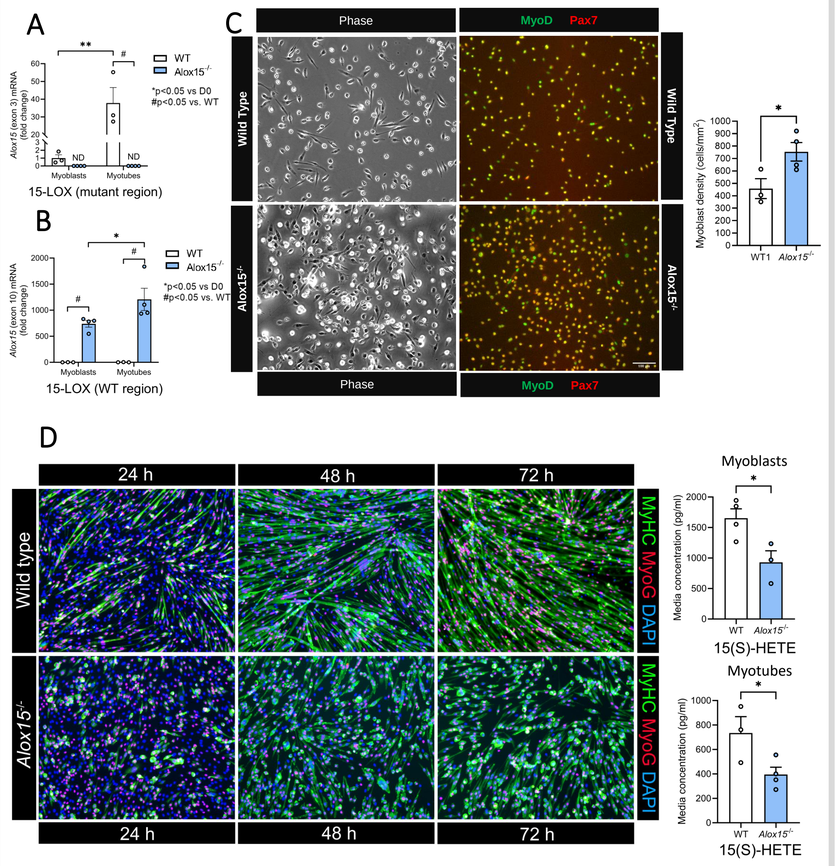

Figure 4: Direct effect of 15-LOX deficiency on primary myoblast proliferation and differentiation/fusion. A-B: Primary muscle cell *Alox15* mRNA expression. The mutant region (exon 3) of *Alox15*$^{-/-}$ mice shows no detectable mRNA expression. C-E: *Alox15*$^{-/-}$ mice show faster myoblast proliferation, but slower myogenic differentiation compared to wild-type mice.

Figure 5

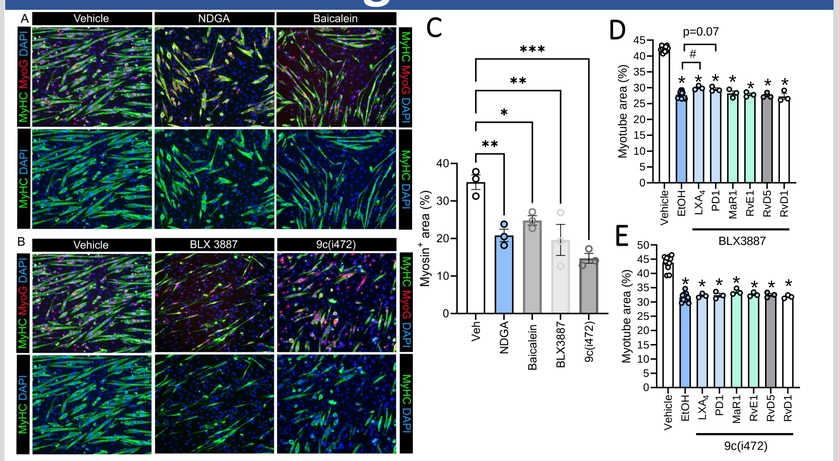

Figure 5: Direct effect of pharmacological inhibition of 15-LOX activity on C2C12 myoblast differentiation/fusion. A-C: NDGA (pan LOX inhibitor), baicalein (dual 12/15 LOX inhibitor), and the 15-LOX specific inhibitors (BLX3887 and 9Ci(472)) significantly inhibit myogenesis in C2C12 myoblast cells. D-E: 15-LOX specific inhibitor rescue experiments with LOX metabolites (mature SPMs)

Conclusions

- Transgenic mice deficient in murine leukocyte-type 15-LOX (12/15-LOX) exhibit more local inflammation and less effective myofiber regeneration following muscle injury.
  - ↑ Immune cell infiltration
  - ↑ Prostaglandin biosynthesis
  - ↓ Myogenic gene expression
  - ↓ Regenerating myofiber number and size
- Primary myoblasts isolated from *Alox15*$^{-/-}$ mice show different behavior *in-vitro.*
  - ↑ Proliferation rate
  - ↓ Differentiation and fusion capacity

People

Markworth Lab

PI: Dr. James F. Markworth

Grad Students: Hamood Ur Rehman, Xinyue Lu

Poster Number: #16

New fluorescent probes for biological imaging of reactive oxygen species

Brooke Steeno

Department of Chemistry

Ratiometric fluorescent probes can be useful for the intracellular imaging of reactive oxygen species (ROS) and metal ions. However, most probe designs are modified versions of existing fluorescent dyes that offer only modest shifts in emission wavelength. We have found 5,Äô-phenyl-2,Äô-pyridylthiazole (PPT) to be an excellent platform for designing chemically responsive fluorophores with sizable emission shifts based on changes in intramolecular charge transfer. For example, a para-borophenyl-PPT derivative (BPPT) can be oxidized by H2O2 into p-hydroxyphenyl-PPT (HPPT) with a 34-nm redshift in fluorescence at pH 7.8. The ratiometric fluorescence of BPPT increases linearly with H2O2 starting at 25 ŒºM and can be used to image H2O2 production during the regeneration of growth cones by Aplysia bag cell neurons. We have also found HPPT derivatives to be sensitive to superoxide anion, which induces a metastable redshift in emission of around 150 nm. Current studies are aimed at identifying novel ROS probes and elucidating the potential roles of ROS in oxidative signaling or stress.

New fluorescent probes for biological imaging of reactive oxygen species

Brooke L. Steeno[1], Yuichiro Watanabe, S. M. Sabbir Alam, Daniel M. Suter[2], and Alexander Wei[1]

Department of Chemistry[1] and Department of Biological Sciences[2], Purdue University, West Lafayette, IN, USA

Fluorescent ICT Probes in Redox Biology

The homeostatic imbalance of reactive oxygen species (ROS) and metal ions can lead to cellular oxidative stress, with strong implications in the progression of neurodegenerative diseases.[1] Redox processes associated with loss of homeostasis can be analyzed using fluorescent probes, with changes in emission wavelengths or intensities in response to specific analytes.[2,3] Most probes are designed by modifying well-known dyes with limited variations in emission shifts.[4] We are designing a class of fluorophores based on 5'-phenyl-2'-pyridylthiazole (PPT), which produce sizable emission shifts via intramolecular charge transfer (ICT) with high quantum yields (example in **Figure 1**). Here we discuss how PPTs can be designed for sensitive detection of various ROS in biological systems.[5,6]

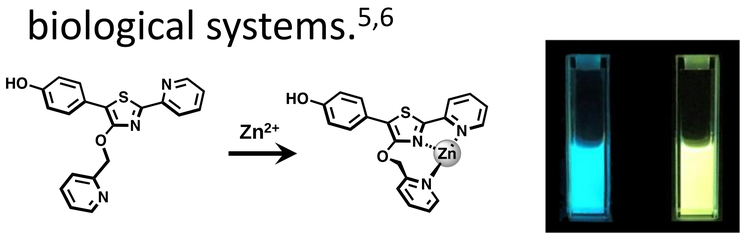

Figure 1. PPT (5"-hydroxy-4'-picolyloxy derivative) produces a 67-nm shift in emission (474 → 541 nm) in response to Zn^{2+} ions (30 μM in CH_3CN).[5]

BPPT: Probe for intracellular imaging of H_2O_2

PPT with a 5"-boropinacolate ester (BPPT **1**) was developed as an imaging dye for intracellular H_2O_2, based on the oxidative cleavage of the C–B bond to produce 5"-hydroxy-PPT (HPPT **2**). Replacing the electron-deficient Bpin ester with electron-rich OH increases ICT, resulting in a 34-nm redshift in emission from blue to green (λ_{em} 472 → 506 nm; **Figure 2**). The synthesis of BPPT (and HPPT) are summarized below (**Scheme 1**).

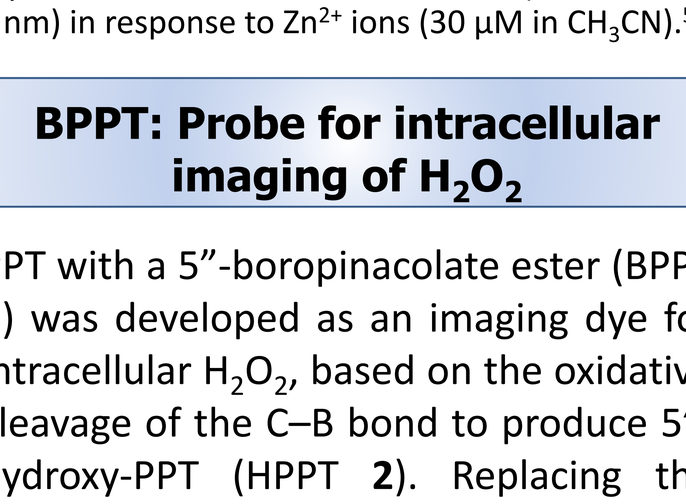

Scheme 1. Synthesis of BPPT (**1**) & HPPT (**2**).

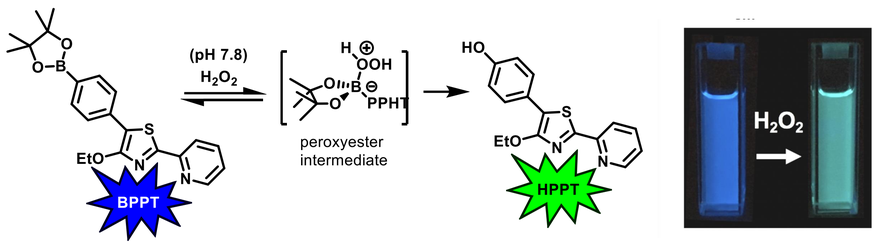

Scheme 1. BPPT oxidation to HPPT by H_2O_2 in artificial sea water with a 34-nm shift in emission (blue → green).

H_2O_2 signaling in neurite regeneration

While excess ROS can cause devastating effects and neurological disorders, small bursts of ROS are needed to signal axonal regeneration and growth.[6] For instance, NAPDH oxidase (Nox) is a membrane-bound enzyme that produces superoxide (O_2^{-}) during neuronal injury, and quickly turns into H_2O_2.[7] BPPT **1** was used to investigate the relationship between Nox and H_2O_2 signaling in injured *Aplysia* bag cell neurons.[8] Mechanically transected neurites were incubated with 4 μM BPPT **1** for 20 minutes then washed prior to *in vitro* H_2O_2 imaging (**Figure 2**). The rate of growth cone regeneration correlated both with higher H_2O_2 concentrations and colocalization of Nox2 (as determined by immunostaining).

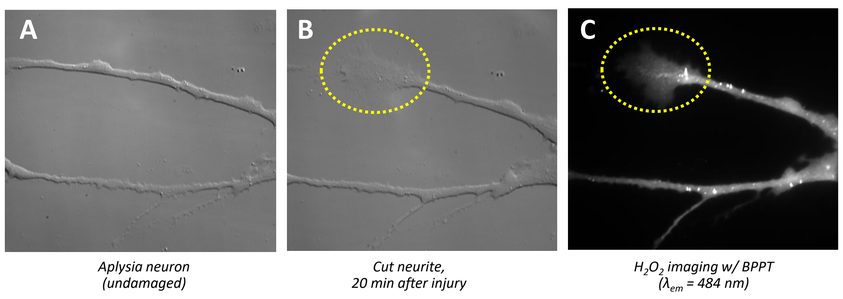

Figure 2. (A,B) Optical DIC microscopy of neurite cells before and after injury. (C) H_2O_2 imaging via BPPT oxidation; injured neurites treated with BPPT for 20 min prior to fluorescence imaging (em 535/40 nm).

To determine the limit of quantification for H_2O_2, the dynamic range and kinetic rate of BPPT oxidation were analyzed in artificial seawater (pH = 7.8) (**Figure 3**). The linear dynamic range was produced by exposing 1.25 μM BPPT to varying H_2O_2 concentrations and, after 10 minutes, measuring the ratiometric [HPPT]/[BPPT] emission (λ_{em} 540/472 nm). The limit of H_2O_2 quantification by BPPT is 25 μM with a first-order oxidation rate.

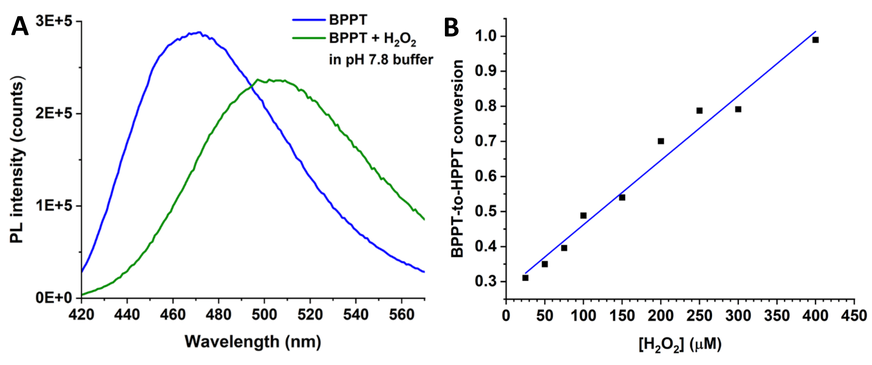

Figure 3. (A) Fluorescence spectra of BPPT and its oxidation into HPPT at pH 7.8. (B) Dynamic H_2O_2 range for conversion to HPPT from BPPT after 10 min. exposure at pH 7.8 (25–400 μM), based on ratiometric emissions (540/472 nm).

HPPT: A new probe for superoxide?

We discovered that HPPT **2** (oxidation product of BPPT **1**) could also be oxidized by O_2^{-}, which has a lifetime of microseconds. HPPT treated with KO_2 in anhydrous DMSO with 18-crown-6 produced a dramatic 150-nm shift from light blue to bright red (λ_{em} 497 → 647 nm; **Figure 4**). More evidence was obtained by treating **2** with NaO_2 (6 M NaOH in 30% H_2O_2) and with electro-chemically generated O_2^{-} in dry DMSO. Treatment of HPPT pivalate ester (λ_{em} 471 nm) with KO_2 produced a similarly large redshift in emission.

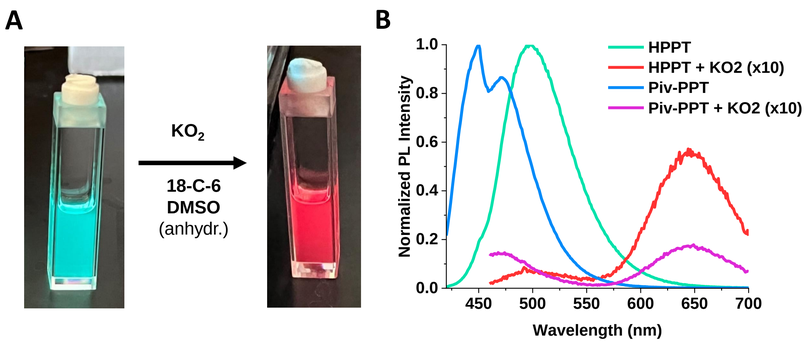

Figure 4. (A) HPPT (5 μM in DMSO, λ_{ex} 365 nm) before and after addition of 5 mM KO_2/18-C-6. (B) PL spectra of HPPT (green) and HPPT-Piv (blue) before and after addition of KO_2 /18-C-6 with dramatic redshifts in emission (red & purple).

Characterization of reaction products from **2** and **3** are in progress. At this time, we postulate a novel quinoidal tautomer (q-HPPT; **Figure 5**). Evidence for q-HPPT includes the absence of a phenolic proton in ^{1}NMR and substantial downfield shifts in ^{13}C NMR signals.

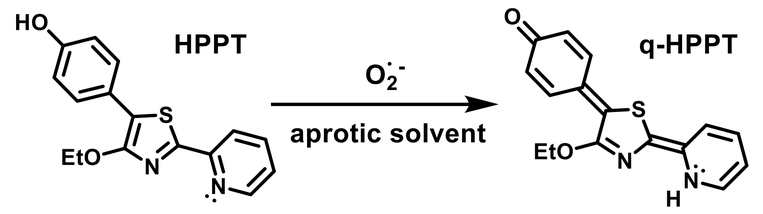

Figure 5. Metastable tautomer (q-HPPT) as the postulated reaction product of HPPT and O_2^{-}.

Summary & Future Directions

PPT derivatives are useful probes for fluorescent ROS imaging, with established potential for H_2O_2 detection in live cells as demonstrated with BPPT. The synthesis is straightforward and easily modified for installation of substituents with specific chemical function. In addition, we have ascertained a novel reaction between HPPT and superoxide (O_2^{-}). PPTs may also be derivatized to direct their localization to cell membranes, mitochondria, and other organelles, enabling cellular redox activities to be imaged with high spatial resolution.

References

1. Anik, M.I. et al. *ACS Appl. Biomater.* **2022**, *5*, 4028.
2. Goshisht, M.K. et al. *Chem. Sci.* **2023**, *14*, 5842.
3. Bigdeli, A. et al. *Anal. Chim. Acta* **2019**, *1079*, 30.
4. Grimm, J.B., & Lavis, L.D. *Nat. Methods* **2022**, *19*, 149.
5. Watanabe, Y. et al. *Mater. Chem. Front.* **2020**, *4*, 899.
6. Meda, F. et al. *Antioxid. Redox Signal.* **2016**, *24*, 299.
7. Bedard K. & Krause, K. *Physiol. Rev.* **2007**, *87*, 245.
8. Alam, S.M.S. et al. *J. Neurochem.* **2023**, *167*, 505.

Acknowledgments. We gratefully acknowledge support from Purdue University (BLS: Ross fellowship), JSPS (YW: fellowship), ACS-PRF (58453-ND4), NIH (R01 NS117701; P30-CA023168), NSF (CHE-2204206), and Indiana State Dept. Health (Contract 26351).

Poster Number: #17

Investigating Proteostasis Modulations from Fic-BiP Interactions by Stable Isotope Labeling
Miranda Weigand
Department of Chemistry

Investigating Proteostasis Modulations from Fic-BiP Interactions by Stable Isotope Labeling

Miranda R. Weigand[1], Radhika Bhaumik[2], Lucas Kramer[3], Christina R. Ferreira[4], Vikki M. Weake[3], Bryon S. Drown[1], Seema Mattoo[2,3]
[1]James Tarpo Jr. and Margaret Tarpo Dept. of Chemistry; [2]Dept. of Biological Sciences; [3]Dept. of Biochemistry; [4]Metabolite Profiling Facility

Unfolded Protein Response Regulates Proteostasis

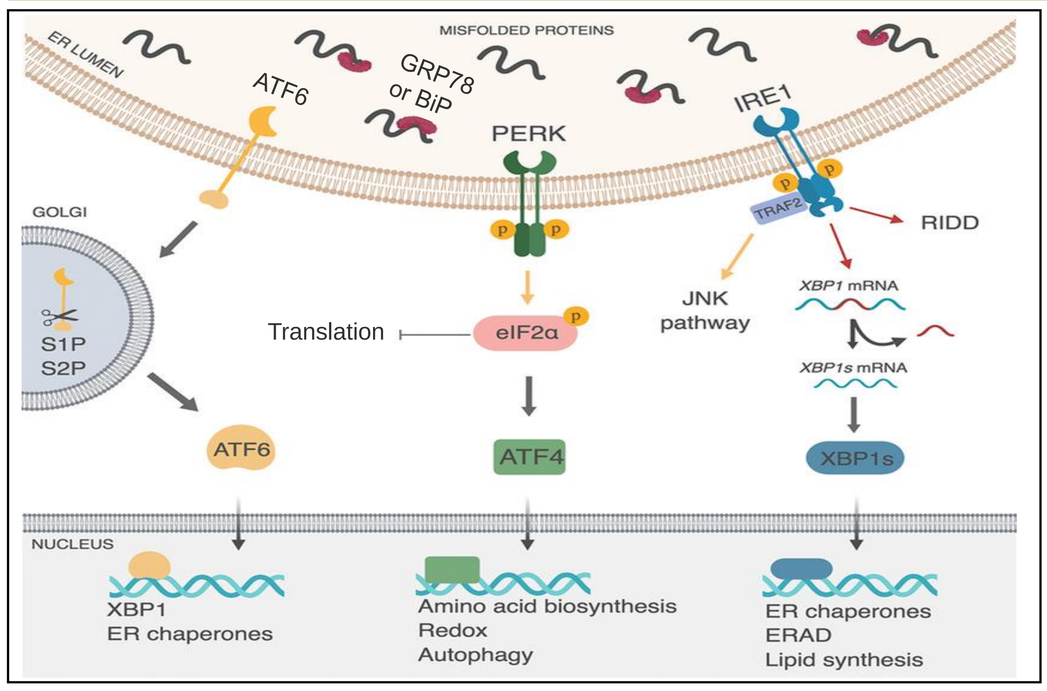

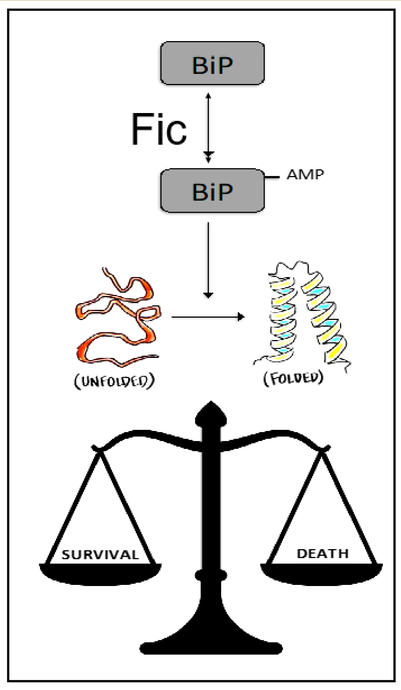

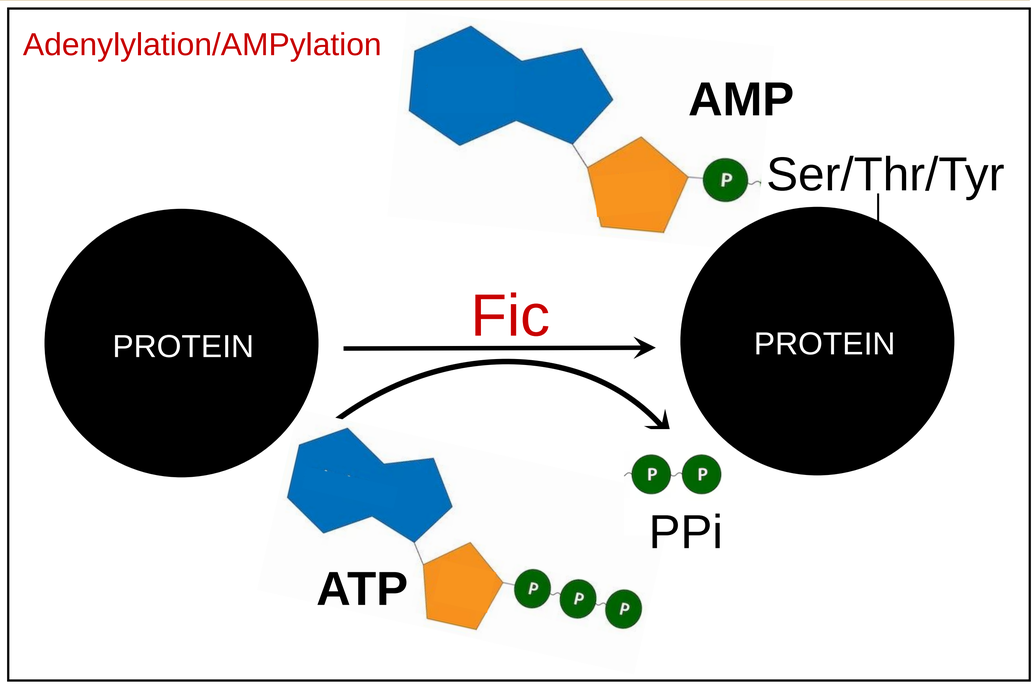

STABLE ISOTOPE LABELING BY AMINO ACIDS IN CELLS (SILAC)

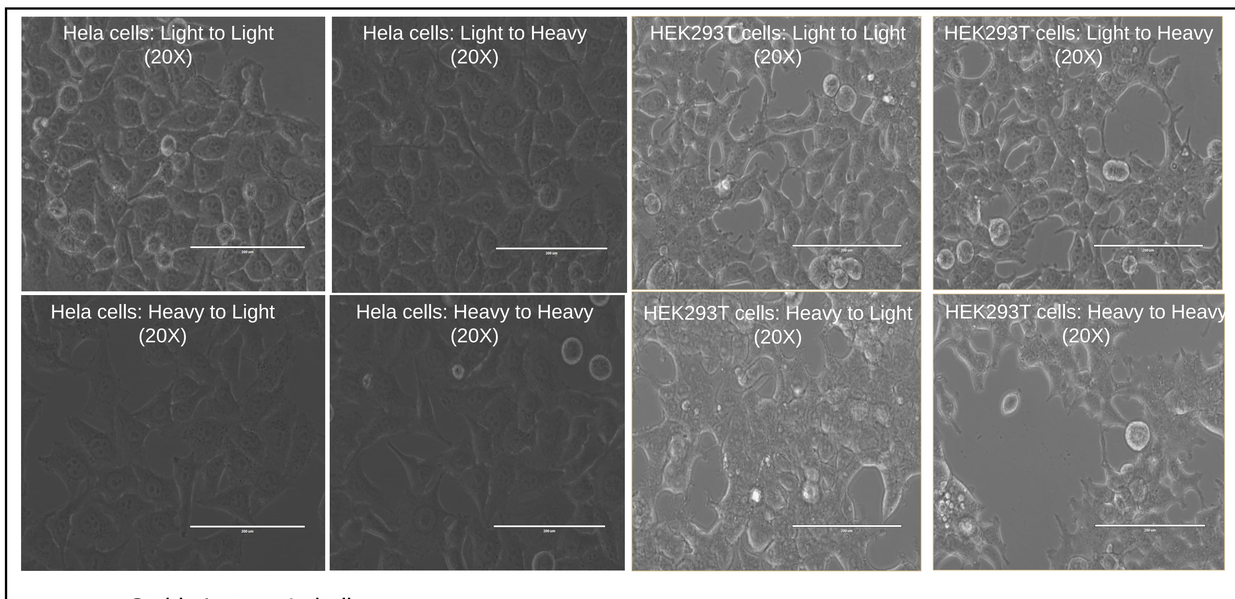

Stable Isotope Labeling

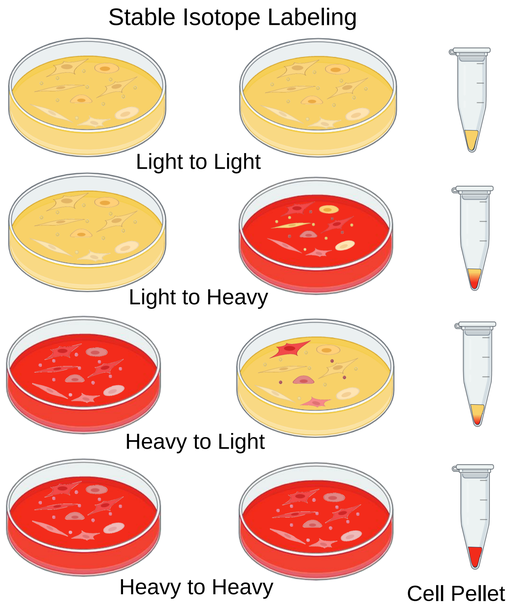

Bottom-up Proteomics Workflow

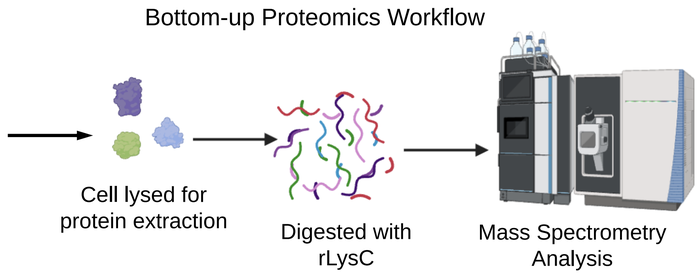

- Isotopically labeled media included $^{13}C_6$-Lysine
- Cells were kept on media for 48 hrs between passages
- Thermo Orbitrap Exploris 480
- Chromatographic separation performed on a Vanquish Neo UHPLC on a PepMap C18 50 cm column and trap column for 120 mins
- Data-dependent acquisition (DDA) was performed with full MS scans at a mass resolution of 120,000 and MS/MS at 22,500 with a normalized collision energy at 30
- Database search with MaxQuant v2.6.3.0

Total number of proteins identified

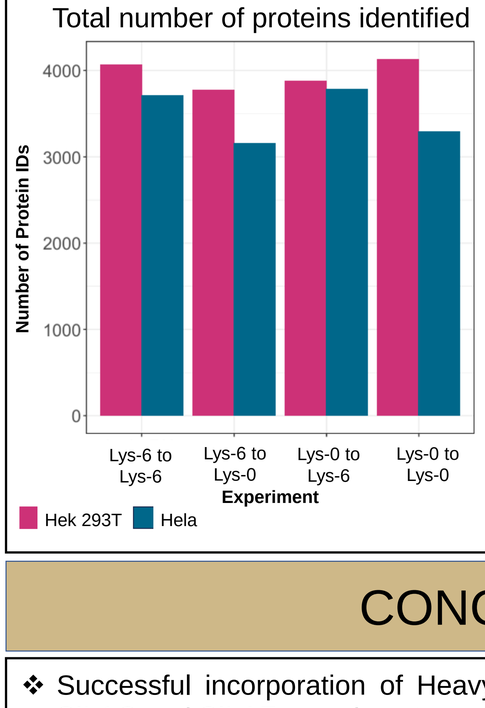

Isotope incorporation at the protein level over time

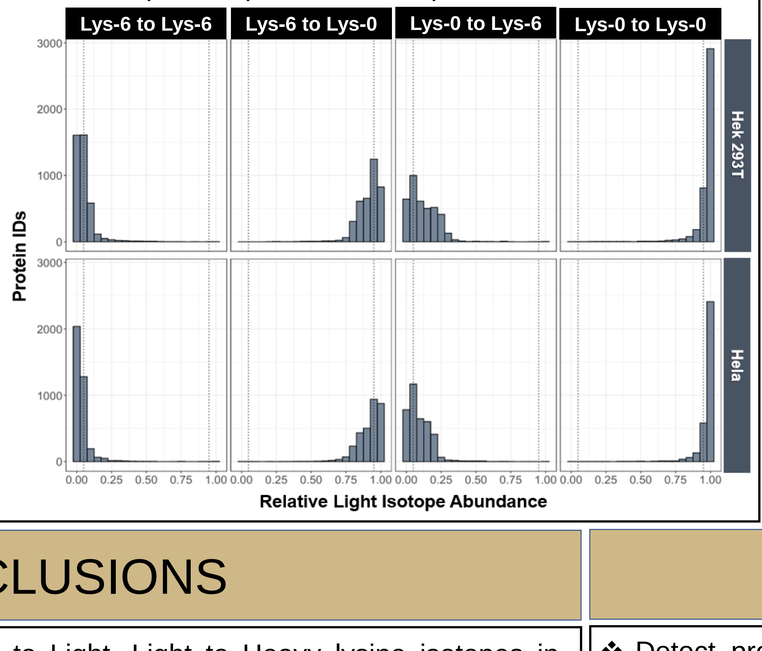

STABLE ISOTOPE LABELING BY AMINO ACIDS IN FLIES (SILAF)

- *Drosophila melanogaster* as a model for diabetic retinopathy
- Nearly all protein misfolding mutations result in various blindness phenotypes
- High metabolic activity in eyes for light signaling making it venerable to metabolic defects
- 10M living with diabetic retinopathy(DR) in US[2]
  - 8M with non-vision threatening DR
  - 2M with vision threatening DR

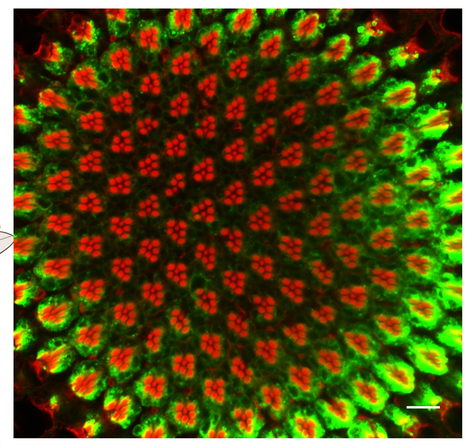

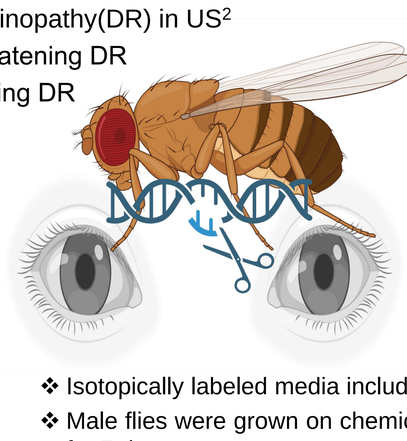

Stable Isotope Labeling

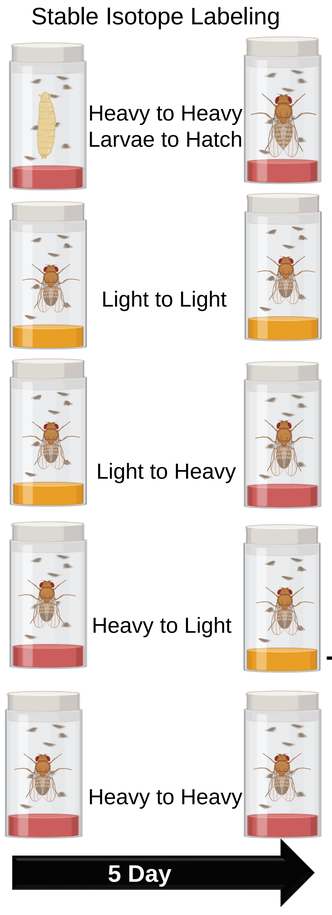

- Isotopically labeled media included $^{13}C_6$-Lysine
- Male flies were grown on chemically defined media for after hatching for 5 days
- Thermo Orbitrap Exploris 480
- Chromatographic separation performed on a Vanquish Neo UHPLC on a PepMap C18 50cm column and trap column for 90 mins
- Data-dependent acquisition (DDA) was performed with full MS scans at a mass resolution of 120,000 and MS/MS at 22,500 with a normalized collision energy at 30
- Database search with MaxQuant v2.6.3.0

Bottom-up Proteomics Workflow

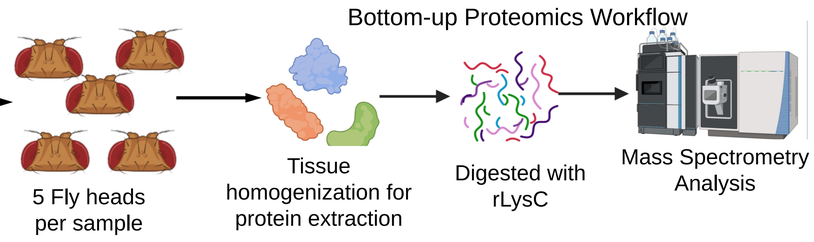

- Successful incorporation of heavy lysine into proteins
- Able to Quantify over 3,500 unique proteins
- A few number of proteins reach more than 50% in 5 days

Isotope incorporation at the protein level over time

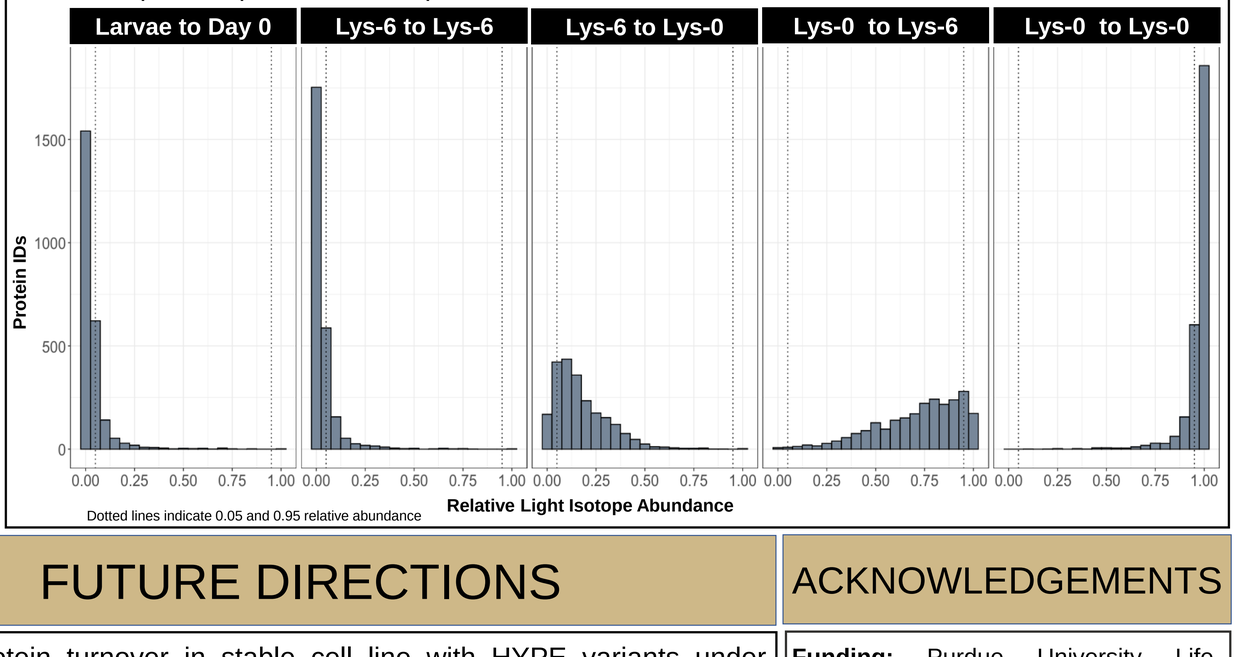

Dotted lines indicate 0.05 and 0.95 relative abundance

CONCLUSIONS

- Successful incorporation of Heavy to Light, Light to Heavy lysine isotopes in SILAC and SILAF experiments.
- Developed a bottom-up proteomics approach analysis of proteins from pSIL samples.
- Successfully quantified 4,000 unique proteins in each experiments.
- *Drosophila melanogaster* is an important model for studying eye-related diseases.

FUTURE DIRECTIONS

- Detect protein turnover in stable cell line with HYPE variants under normal and ER stress conditions.
- Detect protein turnover in stable cell line with BiP variants in normal conditions and ER stress conditions.
- pSILAC and pSILAF across several timepoints for protein turnover analysis.
- Comparison of data acquisition strategies for proteome-wide measurements.

ACKNOWLEDGEMENTS

Funding: Purdue University Life Sciences Summit initiative
Team (labs): Fang Huang, Jonathan Schlebach, Ramaswamy Subramanian, Daniel Flaherty, Alex Chortos, Eugenio Culurciello

References

(1) Cell 140, 4, 2010, 590-590.e2
(2) JAMA Ophthalmol. 2023 Aug 1;141(8):747-754

Poster Number: #18

Inhibition and Bactericidal Effect of GroEL Chaperone Inhibitors against Clostridioides difficile

Lijia Zhang

Comparative Pathobiology

Clostridioides difficile infection (CDI) is a major health concern, causing significant morbidity, mortality, and healthcare costs. CDI is often triggered after the disruption of the normal gut microbiota due to antibiotic use, allowing C. difficile to colonize the gastrointestinal tract and secrete toxins. Current antibiotic treatments (metronidazole, vancomycin, and fidaxomicin) suffer several limitations, including high recurrence rates and treatment failure. The Centers for Disease Control and Prevention (CDC) emphasized the urgency for new therapeutic approaches for CDI. GroEL, an essential chaperone protein in C. difficile, plays a crucial role in protein folding and is a promising target for antimicrobial drugs. This study aimed to identify effective GroEL inhibitors against C. difficile, determine their minimum inhibitory concentrations (MICs), minimum bactericidal concentrations (MBCs), and their killing kinetics. A library of about a hundred GroEL inhibitors was screened for their activity against one strain of C. difficile. Active hits were tested against multiple C. difficile strains, including hypervirulent clinical isolates. Further research is planned to investigate the structure-activity relationships of the active compounds, evaluate their cytotoxicity in vitro and safety in vivo, and analyze their pharmacokinetic properties and efficacy in treating CDI in vivo.

Tau pathology, caused by the abnormal accumulation of the microtubule-associated protein tau, is a major pathological hallmark of AD and other tauopathies, such as frontotemporal dementia (FTD)[3,4].

Inhibition and Bactericidal Effect of GroEL Chaperone Inhibitors against *Clostridioides difficile*

Lijia Zhang [1], Ahmed AbdelKhalek Hassan [1,*]

[1] Department of Comparative Pathobiology, Purdue University, West Lafayette, IN 47907

PURDUE UNIVERSITY

INTRODUCTION

Clostridioides difficile infection (CDI), a leading cause of antibiotic-associated gastrointestinal disease, characterized by high morbidity, mortality, and substantial healthcare costs. The pathogenesis of CDI involves the disruption of the normal intestinal microbiota by antibiotics, leading to colonization by *C. difficile* and subsequent toxins.

The epidemiology of CDI has evolved, with escalating incidence, severity, and recurrence rates attributed to the emergence of hypervirulent strains such as BI/NAP1/027. These challenges are exacerbated by the limitations of current treatment options, which include metronidazole, vancomycin, and fidaxomicin, but are often associated with high recurrence rates. This has aroused interest in developing effective drug development, among which compounds hold promising potential to reduce CDI's incidence and impact significantly.

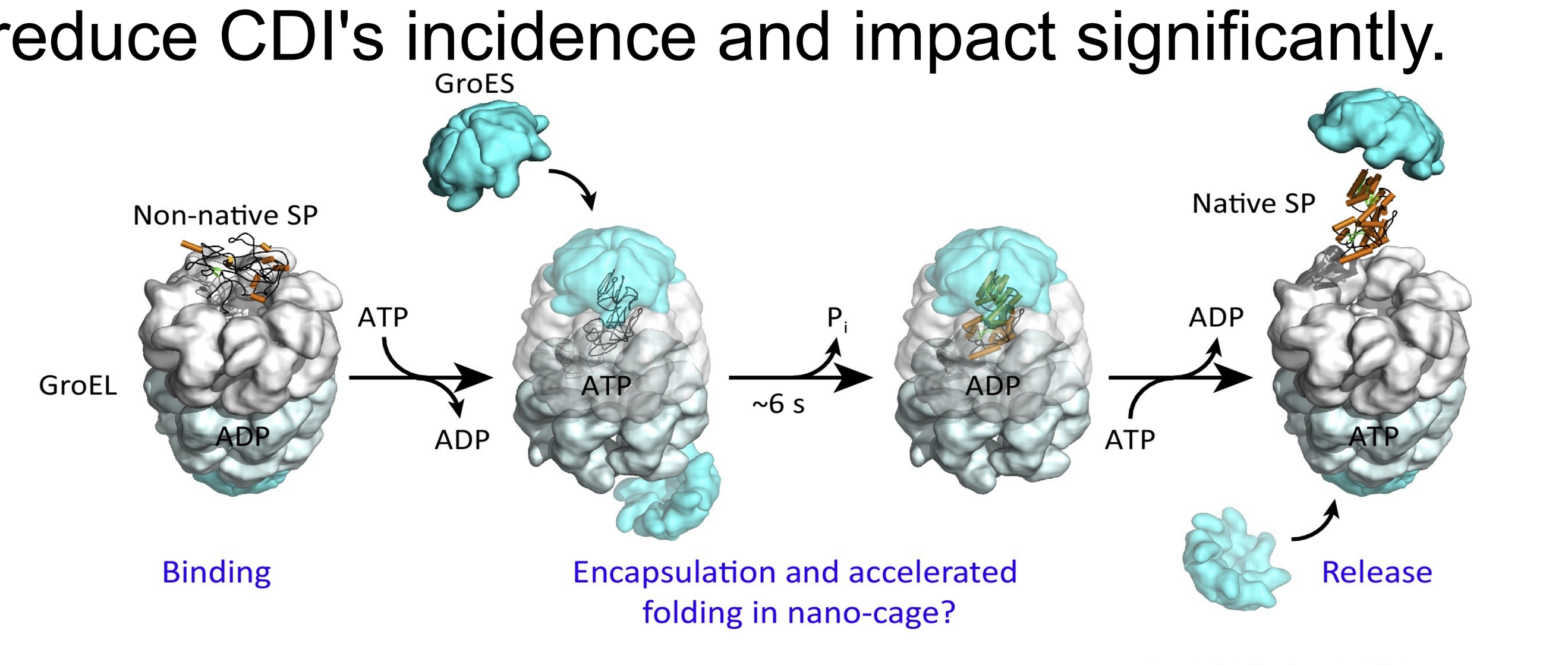

In this study, we ***aim to*** **(1)** screen effective GroEL inhibitors against *C. difficile* and (2) evaluate their minimum inhibition, minimum bactericidal concentration, and time needed to kill *C. difficile.*

METHODS

Microdilution assay

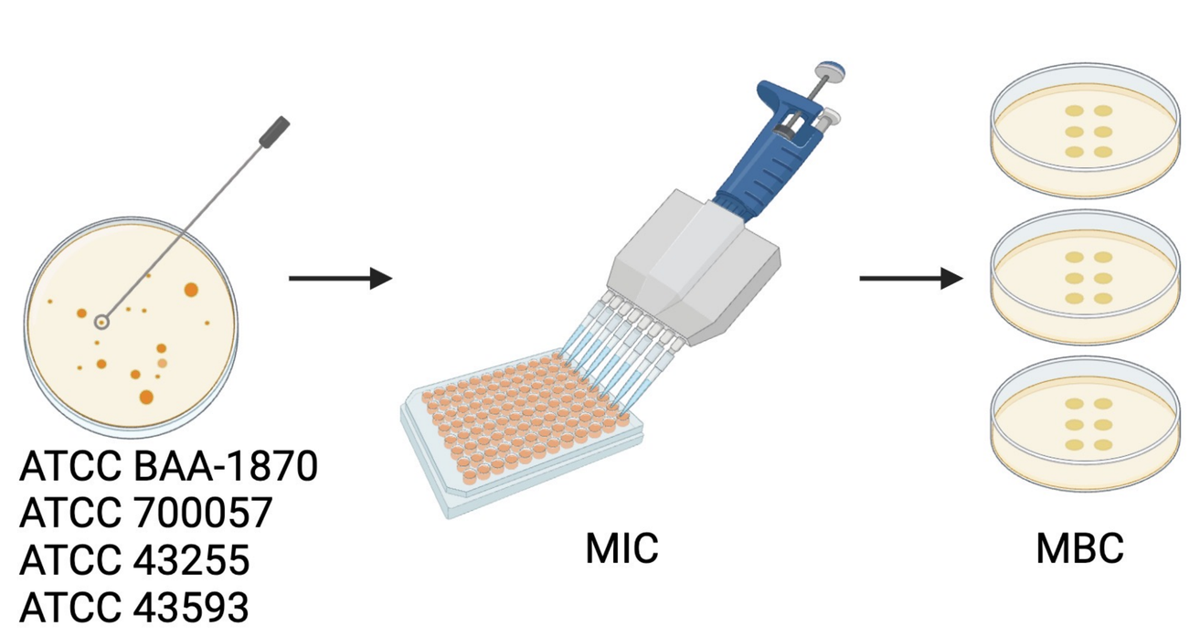

Time-kill assay

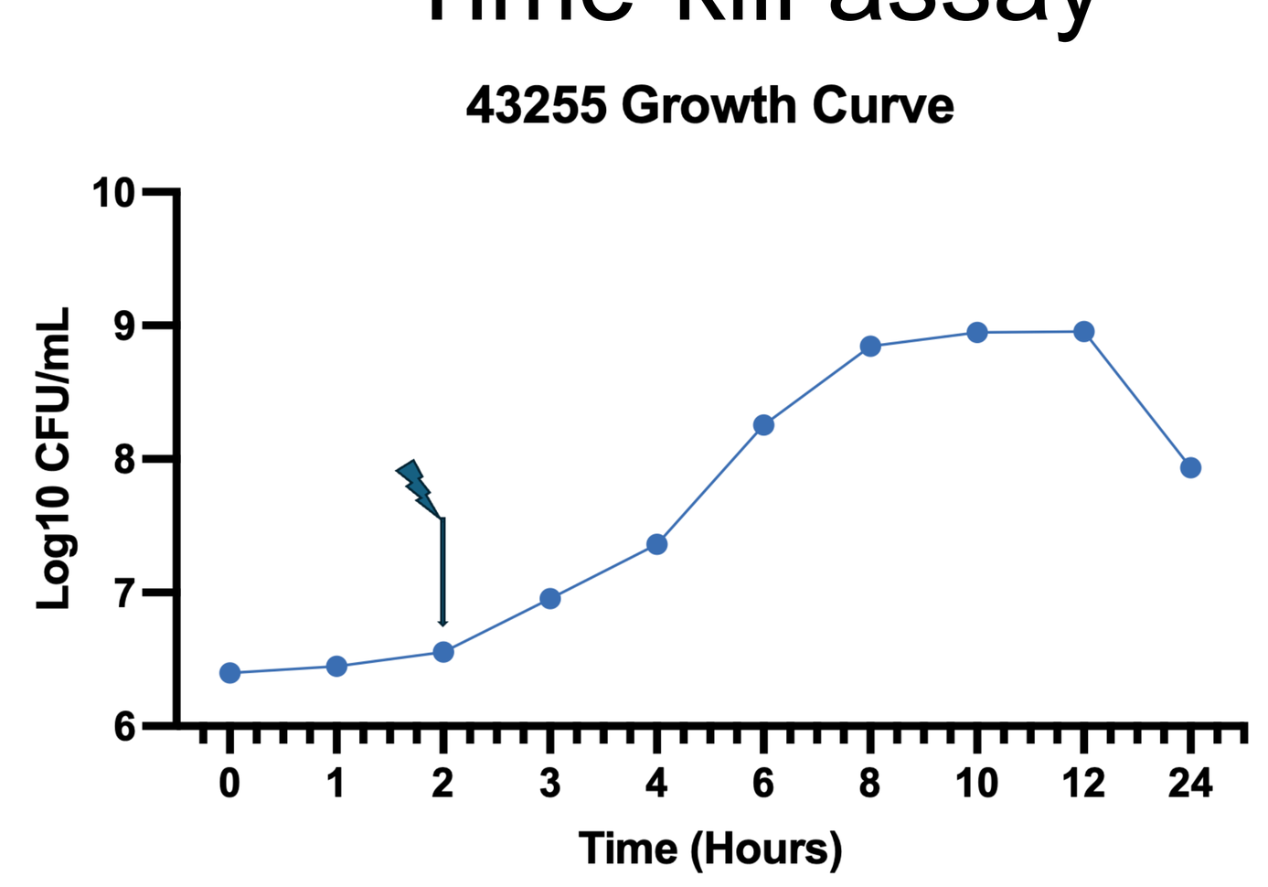

RESULTS

1. Pre-screening results of active compounds against ATCC BAA-1870 *C. difficile strain*.

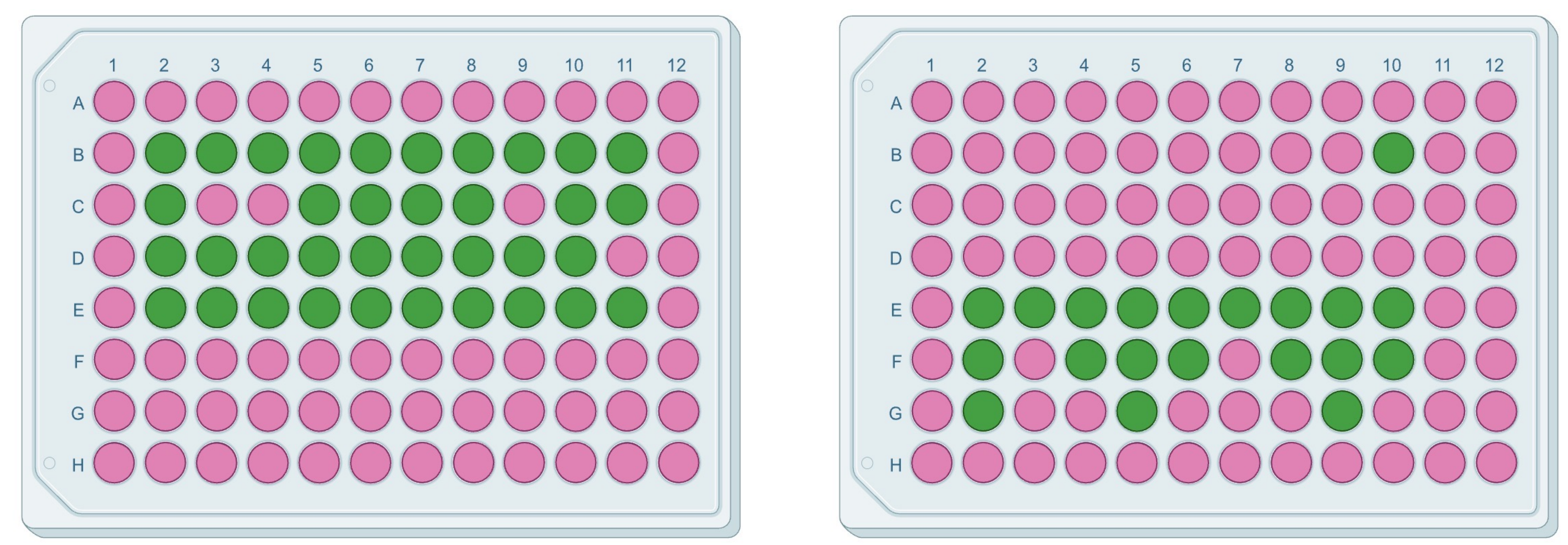

2. The minimum inhibitory concentrations (MICs, µM).

Compouns /strains	Well location	Chemical group	1870	700057	43255	43593
1289	C10	SCA	8	4	8	8
1376	C11	SCA	2	2	4	4
1384	D2	SCA	16	64	32	16
1385	D3	SCA	4	4	8	4
1675	D4	SCA	1	2	2	4
1780	D5	SCA	16	16	16	16
2079	D6	SCA	16	8	8	8
2080	D7	SCA	0.5	0.5	0.5	0.5
2099	D8	SCA	32	32	32	32
1817	E2	NF	16	16	32	32
1845	E4	NF	32	16	64	16
1846	E5	NF	16	8	16	8
1848	E6	NF	16	16	32	16
1860	E8	NF	8	32	32	32
1862	E9	NF	8	8	32	16
1486	E2	SCA	2	2	1	2
1537	E3	SCA	2	1	4	8
1389	E4	SCA	4	4	8	8

3. The minimum bactericidal concentrations (MBCs, µM).

Compouns /strains	Well location	Chemical group	1870	700057	43255	43593
1289	C10	SCA	16	32	16	16
1376	C11	SCA	4	4	4	8
1384	D2	SCA	16	64	>64	64
1385	D3	SCA	8	4	8	8
1675	D4	SCA	2	2	4	8
1780	D5	SCA	16	16	16	16
2079	D6	SCA	32	8	16	8
2080	D7	SCA	0.5	0.5	0.5	1
2099	D8	SCA	64	64	32	64
1817	E2	NF	16	16	32	32
1845	E4	NF	32	16	64	16
1846	E5	NF	16	8	16	8
1848	E6	NF	16	16	32	16
1860	E8	NF	8	32	32	32
1862	E9	NF	8	8	32	16
1486	E2	SCA	8	2	8	2
1537	E3	SCA	8	4	16	8
1389	E4	SCA	32	8	16	8

2. The minimum inhibitory concentrations (µM)[cont.].

Compouns /strains	Well location	Chemical group	1870	700057	43255	43593
1373	E5	SCA	4	4	8	8
1390	E6	SCA	4	4	4	8
1669	E9	SCA	16	16	16	16
1392	E10	SCA	16	32	32	32
1674	F2	SCA	16	16	16	16
1781	F4	SCA	1	1	0.5	1
1589	F5	SCA	32	4	32	32
1500	F6	SCA	16	1	16	8
1818	F9	NF-NAH	32	32	32	32
1861	F10	NF-NAH	16	32	64	32
Vancomycin			1	1	1	1

3. The minimum bactericidal concentration (µM)[cont].

Compouns /strains	Well location	Chemical group	1870	700057	43255	43593
1373	E5	SCA	8	8	16	16
1390	E6	SCA	16	16	8	8
1669	E9	SCA	32	32	32	32
1392	E10	SCA	>32	32	>32	>32
1674	F2	SCA	32	16	32	16
1781	F4	SCA	8	2	4	2
1589	F5	SCA	32	4	32	32
1500	F6	SCA	4	1	16	16
1818	F9	NF-NAH	32	32	>32	32
1861	F10	NF-NAH	32	32	64	32
Vancomycin			2	2	2	2

4. Time-kill assay of compounds D4,D7,E5,E9, and control groups for ATCC 43255 *C. difficile strain*.

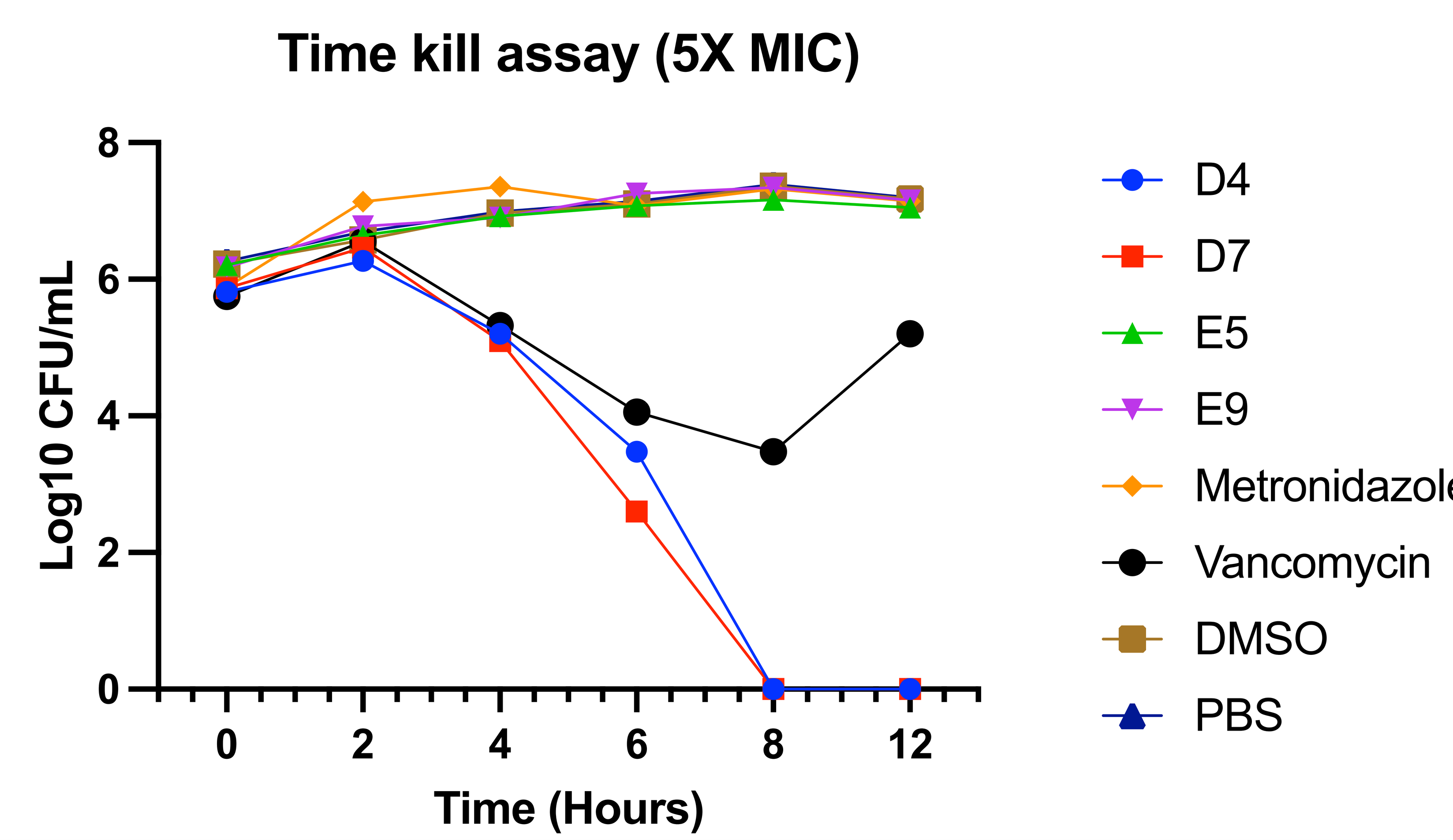

FUTURE PLANS

1. Analyze the structure-activiy relationship among all the active compounds.
2. Cytotoxicity assay in vitro and safety evaluation in vivo.
3. Pharmacokinetic evaluation and activity in vivo.

ACKNOWLEDGEMENT

We appreciate the support from Professor Steven M. Johnson at Indiana University, who provided all the compounds.

REFERENCES

Hayer-Hartl, M., Bracher, A., & Hartl, F. U. (2016). The GroEL–GroES chaperonin machine: a nano-cage for protein folding. Trends in biochemical sciences, 41(1), 62-76.

Godek, J., Sivinski, J., Watson, E. R., Lebario, F., Xu, W., Stevens, M., ... & Chapman, E. (2024). Bis-sulfonamido-2-phenylbenzoxazoles Validate the GroES/EL Chaperone System as a Viable Antibiotic Target. Journal of the American Chemical Society, 146(30), 20845-20856.